UNIVERSITY OF OKLAHOMA

GRADUATE COLLEGE

METABOLIC DEPENDENCIES DRIVE SPECIES INTERACTIONS IN THE MICROBIAL COMMUNITIES

A DISSERTATION

SUBMITTED TO THE GRADUATE FACULTY

in partial fulfillment of the requirements for the

Degree of

DOCTOR OF PHILOSOPHY

BY

Dongyu Wang

Norman, Oklahoma

2024

METABOLIC DEPENDENCIES DRIVE SPECIES INTERACTIONS

IN THE MICROBIAL COMMUNITIES

A DISSERTATION APPROVED FOR THE

SCHOOL OF BIOLOGICAL SCIENCES

BY THE COMMITTEE CONSISTING OF

Dr. Chongle Pan, Chair

Dr. Jizhong Zhou

Dr. Kara B. De León

Dr. J.P. Masly

Dr. Qinggong Tang

Acknowledgements

Pursuing a PhD far from home has been one of the most challenging yet rewarding experiences of my life. Living in a new country, thousands of miles away from my family and friends, presented a unique set of challenges. However, these past five years have been filled with growth, learning, and the invaluable support of many wonderful people. Without their constant encouragement, generosity, and assistance, this journey would have been significantly more difficult. I would like to express my deepest gratitude to everyone who helped me along the way, making it possible for me to complete this PhD.

First, I would like to express my sincere gratitude to my supervisor, Dr. Chongle Pan. I am grateful for his support and for giving me the opportunity and freedom to pursue research in areas that interest me. This journey has equipped me with cutting-edge skills and knowledge in microbial communities, profoundly shaping both my academic and professional growth.

I would also like to extend my heartfelt thanks to my advisory committee members, Dr. Jizhong Zhou, Dr. Kara B. DeLeón, Dr. John P. Masly, and Dr. Qinggong Tang, for their unwavering support and guidance in helping me strive for better science and a better life. A special thanks goes to Dr. Jizhong Zhou for his generous assistance with my experiments, computational analyses, and overall academic development. I truly aspire to become not only a great scientist but also a kind and supportive person, like Dr. Zhou. I am deeply thankful to Dr. Kara B. DeLeón for her practical advice on my research and guidance throughout my PhD studies. Her support ensured I stayed on track, both in research and academics, during this journey. I would also like to express

my gratitude to Dr. John P. Masly for his invaluable teaching during my first year in the course *R for Biology*, which laid a strong foundation for the statistical analyses in my PhD research. A sincere thank you to Dr. Qinggong Tang, who, despite joining my committee for only a short period, played a crucial role in ensuring that I graduate on time in Fall 2024.

In addition, I would like to thank several professors in the Department of Microbiology and Plant Biology at OU. Special thanks to Dr. Michael J. McInerney and Dr. Ralph S. Tanner for their mentorship and support in nearly all of my environmental microbial research projects. From them, I learned the importance of enjoying science, and their encouragement made it possible for me to complete the program smoothly. I am also grateful to Dr. Aifen Zhou for helping me adjust to life at OU, both academically and personally, and for her consistent support, which helped me settle into my new environment quickly. A special note of thanks goes to Dr. Susan Schroeder, who supported me during difficult times and offered constructive advice at critical stages of my PhD journey. Without the help of all of you, this dissertation would not have been possible.

I must also thank my collaborators at the University of Washington, including David A. Stahl, Mari-Karoliina H. Winkler, Pieter Candry, and Kristopher A. Hunt. It has been a great experience working on wetland microbial communities with all of you, and this collaboration forms a significant part of my PhD dissertation.

Finally, I extend my deepest appreciation to my parents and extended family. I am fortunate to have been born into a loving family, and it is your unwavering and unconditional support that has opened my eyes to a broader and more exciting world.

You are my eternal refuge and my constant source of courage to aim high and explore new possibilities. You make my life truly exciting. Most importantly, I dedicate my deepest appreciation to my grandfather. It was you who gave me endless love and favoritism, leaving a LIFELONG IMPACT on me to work hard, be resilient, and strive to be a great person. How I wish you were here to see me grow and become someone you would be proud of.

Table of Content

Acknowledgements IV
List of Tables XI
List of Figures XII
Abstract XIX
Chapter 1: Introduction 1
1.1 Abstract 1
1.2 Microbial Communities: Foundations of Ecosystem Function and Stability 2
1.4 Modeling Microbial Interactions 6
1.5 Integrating Multi-Omics and Modeling Approaches for a Holistic Understanding of Microbial Communities 9
1.6 Future perspectives and conclusion 12
Chapter 2. Cross-feedings, competitions, positive and negative synergies in a four-species synthetic community for anaerobic degradation of cellulose to methane 14
2.1 Abstract 14
2.2 Introduction 16
2.3 Materials and Methods 18
2.3.1 Strains 18
2.3.2 Cultures, Growth Conditions and Experimental Design 18
2.3.3 Chemical analysis 19
2.3.4 Protein Identification and Quantification 20
2.3.5 Construction of Stoichiometric Model 21
2.3.6 Statistical analysis 22
2.3.7 Data availability 22
2.4 Results 23
2.4.1 Overview of the experimental design 23
2.4.2 Metabolism of cellulolytic bacterium *Ruminiclostridium cellulolyticum* 26
2.4.3 Metabolism of hydrogenotrophic methanogen *Methanospirillum hungatei* and acetoclastic methanogen *Methanosaeta concilii* 30
2.4.4 Metabolism of sulfate-reducing bacterium *Desulfovibrio vulgaris* 33
2.4.5 Modeling of carbon and energy flow through the synthetic community 37

2.5 Discussion 40
Chapter 3. Metabolic dependencies drive species interactions in a synthetic microbial community 46
3.1 Abstract 46
3.2 Introduction 48
3.3 Materials and Methods 51
3.3.1 Genome-scale metabolic model building and Community simulation 51
3.3.2 Protein Identification and Quantification 51
3.3.3 Construction of the stoichiometric model 53
3.3.4 Statistical analysis 53
3.3.5 Data availability 53
3.4 Results 54
3.4.1 Overview of metabolic cooperation and competition in microbial communities 54
3.4.2 Enhanced cellulose degradation through multi-species metabolic interactions 57
3.4.3 Enhanced reliance and methanogenesis of *M. concilii* in complex communities 62
3.4.4 Reduced metabolic contribution of *M. hungatei* and enhanced methanogenesis 64
3.4.5 Decreased lactate and hydrogen metabolism in multiple-species interactions 66
3.4.6 Microbial interactions from modeling carbon and energy flow 69
3.5 Discussion 72
Chapter 4. Metaproteomics-informed stoichiometric modeling reveals the responses of wetland microbial communities to oxygen and sulfate exposure 76
4.1 Abstract 76
4.2 Introduction 78
4.3 Materials and Methods 82
4.3.1 Sampling and soil microcosm set up 82
4.3.2 Chemical analysis 83
4.3.3 DNA extraction and metagenomic sequencing 83

4.3.4 Metagenomic data processing 84
4.3.5 Metaproteomics measurement 84
4.3.6 Construction of the stoichiometric model 86
4.3.7 Statistical analysis 86
4.3.8 Data availability 87
4.4 Results 88
4.4.1 SO_4^{2-} and O_2 additions changed community structure and activities 88
4.4.2 SO_4^{2-} and O_2 additions altered depolymerization of plant polysaccharides 91
4.4.3 SO_4^{2-} and O_2 decreased methanogenesis and promoted methane oxidation 94
4.4.4 SO_4^{2-} and O_2 additions changed metabolic behaviors of sulfate-reducing bacteria 102
4.4.5 Modeling of Carbon and Energy Flow Through the Microbial Communities 106
4.5 Discussion 110
Chapter 5. Maternal Complex Carbohydrates Diet Enhances Taxonomic Diversity and Metabolic Activities of the Microbiome in Gestational Diabetes and in Their Infants 115
5.1 Abstract 115
5.2 Introduction 117
5.3 Materials and Methods 121
5.3.1 Assembly-Based Data Analysis 121
5.3.2 Core Protein Family Construction, Annotation, and Clustering 121
5.3.3 Metaproteomics Measurement 122
5.4 Results 125
5.4.1 Diet-Induced Differences in Microbial Species and Functional Diversity 125
5.4.2 Species Composition Changes in the Microbiomes of Mother and Infant 128
5.4.3 Functional Metabolic Pathway Shifts in the Microbiomes of Mother and Infant 130
5.4.4 Species-Specific Alterations in Metabolic Functions in the Mother's Microbiome 133
5.4.5 Species-Specific Metabolic Function Changes in the Infant's Microbiome 137
5.5 Discussion 140
Chapter 6 Summary and Outlook 145
6.1 Summary of Findings 145

6.1.1 Ecological and Biotechnological Implications of Microbial Metabolic Dependencies 145
6.1.2 Emergent Properties of Quad-Culture Microbial Communities 146
6.1.3 Higher-Order Interactions in Anaerobic Microbial Communities 147
6.1.4 Effects of Climate Change on Wetland Microbial Communities 148
6.1.5 Gut Microbiome and Gestational Diabetes Mellitus (GDM) 149
6.2 Outlook and Future Directions 149
6.2.1 Advances in Multi-Omics and Computational Modeling 150
6.2.2 Synthetic Microbial Communities for Biotechnological Innovation 150
6.2.3 Microbial Responses to Climate Change 151
6.2.4 Precision Medicine and the Human Microbiome 151
6.3 Conclusion 152
Appendix A: Supplementary Figures 153
Appendix B: Supplementary Tables 160
Reference 164

List of Tables

Table 2.1 Effects of SO_4^{2-} and O_2 exposures on plant polysaccharide degradation..... 28

Table 4.1 Accumulation of metabolic products in the microcosms under the four incubation conditions. 94

Table 4.2 Proteins in methane metabolism and sulfate reduction pathway. 101

List of Figures

Figure1.1 Microbial communities play critical roles in geochemical cycling, health, and industrial productivity. 4
Figure 1.2 Carbon Cycling and Trophic Cascades in Microbial Communities[44]..... 6
Figure 1.3 Microbial Interactions and Community Dynamics in Microbiomes. 9
Figure 1.4 Proposed systems and methods that used for the study of microbial interactions. 12
Figure 2.1 Perturbation of the synthetic communities by sulfate addition. (A) Schematics of the synthetic community assembly. (B) Proteome composition of the quad-cultures in the control and sulfate addition conditions. (C) and (D) Distribution of the fermentation products in R. cellulolyticum mono-culture and the quad-culture by carbon molarity (C) and electron molarity (D). Rc: *Ruminiclostridium cellulolyticum*, Mh: *Methanospirillum hungatei*, Mc: *Methanosaeta concilii*, Dv: *Desulfovibrio vulgaris*. 25
Figure 2.2 Metabolism of *R. cellulolyticum*. (A) Cellulose consumption. (B) Accumulation of acetate and lactate in the liquid phase. (C) Accumulation of H_2 and CO_2 in the gas phase. Significant differences (* for *p*-value < 0.05, ** for *p*-value < 0.01 and *** for *p*-value < 0.001) indicate targeted biological hypotheses. (D) Protein expression profile of the major carbon metabolism pathways in *R. cellulolyticum*. Enzymes are color-coded based on their protein abundance changes induced by sulfate addition. Unidentified enzymes are not labeled. Sat: sugar related ABC transporter; Pfo: Pyruvate flavodoxin/ferredoxin oxidoreductase; Hyd: Hydrogenase, Fe-only; Nhd: flavin oxidoreductase/NADH oxidase; Ldh: L-lactate dehydrogenase; Aad: Acetaldehyde dehydrogenase; Alr: alcohol dehydrogenase; Ads: AMP-dependent synthetase; Ack: Acetate kinase; Pta: phosphate acetyltransferase. 29
Figure 2.3 Metabolism of *Methanospirillum hungatei* and *Methanosaeta concilii*. (A) H_2 accumulation. (B) acetate accumulation. (C) CH_4 accumulation. The table on the x-axis marks the species included in each culture and the presence or absence of sulfate addition. Significant differences (*** for *p*-value < 0.001) indicate targeted biological hypotheses. (D) Hydrogenotrophic methanogenesis in *M. hungatei*. (E) Acetoclastic methanogenesis in *M. concilii*. Enzymes are color-coded based on their protein abundance changes induced by sulfate addition. Unidentified enzymes are not labeled.

Fmd: formylmethanofuran dehydrogenase; Fdh: formate dehydrogenase; Acs: acetyl-coenzyme A synthetase; Cds: CO dehydrogenase/acetyl-CoA synthase; Cmd: carbon monoxide dehydrogenase CoM; Mtf: tetrahydromethanopterin S-methyltransferase; Mcr: methyl-coenzyme M reductase; Bmr: CoB-CoM reductase..... 32
Figure 2.4 Metabolism of *D. vulgaris.* (A) lactate accumulation. A column represents daily lactate accumulation in a culture over 7 days of cultivation. The cultures with sulfate additions were clustered together. (B) Acetate accumulation. (C) H_2 accumulation. (D) CH_4 accumulation. (E) CO_2 accumulation. Significant differences (* for *p*-value < 0.05 and ** for *p*-value < 0.01) indicate targeted biological hypotheses. (F) Hydrogenic lactate fermentation in D. vulgaris. (G) Sulfidogenic lactate oxidation and sulfidogenic hydrogenic oxidation in D. vulgaris. Cyt c3: cytochrome C3; Hmc: high-molecular cytochrome; Hdy: hydrogenase; Lpe: L-lactate permease; Coo: membrane-bound Coo hydrogenase; H_2ase: hydrogenase; Fca: FeS cluster assembly ATPase; Ldh: lactate dehydrogenase; Srd: sulfite reductase. The table on the x axis marks the species included in each culture and the presence or absence of sulfate addition. 36
Figure 2.5 Community stoichiometric modeling. (A) Model fitting in the control condition. (B) Model fitting in sulfate addition condition. (C) Cross-feeding fluxes among the four species under the control condition and sulfate addition conditions..... 39
Figure 3.1 Synthetic community assembly. (A) Schematics of the combinatorial experimental setup. (B) Metabolic Interaction Potential (MIP) and Metabolic Resource Overlap (MRO) across seven synthetic microbial communities. (C) Cumulative production of fermentation products quantified by carbon molarity and electron molarity in different co-cultures, with correlations to MIP and MRO scores. (D) Fluxes of key metabolic reactions contributing to methane (CH_4) and carbon dioxide (CO_2) production. The cycles represent seven days of reaction fluxes, and error bars indicate the range of fluxes observed in CH_4 and CO_2 production across eight microbial assemblies. Rc: *Ruminiclostridium cellulolyticum,* the cycle represents the seven days' fluxes though reactions, and the error bar represent the range of fluxes producing CH_4 and CO_2 from each reaction across eight microbial assemblies. Mh: *Methanospirillum hungatei,* Mc: *Methanosaeta concilii*, Dv: *Desulfovibrio vulgaris.* 57

Figure 3.2 Metabolic activities of *R. cellulolyticum* in synthetic communities. (A)Comparison of cellulose consumption by *R. cellulolyticum* among different cultures. Significant differences with *p*-values determined using Student's t-test, and adjusted for the false discovery rate, are marked by * for *p*-value < 0.05, ** for *p*-value < 0.01 and *** for *p*-value < 0.001. The error bars are defined as standard deviation. (B) Cross-feeding interactions between *R. cellulolyticum* and other species in all the synthetic communities. (C) Protein expression profile of the major carbon metabolism pathways in *R. cellulolyticum*. (D) Fluxes of the key reactions in *R. Cellulolyticum* modeled in all cultures. Rc: *Ruminiclostridium cellulolyticum,* Mh: *Methanospirillum hungatei,* Mc: *Methanosaeta concilii*, Dv: *Desulfovibrio vulgaris.* 61
Figure 3.3 Metabolic activities of *M. concilii* in synthetic communities. (A) Cross-feeding interactions between *M. concilii* and other species in all synthetic communities. (B) Functional proteins profiling of acetoclastic methanogenesis. (C) Flux of acetoclastic methanogenesis modeled in *M. concilii*. Rc: *Ruminiclostridium cellulolyticum,* Mh: *Methanospirillum hungatei,* Mc: *Methanosaeta concilii*, Dv: *Desulfovibrio vulgaris.* 63
Figure 3.4 Metabolic activities of *M. hungatei* in synthetic communities. (A) Cross-feeding interactions between *M. hungatei* and other species in all synthetic communities. (B) Functional proteins profiling of hydrogenotrophic methanogenesis. (C) Flux of hydrogenotrophic methanogenesis modeled in *M. hungatei*. Rc: *Ruminiclostridium cellulolyticum,* Mh: *Methanospirillum hungatei,* Mc: *Methanosaeta concilii*, Dv: *Desulfovibrio vulgaris*..... 65
Figure 3.5 Metabolic activities of *D. vulgaris* in synthetic communities. (A) Comparison of H_2 accumulation in the co-cultures with *D. vulgaris*. (B) Cross-feeding interactions between *M. hungatei* and other species in all synthetic communities. (C) Functional proteins profiling of hydrogenic lactate oxidation. (D) Flux of hydrogenic lactate oxidation modeled in *D. vulgaris*. Rc: *Ruminiclostridium cellulolyticum,* Mh: *Methanospirillum hungatei,* Mc: *Methanosaeta concilii*, Dv: *Desulfovibrio vulgaris.* 68
Figure 3.6 Stoichiometric modeling of synthetic communities. (A) Conceptual metabolic network among four microbial species in the synthetic community. (B) Exchanging fluxes estimating the metabolic interactions between species. The edges represent the exchange flux, and the circles represent the biomass. Rc: *Ruminiclostridium*

cellulolyticum, Mh: *Methanospirillum hungatei,* Mc: *Methanosaeta concilii*, Dv: *Desulfovibrio vulgaris.* 71
Figure 4.1 Schematic diagram of study design. Emissions of methane and carbon dioxide from wetland ecosystems can be severely perturbed by climate-change-induced stressors, such as seawater intrusions and droughts. To investigate this, we constructed laboratory microcosms using freshwater wetland soils under four incubation conditions, including anoxic non-sulfate addition (S-O-), anoxic sulfate-addition (S+O-), oxic non-sulfate addition (S-O+) and oxic sulfate-addition conditions. The soil communities were characterized by integrating geochemical analysis, metagenomics, metaproteomics and stoichiometric modeling. The results uncovered the molecular mechanism on how wetland microbial communities modulate greenhouse gas fluxes under future climate scenarios..... 81
Figure 4.2 Effects of SO_4^{2-} and O_2 exposures on microbial community composition and activities. (A) Relative proteomic abundance of microbial phyla under four treatment scenarios. The relative proteomic abundance is expressed as the proportion of total proteins attributable to each microbial species. (B-C) Community species diversity indices, with (B) showing the richness and (C) the evenness across the four experimental conditions. Significant differences with p-values determined using Student's t-test and adjusted for the false discovery rate, are marked by * for *p*-value < 0.05, ** for *p*-value < 0.01 and *** for *p*-value < 0.001. (D) Correlation between microbial species diversity and the accumulations of CH_4 and CO_2, where each dot represents an experimental measurement (X-axis for geochemical measurements, Y-axis for metaproteomic measurements) from the four conditions with three replicates, and the red line displays best linear fit. r is the Pearson correlation coefficient, and p values were determined by t-statistic. (E-F) Cumulative amounts of fermentation products are measured by carbon molarity (E) and electron molarity (F) within the microcosms. The error bars are defined as standard deviation..... 90
Figure 4.3 Effects of SO_4^{2-} and O_2 exposures on plant polysaccharide degradation. (A) Correlation analysis between the relative abundances of plant polymer degradation species and CAZymes with the accumulation of CH_4 and CO_2, where each dot represents experimental measurements (X-axis for geochemical measurements, Y-axis

for metaproteomic measurements) from four conditions with three replicates, and the red line is the result of linear fitting. r is the Pearson correlation coefficient, and *p*-values were determined by t-test. (B) Protein abundances of CAZyme under the four conditions. The error bars are defined as standard deviation. 93
Figure 4.4 Modulation of methane metabolism by SO42- and O2 exposures. (A-B) Changes in molar mass of CH4 (A) and CO2 (B) under the four conditions, over a 30-day incubation. (C-E) Comparison of methanogens and methanotrophs in terms of relative abundance (C), richness (D) and evenness (E) under the four conditions. Relative abundance is quantified as the aggregate of protein abundances attributable to a specific species. (F) Schematic representation of methane metabolic pathways. The boxes in the pathway map, arranged from left to right, correspond to the S-O-, S+O-, S-O+ and S+O+ conditions. The color gradient from red to blue represents the relative abundance ranking of proteins among the four conditions, with red indicating the highest ranked relative abundance and blue the lowest. The grey color indicates proteins not detected by LC-MS/MS. Significant differences with *p*-values determined using Student's t-test, and adjusted for the false discovery rate, are marked by * for *p*-value < 0.05, ** for *p*-value < 0.01 and *** for *p*-value < 0.001. The error bars are defined as standard deviation. 99
Figure 4.5 Effects of SO42- and O2 exposures on sulfate reduction and sulfite/sulfide oxidation processes. (A-B) Changes in molar mass of lactate (A) and H2S (B) over the 30 days of incubation. (C-E) Relative abundances (C), richness (D) and evenness (E) of sulfate-reducing bacteria (SRB) and sulfide/sulfur-oxidizing bacteria (SOB). Significant differences with p-values determined using Student's t-test, and adjusted for the false discovery rate, are marked by * for *p*-value < 0.05, ** for *p*-value < 0.01 and *** for *p*-value < 0.001. (F) Sulfur metabolism pathways. The boxes in the pathway map, arranged from left to right, correspond to the S-O-, S+O-, S-O+ and S+O+ conditions. The color gradient from red to blue represents the relative abundance ranking of proteins among the four conditions, with red indicating the highest ranked relative abundance and blue the lowest. The grey color indicates proteins not detected by LC-MS/MS. The error bars are defined as standard deviation. 105

Figure 4.6 Stoichiometric modeling of the wetland microbial community. (A-D) fluxes of the key reactions under four experimental conditions. (E-F) Production (+) and consumption (-) of CO2 and CH4 by these reactions. The error bars are defined as standar. 109
Figure 4.7 Conceptual food web responding to SO42- and O2 perturbations. The S-O- condition serves as the baseline. Circle size corresponds to the relative abundance of marker proteins within the reaction, with larger circles indicating higher abundance, and smaller circles denoting lower abundance. Numbers alongside circles indicate the fold change in metabolic fluxes as inferred from stoichiometric models relative to the control. Edge thickness represents the magnitude of fluxes that consume or produce metabolites. Dashed lines indicate fluxes for nearly eliminated hydrogenotrophic methanogenesis post-treatment. Statistical significance was assessed by Wald type II χ^2 tests, with *p*-values adjusted for the false discovery rate indicated by: *** $p < 0.001$, ** $p < 0.01$, * $p < 0.05$. 112
Figure 5.1 Comparison of species composition and functional diversity between CONV and CHOICE samples. (A) Comparing species diversity between conventional (CONV) and CHOICE treatments based on metagenome and metaproteome data. (B) Comparing functional diversity between CONV and CHOICE samples based on metagenome and metaproteome data. *P*-values indicate the statistical significance of the differences in function between the two treatments, as evaluated by PERMANOVA. (C) Shannon Index comparing the alpha diversity of species in the metagenome and metaproteome datasets between CONV and CHOICE groups. (D) Rao's Quadratic Entropy, a measure of functional diversity, showing differences between CONV and CHOICE treatments in both the metagenome and metaproteome datasets..... 127
Figure 5.2 Species composition changes in the microbiomes of mother and infant. (A) the species composition changes in the mother’s microbiome at the metagenomic and metaproteomic levels. (B) Species composition changes in the infant’s microbiome at the metagenomic and metaproteomic levels. Each point represents a bacterial species, the size of the points indicating fold change. Positive effect sizes represent species that increased in abundance, while negative effect sizes represent species that decreased. 130

Figure 5.3 Changes in functional metabolic pathways in the microbiomes of mother and infant. (A) Metagenomic and metaproteomic analyses of the mother's microbiome. (B) Metagenomic analysis of the infant's microbiome. Pathways are categorized into functional groups: energy metabolism, carbohydrate metabolism, nucleotide metabolism, amino acid metabolism, and lipid metabolism. Circle size corresponds to fold change, with larger circles indicating greater fold changes. Positive effect sizes indicate an increase in the relative abundance of the pathway, while negative effect sizes represent a decrease. 133
Figure 5.4 Species-specific changes in key metabolic pathways in the mother's microbiome. (A) Energy metabolism. (B) Carbohydrate metabolism. (C) Amino acid metabolism. Circle colors correspond to effect sizes (as shown in the color bar), and circle size indicate the magnitude of the fold change in pathway enrichment for each species. Metagenomic data reflect the genomic potential for functional activity, while metaproteomic data indicate active protein expression in these pathways. 137
Figure 5.5 Species-specific changes in metabolic pathways in the infant's microbiome. (A) Energy Metabolism. (B) Carbohydrate Metabolism. (C) Amino Acid Metabolism. Circle size represents the fold change, and color indicates the effect size for each species across the different metabolic pathways. Positive effect sizes reflect increased species contributions to specific metabolic functions, while negative values indicate decreased contributions. 139

Abstract

Microbial interactions are fundamental to ecosystem dynamics, influencing processes such as nutrient cycling, energy flow, and ecosystem stability. This dissertation explores the complexity of microbial communities across diverse contexts, from environmental ecosystems to human health, using advanced multi-omics technologies and computational modeling. By examining both natural and synthetic microbial consortia, the research presented here highlights how metabolic dependencies, such as cross-feeding and syntrophy, shape community structure, stability, and functionality.

A key focus of the research is on microbial metabolic dependencies and their role in ecological processes such as nutrient cycling and organic matter decomposition. Recent advances in multi-omics approaches have revealed how these dependencies influence the assembly, stability, and adaptation of microbial communities, with implications for agriculture, environmental management, and biotechnology.

Further investigations into synthetic microbial consortia reveal how higher-order interactions lead to emergent properties that are not present in simpler systems. A synthetic quad-culture, composed of microorganisms responsible for cellulose degradation and methane production, exhibited both positive and negative synergies, demonstrating enhanced methane production and reduced cellulose degradation compared to simpler consortia. These findings highlight the potential for engineering microbial communities for industrial applications such as bioenergy production and waste management.

The dissertation also examines the effects of environmental stressors, such as oxygen and sulfate exposure, on microbial communities in wetland soils, key players in global carbon cycling. The research reveals that elevated sulfate and oxygen levels suppress methane emissions while increasing carbon dioxide production, providing insights into how microbial communities respond to climate change and influence greenhouse gas dynamics.

In the clinical context, this work explores the effects of dietary interventions on the gut microbiomes of women with gestational diabetes mellitus (GDM) and their infants. The results demonstrate that targeted dietary modifications can significantly alter microbial diversity and function, with potential implications for managing metabolic disorders through personalized nutrition and microbiome-based therapies.

Overall, this dissertation contributes to a deeper understanding of microbial interactions, emphasizing their role in ecosystem stability, industrial processes, and human health. By leveraging the power of multi-omics technologies and computational models, this work provides a framework for predicting microbial community behavior and designing targeted interventions for both environmental and clinical applications.

Chapter 1: Introduction

1.1 Abstract

Microbial interactions are critical drivers of ecosystem dynamics, influencing essential processes such as nutrient cycling, plant growth, and human health. These communities are organized through complex metabolic dependencies, including cross-feeding, syntrophy, and resource partitioning, which regulate their stability and functionality. By exchanging metabolites and energy, these interactions underpin key ecological functions such as nutrient cycling, organic matter decomposition, and energy flow. Recent advancements in multi-omics technologies—such as metagenomics, metaproteomics, and metabolomics—paired with computational modeling, have greatly enhanced our understanding of these metabolic dependencies. This chapter synthesizes current research on the ecological and biotechnological implications of microbial metabolic dependencies, emphasizing their roles in community assembly, stability, and resilience under environmental changes. Additionally, recent findings on trophic networks—where the metabolic byproducts of one species serve as resources for another—are discussed, revealing complex interaction networks that shape community dynamics. By integrating these insights, this chapter presents a comprehensive framework for understanding microbial community dynamics, with applications in health, agriculture, and environmental management.

Keywords: Microbial communities, Multi-omics, Metabolic modeling, Biogeochemical cycling, Trophic network, Species interactions

1.2 Microbial Communities: Foundations of Ecosystem Function and Stability

Microbial communities are vital components of nearly every environment on Earth, from soils, freshwater bodies, and marine environments to extreme habitats such as deep-sea hydrothermal vents and the human gut (Figure 1.1). These communities play crucial roles in key ecological processes, including the decomposition of organic matter, biogeochemical cycling, and primary production [1-3]. The interactions within microbial communities are driven by complex metabolic dependencies—such as cross-feeding, syntrophy, and resource partitioning—that are fundamental to maintaining community stability and functionality [4-6].

Microbial communities form the cornerstone of ecosystem stability and functioning by regulating essential processes like geochemical cycling, health maintenance, and industrial productivity [7-9]. These microorganisms are integral to the cycling of critical elements, including carbon, nitrogen, sulfur, and phosphorus, all of which are vital to sustaining life on Earth [10-13]. In marine ecosystems, for example, microbes drive the global carbon cycle by transforming dissolved organic carbon into biomass, which is eventually recycled back into carbon dioxide [14]. In soils, nitrogen-fixing bacteria and other microbes decompose organic matter, releasing essential nutrients such as nitrogen and phosphorus, which support plant growth and maintain soil fertility [15]. Without these microbial processes, ecosystems would lose their ability to recycle nutrients, which would ultimately jeopardize global ecosystem productivity [16, 17].

In human and animal health, microbial communities—especially the gut microbiota—are essential for regulating digestion, immune responses, and disease

prevention [18-21]. Microbes in the gut engage in intricate metabolic interactions, breaking down dietary fibers and producing short-chain fatty acids that promote gut health and protect against inflammation [22, 23]. Additionally, the microbiome plays a pivotal role in immune modulation, helping the body defend against pathogens and fostering immune tolerance [24, 25]. Disruptions in these microbial communities can lead to dysbiosis, contributing to various conditions such as inflammatory bowel disease, obesity, and metabolic disorders [26-28]. This highlights the critical importance of maintaining a balanced microbial ecosystem for overall health.

Beyond their ecological and health roles, microbial communities have significant industrial applications. In biotechnology, microbes are utilized in processes like biofuel production, wastewater treatment, and agricultural enhancement [29-31]. Microbial consortia are engineered to convert plant biomass into bioethanol, degrade pollutants in wastewater, and improve soil fertility by enhancing nutrient availability for crops. These applications highlight the immense potential of microbial communities in promoting sustainable industrial practices, helping to address global challenges such as energy security, environmental pollution, and food production. By deepening our understanding of microbial interactions, we can develop innovations that enhance ecosystem resilience, improve human health, and boost industrial efficiency.

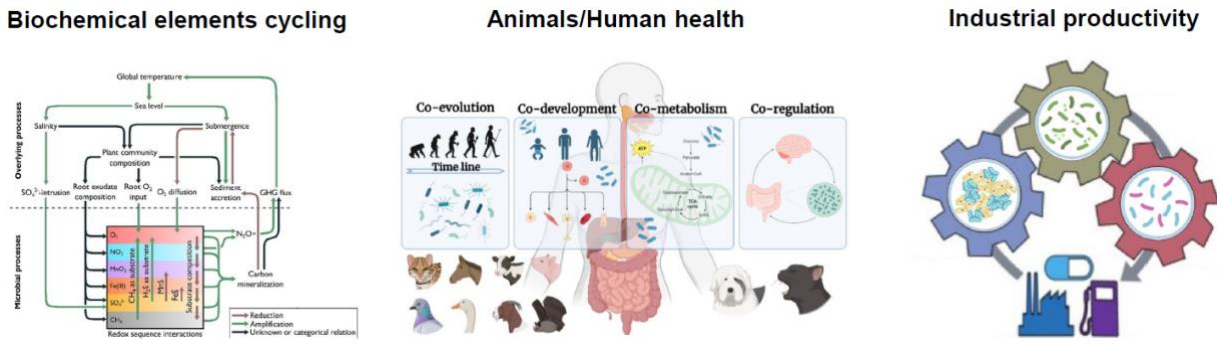

Figure1.1 Microbial communities play critical roles in geochemical cycling, health, and industrial productivity.

1.3 Types of Microbial Interactions

Microbial interactions manifest in various forms, ranging from mutualism and commensalism to competition and parasitism [32]. These interactions often form complex networks, influenced by the presence of other species, which makes them difficult to predict. Within these networks, the metabolic activities of one species can directly impact the growth, survival, or activity of others, creating a dynamic system of cooperation, competition, and resource-sharing [33-36].

Mutualistic interactions involve reciprocal benefits for both partners. For example, nitrogen-fixing bacteria (*Rhizobium spp*.) form symbiotic relationships with leguminous plants, providing ammonia in exchange for carbohydrates. These interactions enhance nutrient availability, significantly contributing to the productivity of both natural and agricultural ecosystems. In contrast, commensal interactions, such as the relationship between *Staphylococcus epidermidis* and its human host, benefit one partner without affecting the other [37, 38]. On the other hand, parasitism involves one organism benefiting at the expense of another, often causing harm or disease. These interactions

are common in microbial communities and are pivotal in shaping ecosystem structure and function [32, 39].

Competition and amensalism occur when species vie for the same resources or when one species inhibits another without deriving any direct benefit, respectively. These interactions play a critical role in community composition and resource allocation, influencing the dominance or exclusion of certain species within a community [40, 41].

Within microbial communities, trophic interactions form a cascade of cross-feeding processes (Figure 1.2). Complex organic matter, such as polysaccharides, is hydrolyzed by primary degraders into simpler compounds. Secondary consumers then process these byproducts of hydrolysis or the metabolic products of the primary degraders. For instance, in anaerobic environments, fermentative bacteria break down organic compounds into hydrogen and acetate, which are then utilized by methanogenic archaea to produce methane [42, 43]. This syntrophic interaction enables the complete degradation of organic matter, demonstrating how metabolic dependencies within trophic networks drive community assembly, stability, and productivity.

Cooperative and competitive interactions within these processes profoundly shape the structure, stability, and functionality of microbial communities, influencing their capacity to perform essential functions for both the environment and host organisms.

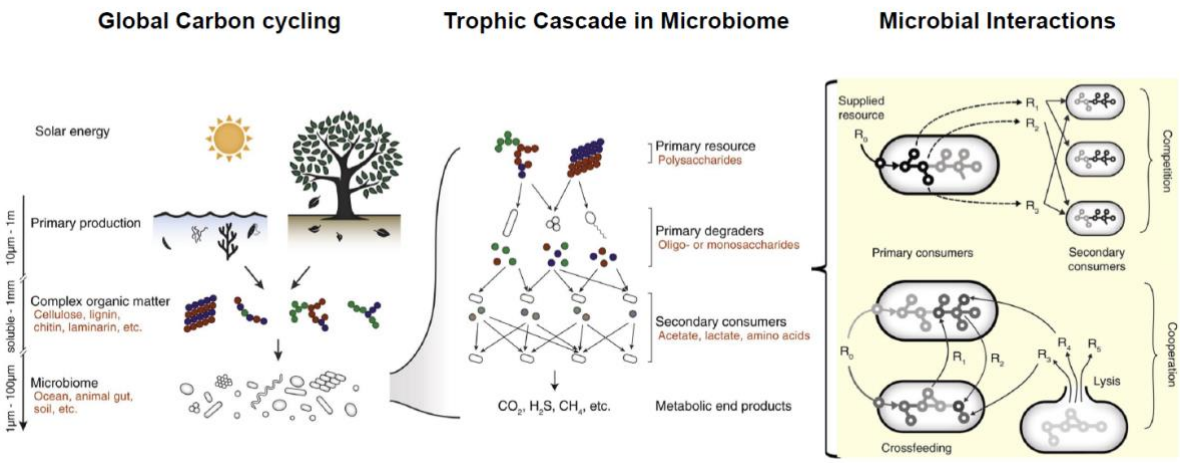

Figure 1.2 Carbon Cycling and Trophic Cascades in Microbial Communities[44]

1.4 Modeling Microbial Interactions

Modeling microbial interactions is essential for understanding the intricate dynamics that govern microbial community structure and function [45-48]. Traditional modeling approaches, such as pairwise interaction models, often assume that species interactions are linear, independent, and context-invariant. These models typically use frameworks like the generalized Lotka-Volterra (gLV) equations to describe competitive or cooperative relationships between species [49-51]. While these models provide useful insights into community dynamics, they have significant limitations when applied to multispecies communities. One major limitation is their inability to account for the influence of additional species and higher-order interactions, which are critical for accurately predicting community behavior [52, 53].

In recent years, numerous omics studies have cataloged gene and species content in various microbial communities, giving us a broad understanding of microbial diversity [54-57]. However, the challenge remains in translating these catalogs into

functionally meaningful units that represent key metabolic or ecological roles within ecosystems [44, 58]. Microbiologists often rely on bottom-up approaches that assume species interact in a pairwise manner. Yet, these pairwise interactions can be modulated by the presence of additional species, fundamentally altering the structure and functionality of the community [45, 59, 60]. This realization has driven the need for more comprehensive models that incorporate higher-order interactions and better capture the complexity of microbial ecosystems (Figure 1.3).

Furthermore, one key limitation of pairwise interaction models is that they assume interactions between two species are sufficient to explain their effects on one another, ignoring the potential for emergent behaviors that arise when multiple species interact simultaneously. In reality, microbial communities are shaped by complex, non-linear interactions [61, 62]. For instance, a bacterium that competes with another species in isolation may switch to a mutualistic or commensal role when a third species is introduced. This complexity underscores the insufficiency of pairwise models in predicting community dynamics, calling for more sophisticated models that can incorporate context-dependent and multi-species interactions [63, 64].

Recent advances in modeling have focused on incorporating higher-order interactions and trophic dependencies into community models. Higher-order interactions occur when the presence of additional species alters the nature or strength of pairwise interactions, leading to emergent properties that cannot be inferred from simpler models [45, 65-67]. Additionally, trophic dependencies, such as cross-feeding and syntrophy, play a crucial role in shaping community structure. These interactions occur when the metabolic byproducts of one species serve as essential resources for another, creating

cascading dependencies that contribute to the overall stability and functionality of the community [44].

To account for these complex interactions, models are evolving from species-centric frameworks to community-wide perspectives that capture the flow of metabolites and energy within microbial ecosystems [68, 69]. For instance, metabolic network models and flux balance analysis (FBA) have been employed to simulate metabolic exchanges between species, allowing researchers to predict how these exchanges influence community assembly and stability [70]. These models, by capturing the flow of resources and energy, offer more accurate predictions of microbial community behavior and provide insight into the emergent properties of microbial ecosystems.

Emerging approaches, such as network-based models and assembly-rule frameworks, represent promising alternatives to traditional pairwise models. Network-based models depict microbial communities as interconnected nodes (species) linked by edges (interactions), enabling a more comprehensive view of community structure [71]. These models allow for the inclusion of different types of interactions, such as competition, cooperation, and facilitation, offering a more holistic perspective on community dynamics. Meanwhile, assembly-rule-based models use qualitative data on species survival in smaller sets of species to predict survival and coexistence in more complex multispecies communities [72]. These models do not rely heavily on quantitative data, making them less prone to overfitting and more robust to various environmental conditions.

By integrating higher-order interactions, trophic dependencies, and network-based approaches, researchers are now developing more sophisticated models that

reflect the true complexity of microbial communities. These advanced modeling techniques hold great promise for predicting community behavior, understanding ecosystem stability, and designing synthetic microbial consortia for various biotechnological applications [73-76].

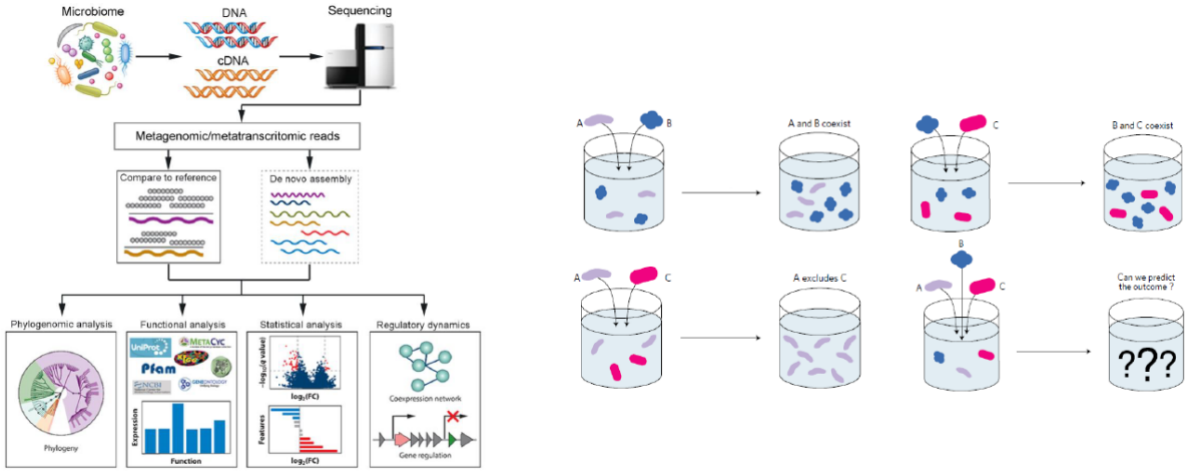

Figure 1.3 Microbial Interactions and Community Dynamics in Microbiomes.

1.5 Integrating Multi-Omics and Modeling Approaches for a Holistic Understanding of Microbial Communities

Recent advancements in multi-omics technologies—such as metagenomics, metatranscriptomics, and metabolomics—have significantly enhanced our understanding of microbial communities, offering deeper insights into their structure, function, and metabolic interactions. These tools have allowed researchers to investigate microbial communities in synthetic systems, lab-controlled environments, and real ecosystems, providing a more comprehensive view of how microbial interactions shape community dynamics across different contexts [77-80].

In synthetic microbial communities, which are simplified systems designed to model microbial interactions in controlled environments, multi-omics approaches enable detailed exploration of how genetic potential is linked to actual metabolic activity [81, 82]. For example, metagenomic data reveal the genetic composition of these communities, while metatranscriptomic data show how genes are expressed under specific conditions. This allows researchers to map out the metabolic dependencies within the community and to predict how different species interact through processes like cross-feeding and syntrophy [83]. Synthetic communities provide an ideal platform for testing hypotheses about microbial behavior and validating computational models before applying these findings to more complex natural environments [46].

Moving from synthetic systems to lab-controlled communities, where environmental factors such as temperature, pH, and nutrient availability can be tightly regulated, researchers can gain further insight into how microbial communities function under specific conditions [84, 85]. Multi-omics data from these environments help link the presence of genes with their active metabolic roles, showing how species interact, compete, or cooperate under controlled variables [86]. By integrating metagenomics and metabolomics, scientists can investigate how shifts in environmental conditions alter microbial interactions and metabolic pathways, offering insights into community stability and adaptation. These lab-based experiments provide essential data for refining models and testing their applicability in more complex, real-world ecosystems [87, 88].

When applied to natural ecosystems, multi-omics methods, combined with computational models, allow for the study of microbial communities in their full complexity [89]. Real-world environments, such as soils, oceans, and the human gut,

host diverse microbial ecosystems shaped by both biotic and abiotic factors. Multi-omics techniques enable researchers to capture the diversity and metabolic potential of these communities, linking genomic data to real-time metabolic activity [90, 91]. However, the challenge in these natural systems lies in translating the vast amounts of omics data into functionally meaningful units that represent key metabolic and ecological roles [77, 89, 92]. To bridge this gap, computational tools such as metabolic network models, flux balance analysis, and machine learning algorithms are employed to predict species interactions and their effects on community dynamics.

The integration of multi-omics data with advanced computational modeling provides a robust framework for understanding microbial communities [91]. By combining genetic, transcriptomic, proteomic, and metabolomic datasets, researchers can map out the complex metabolic networks that define microbial ecosystems [79]. This approach allows for the identification of key species, metabolic pathways, and interaction networks that are crucial for community function and stability. Moreover, by incorporating machine learning and other predictive modeling techniques, scientists can forecast how microbial communities will respond to environmental changes, such as shifts in nutrient availability or the introduction of new species.

In sum, the integration of multi-omics technologies and computational modeling offers a holistic approach to studying microbial communities. From synthetic and lab-controlled systems to natural ecosystems (Figure 1.4), this combined methodology allows for a deeper understanding of microbial interactions and offers the potential to predict how these communities will behave in response to changing environmental

conditions. These insights are critical for applications ranging from ecosystem management and agriculture to human health and industrial biotechnology.

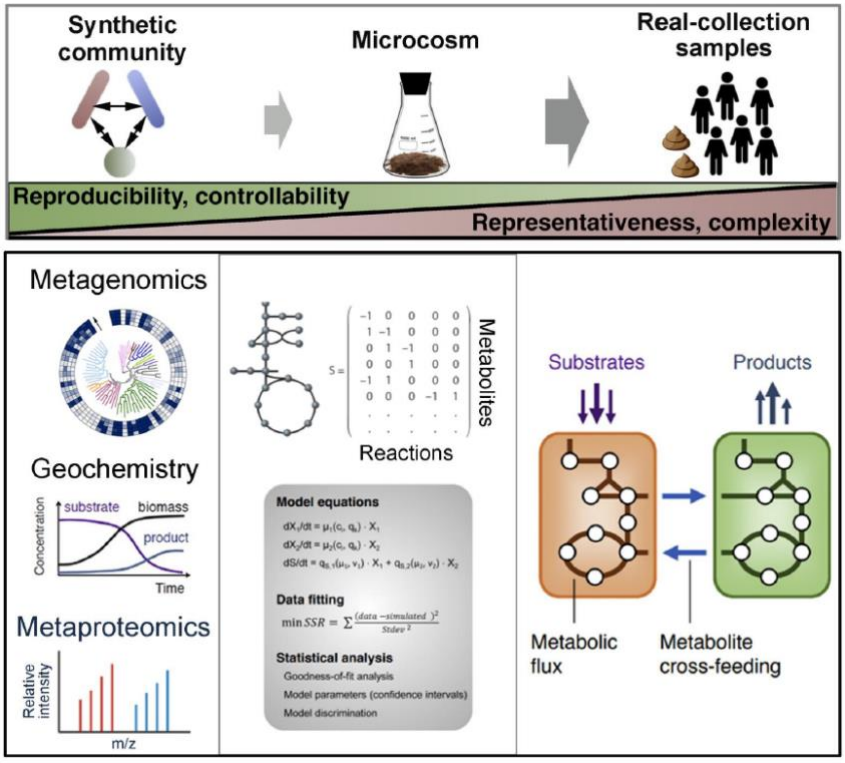

Figure 1.4 Proposed systems and methods that used for the study of microbial interactions.

1.6 Future perspectives and conclusion

Despite significant advances, understanding microbial interactions remains challenging due to their complexity and context-dependence. Future research should focus on integrating multi-omics data to build comprehensive models of microbial networks and explore community-wide trophic interactions.

Microbial interactions are foundational to ecosystem functioning and have broad implications for human health, agriculture, and environmental management. Although

traditional pairwise models have provided valuable insights, a community-wide approach that incorporates trophic interactions offers a more comprehensive framework for understanding microbial community assembly. By integrating qualitative survival data, multi-omics datasets, and computational models, researchers can better predict community structure and design functional microbial communities de novo.

Chapter 2. Cross-feedings, competitions, positive and negative synergies in a four-species synthetic community for anaerobic degradation of cellulose to methane

2.1 Abstract

Complex interactions exist among microorganisms in a community to carry out ecological processes and adapt to changing environments. Here, we constructed a quad-culture consisting of a cellulolytic bacterium (*Ruminiclostridium cellulolyticum*), a hydrogenotrophic methanogen (*Methanospirillum hungatei*), an acetoclastic methanogen (*Methanosaeta concilii*) and a sulfate-reducing bacterium (*Desulfovibrio vulgaris*). The four microorganisms in the quad-culture cooperated via cross-feeding to produce methane using cellulose as the only carbon source and electron donor. The community metabolism of the quad-culture was compared with those of the *R. cellulolyticum*-containing tri-cultures, bi-cultures and mono-culture. Methane production was higher in the quad-culture than the sum of the increases in the tri-cultures, which was attributed to a positive synergy of four species. In contrast, cellulose degradation by the quad-culture was lower than the additive effects of the tri-cultures, which represented a negative synergy. The community metabolism of the quad-culture was compared between a control condition and a treatment condition with sulfate addition using metaproteomics and metabolic profiling. Sulfate addition enhanced sulfate reduction and decreased methane and CO_2 productions. The cross-feeding fluxes in the quad-culture in the two conditions were modeled using a community stoichiometric model. Sulfate addition strengthened metabolic handoffs from *R. cellulolyticum* to *M. concilii* and *D. vulgaris* and intensified substrate competition between *M. hungatei* and *D. vulgaris*. Overall, this study uncovered emergent properties of higher-order microbial interactions using a four-species synthetic community.

A synthetic community was designed using four microbial species that together performed distinct key metabolic processes in the anaerobic degradation of cellulose to methane and CO_2. The microorganisms exhibited expected interactions, such as cross-feeding of acetate from a cellulolytic bacterium to an acetoclastic methanogen and competition of H_2 between a sulfate reduction bacterium and a hydrogenotrophic methanogen. This validated our rational design of the interactions between microorganisms based on their metabolic roles. More interestingly, we also found positive and negative synergies as emergent properties of high-order microbial interactions among three or more microorganisms in co-cultures. These microbial interactions can be quantitatively measured by adding and removing specific members. A community stoichiometric model was constructed to represent the fluxes in the community metabolic network. This study paved the way towards a more predictive understanding of the impact of environmental perturbations on microbial interactions sustaining geochemically significant processes in natural systems.

Key words: Cellulose, Methane, Carbon dioxide, Synthetic community, Geochemical analysis, Metaproteomics, Stoichiometric modeling.

2.2 Introduction

Complex anaerobic microbial communities can degrade cellulose to methane, CO_2 and other products in many anoxic ecosystems, including wetlands [93], rumen gut [94], waste treatment systems [95], and biogas digesters [96]. In these communities, cellulolytic bacteria metabolize cellulosic materials primarily to CO_2, hydrogen (H_2) and a variety of organic acids such as acetate, lactate, formate and succinate [30]. Then, H_2 and CO_2 are converted to CH_4 by hydrogenotrophic methanogens and acetate is metabolized to CH_4 by acetoclastic methanogens. When sulfate is available, sulfate-reducing bacteria (SRB) may oxidize acetate and lactate to CO_2 and reduce sulfate to H_2S. When sulfate is limited, some SRB grow as syntrophic oxidizers, fermenting lactate to acetate, H_2 and CO_2 [97]. The overall methane and CO_2 emissions are determined by the nutrient and redox potential of their local environments that eventually drive the interactions among these functional guilds [98-100]. Increased sulfate availability caused by, for example, intrusion of sulfate-laden seawater to estuarine wetlands [101], will likely enable SRB to produce more H_2S, utilizing H_2 and/or organic acids such as acetate and lactate as electron donors. The competition from SRB for H_2 and acetate may reduce methane production by hydrogenotrophic and acetoclastic methanogens [98, 102]. Characterization of these microbial interactions will provide insights into community metabolism under changing environmental conditions and allow modeling of metabolic fluxes rates among community members.

It is a challenge to mechanistically study complex microbial interactions in natural communities. Synthetic communities provide a complementary reductionist system to characterizing microbial interactions from microbiological, ecological and biochemical

perspectives. Synthetic communities can be directly manipulated and the response of individual community members can be identified [103, 104]. Previous synthetic community studies have investigated mutualistic interactions between *Methanococcus maripaludis* and *Desulfovibrio vulgaris* in bi-cultures [100], cooperative interaction between *Geobacter metallireducens* and *Geobacter sulfurreducens* [105], cross-feeding between *Escherichia coli* and *Rhodopseudomonas palustris* [106], and competitive interaction in a synthetic community of *Pseudomonas aeruginosa* and *Agrobacterium tumefaciens* [107]. Rationally designed synthetic communities are experimentally more tractable and enable identifying interactions between key functional guilds that are challenging to assess in environmental communities.

In this study, we developed a simplified, yet functionally complete, synthetic community to study the microbial interactions and carbon exchanges during anaerobic carbon degradation. Our synthetic microbial community was composed of the major functional guilds (cellulolytic fermenter, sulfate reducer, hydrogenotrophic methanogen and acetoclastic methanogen) that mediate the anaerobic conversion of cellulosic biomass to CH_4 and CO_2. The choice of a sulfate-reducing bacterium (*Desulfovibrio vulgaris* Hildenborough) introduced metabolic versatility and enabled investigations into the community response to sulfate intrusion. We characterized the biochemical and physiological response of each microorganism in the synthetic community, investigated the ecological and metabolic functions, and modeled the inter-species interactions governing carbon exchange among these four organisms. This study provides a foundation for the development of mechanistic metabolic models of anaerobic degradation of cellulose to methane, CO_2, and H_2S.

2.3 Materials and Methods

2.3.1 Strains. The strains used in this study including, *Ruminiclostridium cellulolyticum* H10 (ATCC 35319), *Desulfovibrio vulgaris* Hildenborough (ATCC 29579), *Methanospirillum hungatei* JF1 (txid323259) and *Methanosaeta concilii* (txid990316). Cultures of *R. cellulolyticum* H10 and *D. vulgaris* Hildenborough were stored in 17%(v/v) glycerol at -80℃, while the methanogens were maintained in a defined medium, which is referred to as RST [108] here after, at room temperature.

2.3.2 Cultures, Growth Conditions and Experimental Design. Four strains were revived by respective media and conditions commonly published in previous studies. Briefly, modified VM medium supplemented with 2.0g/L yeast extract and LS4D medium were used for *R. cellulolyticum H10* and *Desulfovibrio vulgaris* Hildenborough respectively, both were cultured at 34 °C [109, 110]. *M. hungatei* JF1 and *M. concilii* were grown in RST medium with H_2 :CO_2 (80:20) in the head space and 50 mM acetate at 37 °C [111]. *M. concilii* required about 5 weeks before noticeable growth and acclimation of acetate occurred. Subsequently, active inocula (OD = 0.5 at the wavelength of 600nm) were transferred to the modified VM medium with 10 g/L cellulose as the sole carbon source for experiments [110].

All fermentation experiments were carried out in 160 mL serum bottles with 20 mL of modified VM medium containing 10 g/L cellulose; the chamber gas contained 3% H_2 and 97% N_2. The modified VM medium contained 1.25 mg/L of $FeSO_4 \cdot 6H_2O$, which introduced approximately 0.14 μmole sulfate to the control condition. Revived cells were counted by flow cytometry; the number of inoculated cells per species was about 5×10^7

for all mixed cultures. All cultures were incubated at 34 °C with shaking at 200 rpm for seven days and sampled each day.

During the sampling, two milliliter of well-shaken culture liquid was sampled, centrifuged at 14000 rpm for 15 min to separate the cells and cellulose from the supernatant, and stored at -80 °C for later analysis. Five milliliter of gas phase were collected in vacuumed Labco exetainer glass vials (cat. 837w) for later analysis of metabolic products.

After sampling, two milliliter fresh medium with 10 g/L cellulose was added to the cultures, pH was adjusted to 7.3 and produced gases vented to restore serum bottle headspace to atmospheric pressure. To mimic seawater intrusion, sulfate-treated experiments received two milliliters of 100mM K_2SO_4 solution every day from the first day of cultivation and the control group received the same volume of sterile water.

2.3.3 Chemical analysis. Cellulose in the medium was measured by phenol-sulfuric acid method as described previously [112]. Headspace pressure was measured daily with a pressure gauge (Cole Parmer SK-68900-24) before sampling liquid and gas phases. Gas composition (H_2, CO_2 and CH_4) was analyzed from the stored LabCo vacuum containers with a gas chromatograph (GC-8A, Shimadzu, Japan). Absolute gas composition in each bottle was calculated with the ideal gas law. The remaining sulfate in the medium was measured by ion chromatography (IC) and used to estimate H_2S production in the cultures. The fermentation products (lactate, acetate) in liquid phase and soluble sugars (cellobiose and glucose) were analyzed by high performance liquid chromatograph (HPLC) as reported previously [113].

2.3.4 Protein Identification and Quantification. Samples from quad-cultures were selected for full metaproteomic analysis. Protein extraction was carried out by a previously reported method [114, 115]. Briefly, harvested cell pellets were washed twice with nanopure water, cells were suspended in lysis buffer (containing 10 mM tris-HCl, 1% SDS, 0.1M DTT), and incubated at 60 °C for 1 h, and then the supernatant was collected after centrifugation. Proteins were then precipitated by trichloroacetic acid overnight at 4 °C and pelleted by centrifugation. Protein pellets were washed by ice-cold acetone three times and resuspended in guanidine buffer. Protein concentrations were quantified by Bicinchoninic Acid Assay [116]. 20 mg samples of proteins were processed using filter-aided sample preparation and digested using Trypsin/LysC mixture. Each sample was analyzed using two-dimensional liquid chromatography-tandem mass spectrometry (2D-LC-MS/MS) on an Orbitrap Fusion Tribrid mass spectrometer (Thermo Fisher Scientific, USA) at the IDeA National Resource for Quantitative Proteomics. Tryptic peptides were separated into 46 fractions on a 100 X 1.0 mm Acquity BEH C18 column (Water) with a 50 min gradient from 99:1 to 60:40 buffer ratio under basic pH conditions, then consolidated into 8 super-fractions. Each super-fraction was then separated by reverse phase XSelect CSH C18 2.5 mm resin (Waters) on an in-line 120 x 0.075 mm column using an UltiMate 3000 RSLCnano system (Thermo Fisher Scientific, USA). Peptides were eluted using a 60-min gradient from 98:2 to 65:35 buffer ratio. Eluted peptides were ionized by electrospray (2.4 kV) followed by mass spectrometric analysis on an Orbitrap Fusion Tribrid mass spectrometer (Thermo Fisher Scientific, USA). MS data were acquired using FTMS analyzer in profile mode at a resolution of 240,000 over a range of 375 to 1500 m/z. Following HCD activation,

MS/MS data were acquired using the ion trap analyzer in centroid mode and normal mass range with normalized collision energy of 28 – 31% depending on charge state and precursor selection range. Mass spectrometry spectra were searched using Sipros Ensemble against a matched protein database constructed from the genomes of the four microorganisms making up the synthetic community [117, 118]. Raw search results were filtered to achieve 1% FDR (false discovery rate) at the peptide level, estimated by the target-decoy approach. Peptide identifications are assigned to proteins or protein groups following the parsimonious rule [117]. A protein group included multiple proteins sharing a set of common peptides, at least one of which cannot be attributed to any other protein or protein group. A minimum of one unique peptide was required for each identified protein or protein group. To avoid ambiguity in data analysis, only proteins were used for biological analysis, while protein groups were not evaluated. Intensity-based label-free quantification for protein was performed using ProRata [119, 120]. The protein abundance was represented by the total peak height of all quantified unique peptides from a protein [121].

2.3.5 Construction of Stoichiometric Model. A set of overall reactions representing the documented metabolisms of the individual species were fit into the daily measured amounts of metabolites in the constructed synthetic communities (Table S 2.1, Table S 2.2). The metabolism of *R. cellulolyticum* was modeled to consume glucose to eliminate artifacts from cellulase production. The overall metabolism of *R. cellulolyticum* was modeled as lactate fermentation, hydrogenic acetogenesis. The low observed ethanol in ethanol/acetate fermentations, accounting for less than 0.36% of the carbon flux, led us to remove this pathway from analysis. *D. vulgaris* was modeled to oxidize lactate to

acetate, coupled to reduction of protons or sulfate, or oxidize H_2 coupled to sulfate reduction. The methanogens were represented by hydrogenotrophic methanogenesis and acetoclastic methanogenesis. Code used for the fitting can be found in the Github https://github.com/thepanlab/Community_stoichiometric_model. The resulting fits indicate the relative contribution of each microorganism to the overall observed transformations and provide a basis for quantifying metabolic contributions. Deviations between the inferred metabolic transformations and the measured transformations indicate uncertainty in our understanding of the metabolic transformations or limitations in analytical capacity.

2.3.6 Statistical analysis. Metabolic measurement data were compared between different conditions using Student's t-test. The differences of protein abundance in metaproteome were analyzed by the Deseq R package [122] and the *p*-values were adjusted to *q*-values using the Benjamini and Hochberg method for multiple comparison correction [123]. Proteins with *q*-values < 0.05 were regarded as statistically significant.

2.3.7 Data availability. Proteomic data are available at the ProteomeXchange Consortium via the PRIDE (Proteomics Identification Database) partner repository with the dataset identifier PXD035759

2.4 Results

2.4.1 Overview of the experimental design

A four-species synthetic community consisting of a cellulolytic bacterium (*Ruminiclostridium cellulolyticum*), a hydrogenotrophic methanogen (*Methanospirilum hungatei*), an acetoclastic methanogen (*Methanosaeta concilii*) and a sulfate-reducing bacterium (*Desulfovibrio vulgaris*) was constructed. To unravel how each species and their interactions contribute to the community metabolism, the growth of this quad-culture was compared with those of a mono-culture, three bi-cultures and three tri-cultures (Figure 2.1A, Table 2.1). All cultures were grown anaerobically in triplicate using the same medium with cellulose as sole carbon source. To simulate the increased sulfate availability from seawater intrusion into a wetland soil community, the *D. vulgaris*-containing cultures received a daily sulfate addition after the first day of cultivation. The growth status of these multi-species cultures was measured over a week by daily analysis of substrate consumption and product accumulation. The quad-cultures were analyzed with metaproteomics at the end of experiment to characterize the community structure and metabolic activities. A stoichiometric model was built to analyze the cross-feeding fluxes through the four species (Figure 2.1A, Table S2.1 and Table S2.2).

Metaproteomics analyses measured the relative proteome abundances of the organisms in the quad-cultures (Figure 2.1B) [121, 124]. A total of 3736 proteins were identified from the four microbial species (Table S2.4). *R. cellulolyticum* was dominant in the quad-cultures as the producer of the growth substrates for the other three microorganisms. Sulfate addition reduced the relative proteome abundance of *R. cellulolyticum* on average from 68% to 59% (p-value = 0.047), while it increased that of

D. vulgaris on average from 19% to 28% (*p*-value = 0.0004). The relative proteome abundances of *M. concilii* and *M. hungatei* remained at 10% and 3%, respectively, in both the control condition and the sulfate addition condition. The fermentation products of the synthetic communities were tracked by carbon molarity (Figure 2.1C) and electron molarity (Figure 2.1D). The mono-culture of *R. cellulolyticum* hydrolyzed cellulose to reducing sugars and fermented these sugars to acetate, lactate, ethanol, H_2 and CO_2. The quad-cultures transferred 1.37 ± 0.03 (29%) mmole of carbon (Figure 2.1C) and 10.99 ± 0.21 (51%) mmole of electrons (Figure 2.1D) to methane in the control condition. The quad-cultures transferred 9.36 ± 0.04 (43%) mmole of electrons (Figure 2.1C) to H_2S in the sulfate addition condition. Sulfate addition reduced the electrons and carbon transferred to methane by 1.28 $\pm$ 0.02 mmole and 0.16 $\pm$ 0.02 mmole, respectively, when compared to the control condition.

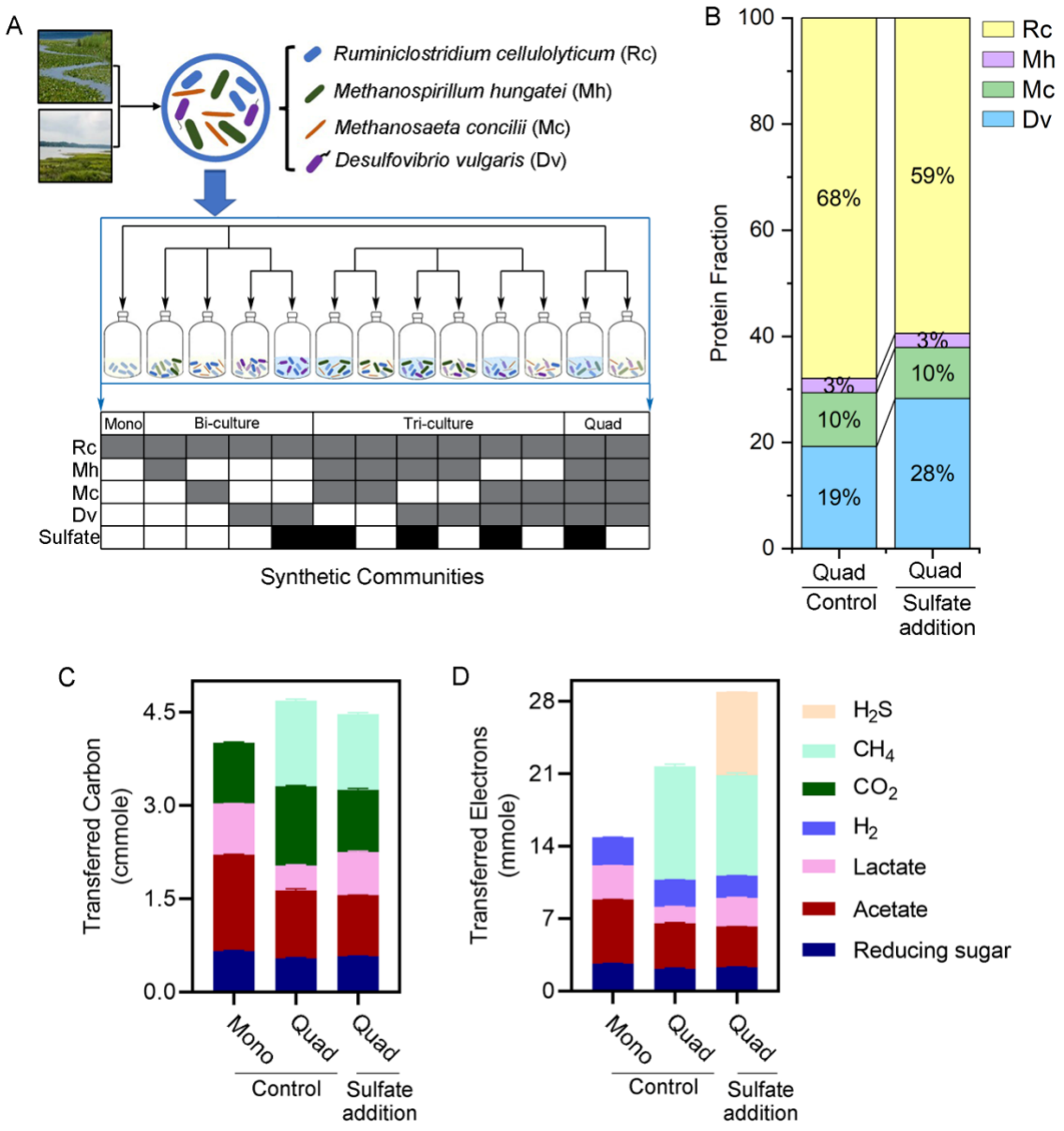

Figure 2.1 Perturbation of the synthetic communities by sulfate addition. (A) Schematics of the synthetic community assembly. (B) Proteome composition of the quad-cultures in the control and sulfate addition conditions. (C) and (D) Distribution of the fermentation products in R. cellulolyticum mono-culture and the quad-culture by carbon molarity (C) and electron molarity (D). Rc: *Ruminiclostridium cellulolyticum*, Mh: *Methanospirillum hungatei*, Mc: *Methanosaeta concilii*, Dv: *Desulfovibrio vulgaris*.

2.4.2 Metabolism of cellulolytic bacterium *Ruminiclostridium cellulolyticum*

Cellulose was the only carbon source provided to all the synthetic communities. After two days of incubation, all cultures began to rapidly consume cellulose (Figure S2.1). Over 7 days of incubation, the *R. cellulolyticum* mono-culture degraded 184.39 ± 0.54 mg of cellulose. Cellulose degradation increased significantly when *R. cellulolyticum* was cultivated with the other three species (*p*-value = 0.0028) (Table 2.1). The highest cellulose degradation was achieved by the quad-culture (210.02 ± 2.10 mg) (Figure 2.2A).

Metaproteomic analysis of the quad-culture identified 64 *R. cellulolyticum* cellulase and 50 *R. cellulolyticum* ABC transporters related to uptake of monosaccharides, disaccharides and oligosaccharides. Glucose and cellobiose produced by cellulose hydrolysis were detected at micromolar concentrations in the medium (Table 2.1). In the *R. cellulolyticum* mono-culture, acetate and lactate accumulated in the medium (Figure 2.2B), and H_2 and CO_2 accumulated in the headspace (Figure 2.2C). These fermentation products from *R. cellulolyticum* can be used by other microorganisms as carbon and/or energy sources in multi-species cultures. Compared with the *R. cellulolyticum* mono-culture, 29.5% less acetate (*p*-value = 0.0006), 51.9% less lactate (*p*-value = 0.0002), 4.4% less H_2 (*p*-value = 0.027) and 30.6% more CO_2 (*p*-value < 0.0001) accumulated in the quad-culture control condition without sulfate addition (Figure 2.2C).

Metaproteomics identified key enzymes in the fermentative pathways in *R. cellulolyticum*, including hydrogenase (Hyd) for H_2 generation, pyruvate flavodoxin/ferredoxin oxidoreductase (Pfo) for CO_2 production, L-lactate dehydrogenase (Ldh) for lactate generation, and phosphotransacetylase (Pta), AMP-forming acetyl-CoA

synthetase (Ads) and acetate kinase (Ack) for acetate generation (Figure 2.2D). The protein abundance of L-lactate dehydrogenase from *R. cellulolyticum* in the quad-culture increased by 3.7-fold in the sulfate addition condition compared to the control condition (*q*-value = 0.04). This may have contributed to the 1.8-fold higher lactate accumulation in the quad-cultures in the sulfate addition condition than the control condition (*p*-value = 0.003) (Figure 2.2B).

Table 2.1 Effects of SO_4^{2-} and O_2 exposures on plant polysaccharide degradation.

Species and metabolites	Mono-culture	Bi-cultures				Tri-cultures						Quad-cultures	
Community assembly													
R. cellulolyticum	Yes	Yes	Yes	Yes	Yes	Yes	Yes	Yes	Yes	Yes	Yes	Yes	Yes
M. hungatei	No	No	Yes	No	No	Yes	No	Yes	Yes	No	Yes	Yes	Yes
M. concilii	No	Yes	No	No	No	Yes	Yes	No	Yes	Yes	No	Yes	Yes
D. vulgaris	No	No	No	Yes	Yes	No	Yes	Yes	No	Yes	Yes	Yes	Yes
Growth condition													
Sulfate addition	No	No	No	No	Yes	No	No	No	Yes	Yes	Yes	No	Yes
Substrate													
Cellulose (mg)	184.39 ± 0.54	197.77 ± 2.23	198.17 ± 2.60	203.73 ± 0.77	205.43 ± 0.31	207.11 ± 1.00	200.98 ± 1.27	200.67 ± 4.09	201.46 ± 0.97	200.49 ± 1.26	197.87 ± 0.47	210.02 ± 2.10	205.44 ± 1.63
Products in gas-phase													
CH_4 (mmole)	0	0.18 ± 0.003	0.42 ± 0.007	0	0	0.62 ± 0.02	0.16 ± 0.01	0.89 ± 0.02	0.53 ± 0.003	0.14 ± 0.001	0.74 ± 0.007	1.37 ± 0.03	1.21 ± 0.03
CO_2 (mmole)	0.98 ± 0.01	1.08 ± 0.03	0.99 ± 0.03	1.04 ± 0.03	0.92 ± 0.003	1.14 ± 0.01	1.11 ± 0.02	1.22 ± 0.03	1.15 ± 0.005	0.99 ± 0.03	0.97 ± 0.005	1.28 ± 0.007	1.00 ± 0.02
H_2 (mmole)	1.36 ± 0.02	1.47 ± 0.03	1.23 ± 0.01	1.52 ± 0.003	1.21 ± 0.002	1.42 ± 0.03	1.30 ± 0.01	1.32 ± 0.03	1.27 ± 0.01	1.09 ± 0.01	1.04 ± 0.01	1.30 ± 0.02	1.07 ± 0.01
H_2S (mmole)*	0	0	0	0	1.17 ± 0.01	0	0	0	0	1.17 ± 0.01	1.17 ± 0.01	0	1.17 ± 0.01
Products in liquid-phase													
Acetate (mmole)	0.78 ± 0.002	0.48 ± 0.01	0.78 ± 0.02	0.65 ± 0.006	0.59 ± 0.03	0.60 ± 0.02	0.52 ± 0.01	0.71 ± 0.02	0.59 ± 0.01	0.44 ± 0.002	0.62 ± 0.005	0.55 ± 0.01	0.49 ± 0.001
Lactate (mmole)	0.27 ± 0.001	0.29 ± 0.005	0.29 ± 0.005	0.13 ± 0.005	0.26 ± 0.006	0.29 ± 0.02	0.15 ± 0.009	0.14 ± 0.001	0.30 ± 0.004	0.27 ± 0.006	0.28 ± 0.005	0.13 ± 0.004	0.23 ± 0.005
Glucose (µmole)	0.35 ± 0.002	0.19 ± 0.02	0.23 ± 0.01	1.51 ± 0.12	1.25 ± 0.03	0.64 ± 0.004	4.51 ± 0.08	2.89 ± 0.13	0.21±0.01	4.40 ± 0.12	2.13 ± 0.09	1.66 ± 0.11	1.15 ± 0.03
Cellobiose (µmole)	2.34 ± 0.02	7.30 ± 1.75	3.71 ± 0.16	9.83 ± 0.24	6.14 ± 0.04	3.55 ± 0.47	15.24 ± 0.01	6.45 ± 0.06	4.08 ± 0.09	13.93 ± 0.06	3.10 ± 0.02	1.70 ± 0.20	2.33 ± 0.11

[a]H2S accumulation inferred from the sulfate consumption. Zero indicates negligible consumption.

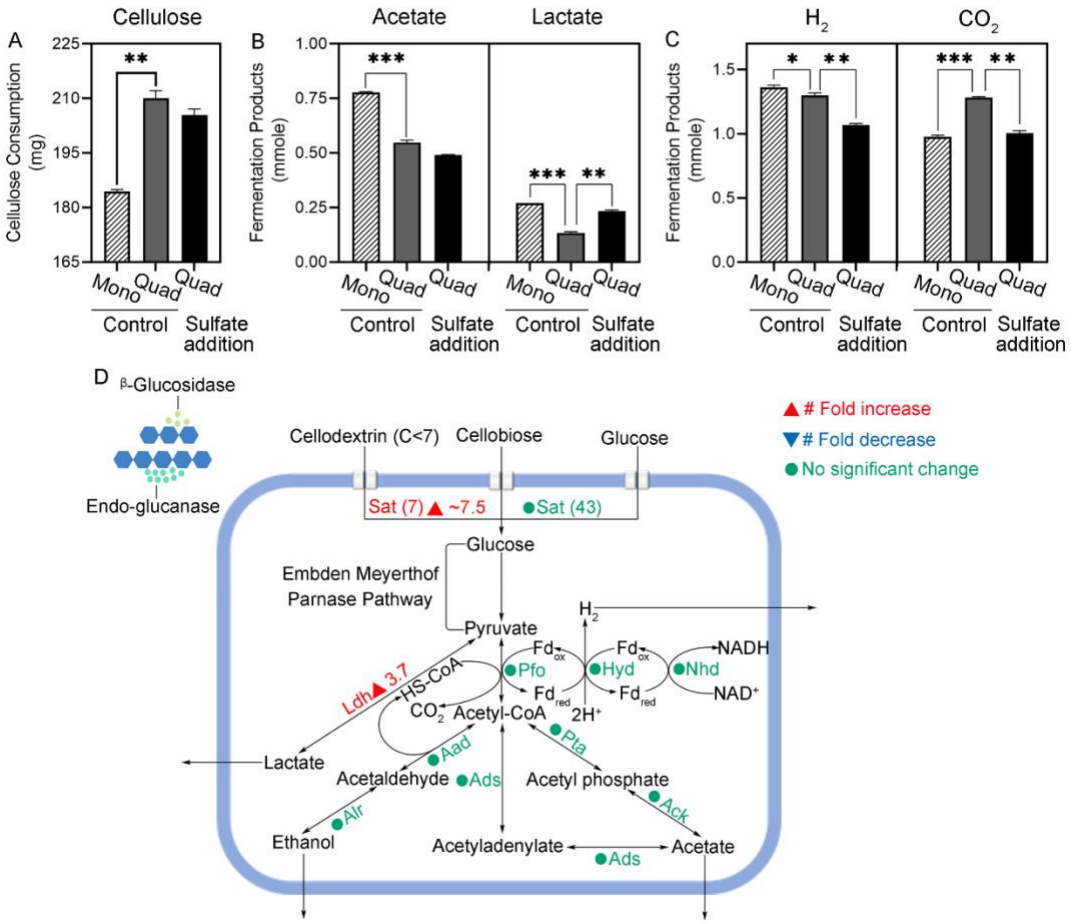

Figure 2.2 Metabolism of *R. cellulolyticum*. (A) Cellulose consumption. (B) Accumulation of acetate and lactate in the liquid phase. (C) Accumulation of H_2 and CO_2 in the gas phase. Significant differences (* for *p*-value < 0.05, ** for *p*-value < 0.01 and *** for *p*-value < 0.001) indicate targeted biological hypotheses. (D) Protein expression profile of the major carbon metabolism pathways in *R. cellulolyticum*. Enzymes are color-coded based on their protein abundance changes induced by sulfate addition. Unidentified enzymes are not labeled. Sat: sugar related ABC transporter; Pfo: Pyruvate flavodoxin/ferredoxin oxidoreductase; Hyd: Hydrogenase, Fe-only; Nhd: flavin oxidoreductase/NADH oxidase; Ldh: L-lactate dehydrogenase; Aad: Acetaldehyde dehydrogenase; Alr: alcohol dehydrogenase; Ads: AMP-dependent synthetase; Ack: Acetate kinase; Pta: phosphate acetyltransferase.

2.4.3 Metabolism of hydrogenotrophic methanogen *Methanospirillum hungatei* and acetoclastic methanogen *Methanosaeta concilii*

M. *hungatei* was selected as a model hydrogenotrophic methanogen. The accumulation of H_2 in the bi-culture of *R. cellulolyticum* and *M. hungatei* over 7 days (1.23 ± 0.01 mmole) was approximately 0.13 mmole lower than in the *R. cellulolyticum* mono-culture (1.36 ± 0.02 mmole) (Figure 2.3A). Methane (0.42 ± 0.007 mmole) accumulated in the bi-culture of *R. cellulolyticum* and *M. hungatei*. Since *M. hungatei* needs to consume 4 H_2 per CH_4 generated, approximately 2.91 mmole of H_2 (0.42 mmole $CH_4 \times 4$ + 1.23 mmole H_2) should be produced by *R. cellulolyticum* in the bi-culture, which was more than twice that in the *R. cellulolyticum* mono-culture (1.36 ± 0.02 mmole). This indicates that *M. hungatei* promoted H_2 production by R. cellulolyticum through the alleviation of product inhibition. The methane production increased from 0.16 ± 0.01 mmole in the tri-culture without *M. hungatei* to 1.37 ± 0.03 mmole in the quad-culture with *M. hungatei* (Figure 2.3C). Two key enzymes in hydrogenotrophic methanogenesis, formylmethanofuran dehydrogenase (Fmd) and formate dehydrogenase (Fdh), were identified in the quad-cultures by metaproteomics (Figure 2.3D). This indicated active hydrogenotrophic methanogenesis by *M. hungatei* in the multi-species cultures.

M. concilii was added as a model acetoclastic methanogen. The net accumulation of acetate in the multi-species cultures containing *M. concilii* increased in the first five or six days and then decreased or leveled off in the last one or two days, which suggested a lag in acetate consumption (Figure S2.2). In the cultures lacking *M. concilii*, the amount of acetate kept increasing during the 7-day growth. The accumulative amount of acetate in the bi-culture of *M. concilii* and *R. cellulolyticum*

(0.48 ± 0.01 mmole) was significantly lower than in the mono-culture of *R. cellulolyticum* alone (0.78 ± 0.002 mmole) (*p*-value = 0.0006). The accumulation of acetate in the quad-culture (0.55 ± 0.01 mmole) was also significantly lower than that in the tri-culture that lacked *M. concilii* (0.71 ± 0.02 mmole) (*p*-value = 0.0005) (Figure 2.3B). Approximately 0.48 mmole more methane accumulated in the quad-culture (1.37 ± 0.03 mmole) than in the tri-culture (0.89 ± 0.02 mmole) without *M. concilii* (Figure 2.3C) (*p*-value < 0.0001). In the *M. concilii* acetoclastic methanogenesis pathway, acetyl-coenzyme A synthetase (Acs), CO dehydrogenase/acetyl-CoA synthase (Cds), tetrahydromethanoprotein S-methyltransferase, methyl-coenzyme A reductase (Mtf) and CoB-CoM reductase (Mcr) were identified by metaproteomics (Figure 2.3E). This indicated active acetoclastic methanogenesis by *M. concilii* in the multi-species cultures.

Sulfate addition reduced quad-culture methane production by 11.7% (*p*-value < 0.0001) (Figure 2.3C). The protein abundance of formate dehydrogenase, involved in the hydrogenotrophic methanogenesis in M. *hungatei,* significantly decreased by 27.8-fold (*q*-value < 0.0001) (Figure 2.3D). In addition, sulfate addition significantly decreased the protein abundances of enzymes involved in acetoclastic methanogenesis. Specifically, the protein abundances of CO dehydrogenase/ acetyl-CoA synthase (*q*-value = 0.03) and methyl-coenzyme M reductase (*q*-value = 0.001) significantly decreased by at least 4-fold (Figure 2.3E). These decreases indicated that the sulfate addition suppressed both hydrogenotrophic methanogenesis and acetoclastic methanogenesis in the quad-culture.

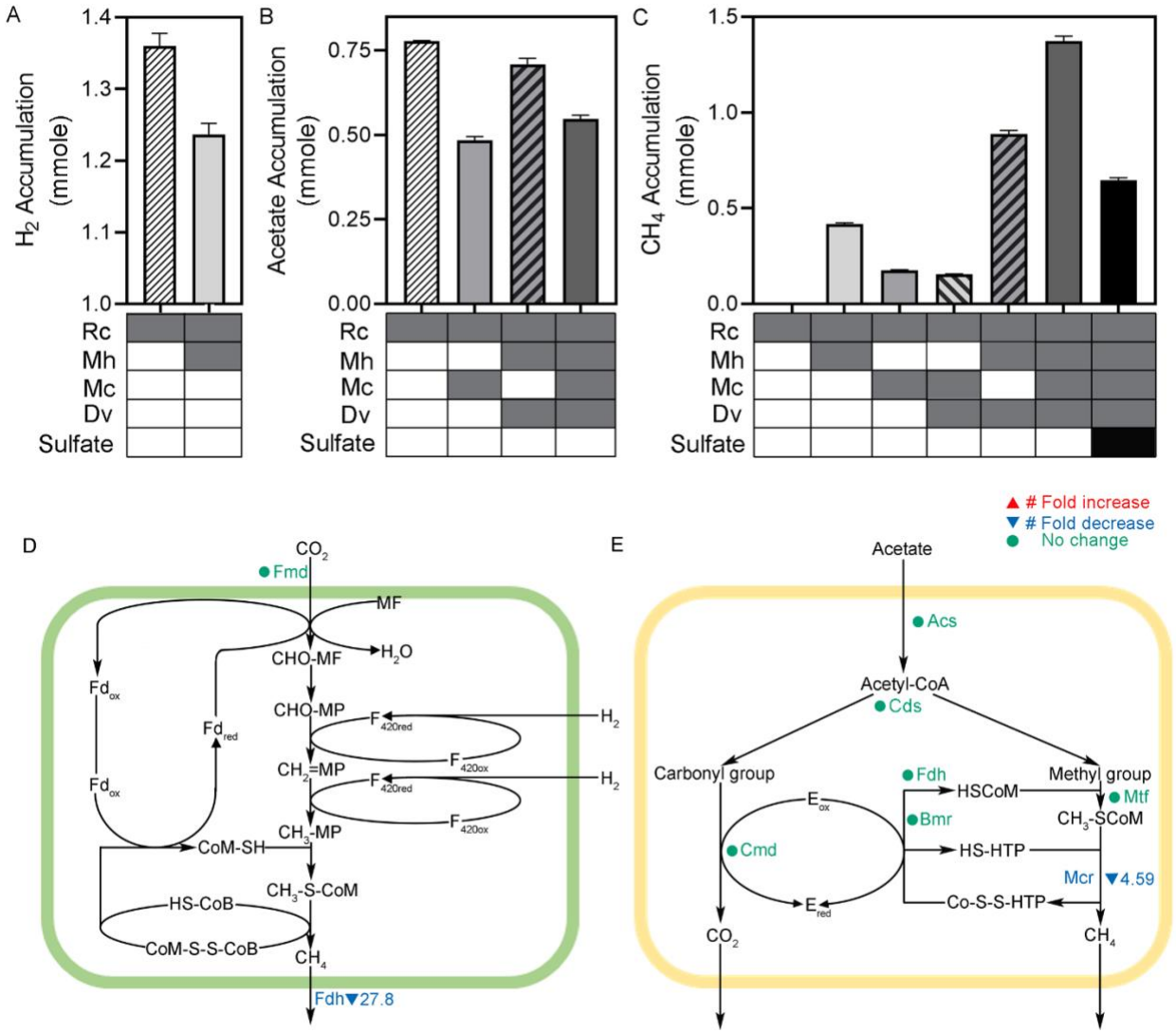

Figure 2.3 Metabolism of *Methanospirillum hungatei* and *Methanosaeta concilii*. (A) H_2 accumulation. (B) acetate accumulation. (C) CH_4 accumulation. The table on the x-axis marks the species included in each culture and the presence or absence of sulfate addition. Significant differences (*** for *p*-value < 0.001) indicate targeted biological hypotheses. (D) Hydrogenotrophic methanogenesis in *M. hungatei*. (E) Acetoclastic methanogenesis in *M. concilii*. Enzymes are color-coded based on their protein abundance changes induced by sulfate addition. Unidentified enzymes are not labeled. Fmd: formylmethanofuran dehydrogenase; Fdh: formate dehydrogenase; Acs: acetyl-coenzyme A synthetase; Cds: CO dehydrogenase/acetyl-CoA synthase; Cmd:

carbon monoxide dehydrogenase CoM; Mtf: tetrahydromethanopterin S-methyltransferase; Mcr: methyl-coenzyme M reductase; Bmr: CoB-CoM reductase.

2.4.4 Metabolism of sulfate-reducing bacterium *Desulfovibrio vulgaris*

D. vulgaris can ferment lactate to acetate, H_2 and CO_2 when sulfate is limited (Figure 2.4F) or reduce sulfate with lactate or H_2 as electron donors (Figure 2.4G) [125]. In the control condition, while lactate in the cultures without *D. vulgaris* accumulated continuously over seven days, lactate in the cultures with *D. vulgaris* increased in the first 3 days and then decreased slightly from day 4 onward. Over 7 days, 0.13 ± 0.005 mmole lactate accumulated in the bi-culture of *R. cellulolyticum* and *D. vulgaris*, which was 51.9% lower than that in the mono-culture (0.27 ± 0.001 mmole) (*p*-value = 0.0005). The lactate accumulation by the tri-culture that lacked *D. vulgaris* (0.29 ± 0.02 mmole) was also higher than that in the quad-culture that included *D. vulgaris* (0.13 ± 0.004 mmole) (*p*-value = 0.002) (Figure 2.4A). Metaproteomics identified cytochrome C_3 (Cyt c3), high-molecular weight cytochrome (Hmc), periplasmic [NiFe] hydrogenase (Hyd), membrane-bound Coo hydrogenase (Coo), lactate dehydrogenase (Ldh) and L-lactate permease (Lpe) in the hydrogenic lactate oxidation pathway of *D. vulgaris* (Figure 2.4F). In the mono-culture of *R. cellulolyticum*, 1.36 ± 0.02 mmole H_2 accumulated at the end of the cultivation, while 1.52 ± 0.003 mmole H_2 accumulated in the bi-culture of *R. cellulolyticum* and *D. vulgaris*. These results suggest that *D. vulgaris* fermented lactate produced by *R. cellulolyticum* to H_2.

The addition of *D. vulgaris* to the bi-culture of *R. cellulolyticum* and *M. concilii* did not significantly increase the methane production. But the addition of *D. vulgaris* to the bi-culture of *R. cellulolyticum* and *M. hungatei* significantly increased the methane production by ~112% (from 0.42 $\pm$ 0.007 mmole to 0.89 $\pm$ 0.02 mmole) (Figure 2.4D). *D.*

vulgaris enhanced hydrogenotrophic methanogenesis likely by producing additional hydrogen from lactate fermentation [100].

We found that the synergy between hydrogenotrophic and acetoclastic methanogenesis depended on the presence of *D. vulgaris*. Methane produced by the tri-culture of *R. cellulolyticum*, *M. concilii* and *M. hungatei* (0.62 ± 0.02 mmole) was close to the sum (0.60 ± 0.01 mmole) of the methane produced by the bi-culture of *R. cellulolyticum* and *M. concilii* (0.18 ± 0.003 mmole) and the bi-culture of *R. cellulolyticum* and *M. hungatei* (0.42 ± 0.007 mmole). However, the methane produced by the quad-culture (1.37 ± 0.03 mmole) was ~30% higher than the sum (1.05 ± 0.02 mmole) of the methane produced by the tri-culture of *R. cellulolyticum*, *D. vulgaris* and *M. concilii* (0.16 ± 0.001 mmole) and the tri-culture of *R. cellulolyticum*, *D. vulgaris* and *M. hungatei* (0.89 ± 0.02 mmole) (Figure 2.4D, Table 2.1). From another perspective to compare, the addition of *D. vulgaris* to the tri-culture of *R. cellulolyticum*, *M. concilii* and *M. hungatei* increased total methane production by 0.75 mmole. This was 67% more than the additive increase of adding *D. vulgaris* to either a *R. celluloltyicum-M hungatei* bi-culture (0.47 mmole increase) or to a *R. cellulolyticum-M. concillii* bi-culture (0.02 mmole decrease) (Figure 2.4D). Both ways of comparisons showed a positive synergistic relationship amongst methanogenesis and fermentation via *D. vulgaris*.

The mono-culture of R. cellulolyticum produced 0.98 ± 0.01 mmole of CO_2. Co-culturing *R. cellulolyticum* with *D. vulgaris* did not significantly increase their CO_2 production (1.04 ± 0.03 mmole). Adding *M. hungatei* to *R. cellulolyticum* did not significantly change the CO_2 production in their bi-culture (0.99 ± 0.03 mmole) either. However, combining both *D. vulgaris* and *M. hungatei* with *R. cellulolyticum* significantly

increased the CO_2 production (1.22 ± 0.03 mmole). Further adding *M. concilii* to this tri-culture did not result in a significant increase of CO_2 production by the quad-culture (1.28 ± 0.007 mmole) (Figure 2.4E). These results suggested a positive synergy between *M. hungatei* and *D. vulgaris* on CO_2 production.

Sulfate addition enhanced sulfate reduction by *D. vulgaris*. At the end of cultivation, the quad-culture consumed 1.17 ± 0.01 mmole of sulfate in the sulfate addition condition (Table 2.1). Sulfate addition increased the relative abundance of sulfite reductase by 2.0 fold (*q*-value = 0.003) (Figure 2.4G). H_2 accumulation significantly decreased in the sulfate addition condition (1.07 ± 0.02 mmole) when compared with the control condition (1.30 ± 0.02 mmole) (*p*-value = 0.003) (Figure 2.4C). Sulfate reduction promoted sulfidogenic lactate oxidation as evidenced by a 1.8-fold increase of the relative abundance of FeS cluster assembly ATPase (Fca) (*q*-value = 0.009) in the sulfate addition condition (Figure 2.4G). However, lactate accumulated in the first three days and then slightly decreased in the following four days in the control condition, but lactate continuously accumulated over the seven days in the sulfate addition condition (Figure 2.4A). The increased accumulation of lactate in the sulfate addition condition, despite the enhanced *D. vulgaris* sulfidogenic lactate oxidation, can be attributed to the increased *R. cellulolyticum* lactate fermentation stimulated by sulfate addition as described above (Figure 2.2D).

Sulfate addition significantly decreased the CO_2 accumulation in the two tri-cultures containing *D. vulgaris* and the quad-culture, but not in the tri-culture without *D. vulgaris* (Figure 2.4E, Table 2.1). Sulfate addition also significantly reduced the acetate accumulation in the two tri-cultures containing *D. vulgaris* and the quad-culture, but not

in the tri-culture without *D. vulgaris* (Figure 2.4B, Table 2.1). These observations can be attributed to the suppression of the *D. vulgaris* fermentation of lactate to acetate and CO_2 by the sulfate addition.

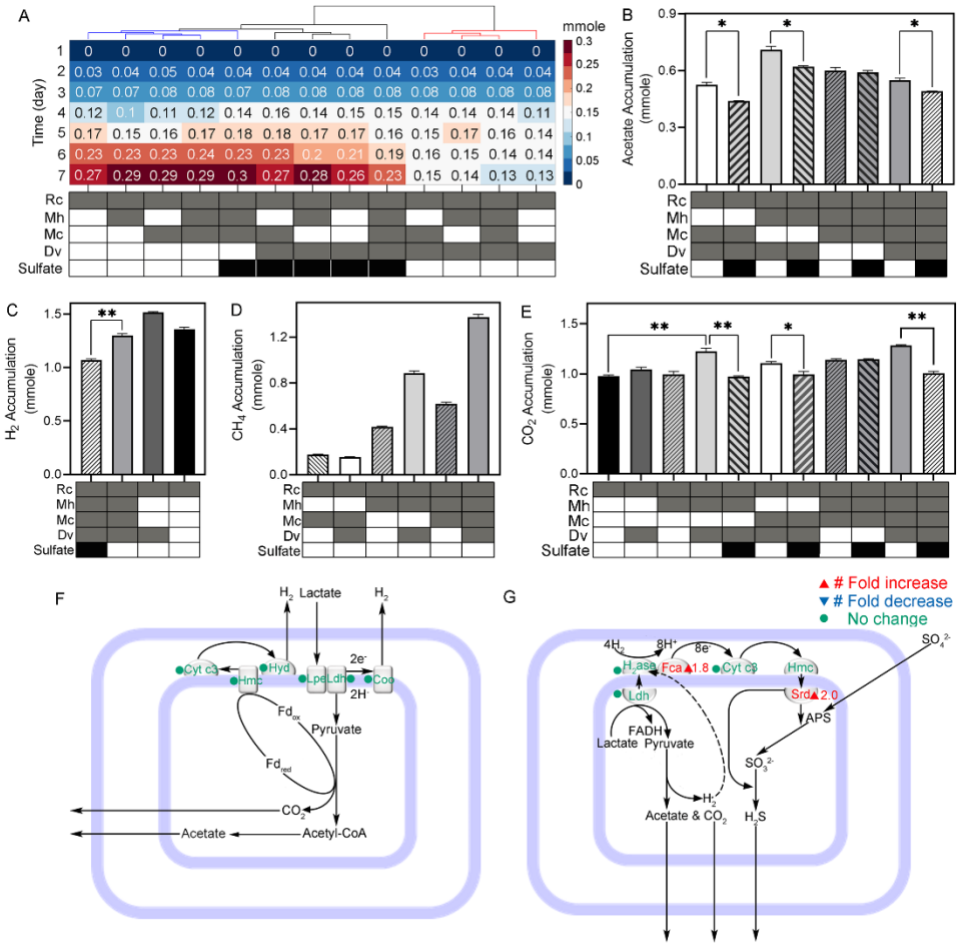

Figure 2.4 Metabolism of *D. vulgaris*. (A) lactate accumulation. A column represents daily lactate accumulation in a culture over 7 days of cultivation. The cultures with sulfate additions were clustered together. (B) Acetate accumulation. (C) H_2 accumulation. (D) CH_4 accumulation. (E) CO_2 accumulation. Significant differences (* for p-value < 0.05 and ** for p-value < 0.01) indicate targeted biological hypotheses. (F) Hydrogenic lactate fermentation in *D. vulgaris*. (G) Sulfidogenic lactate oxidation and sulfidogenic hydrogenic oxidation in D. vulgaris. Cyt c3: cytochrome C3; Hmc: high-molecular cytochrome; Hyd: hydrogenase; Lpe: L-lactate permease; Coo: membrane-

bound Coo hydrogenase; H_2ase: hydrogenase; Fca: FeS cluster assembly ATPase; Ldh: lactate dehydrogenase; Srd: sulfite reductase. The table on the x axis marks the species included in each culture and the presence or absence of sulfate addition.

2.4.5 Modeling of carbon and energy flow through the synthetic community

A stoichiometric model was constructed to simulate fluxes through the primary energy production pathways in the four organisms (Table S2.1, Table S2.2). For simplicity, extracellular cellulose hydrolysis was omitted and *R. cellulolyticum* was considered to ferment glucose. The overall model had seven reactions, including two for *R. cellulolyticum*, three for *D. vulgaris*, and one for each methanogen (Table S2.1, Table S2.2). Reactions that were not expected to be active were removed based on either genetic or nutrient availability in the system (i.e., sulfidogenic reactions were removed in the absence of sulfate and acetoclastic methanogenesis was removed in the absence of *M. concilii*). The contributions of each reaction were fitted to the accumulative mmoles of glucose, acetate, lactate, H_2, CH_4 and H_2S produced or consumed over the 7 days of incubation. To access redundancy of metabolic pathways in this stoichiometric model, each reaction pathway was sequentially excluded before fitting and the impact on model fit was evaluated. These simulations identified two and three possible flux distributions through the quad-culture in the control and sulfate addition conditions (Table S2.1, Table S2.2 and Table S2.3) with equal goodness of fit to the experimental data. The correlation coefficients, R^2, exceeded 0.9 in both conditions. The NRMSEs (normalized root mean square errors) were 0.11 ± 0.006 in the control condition and 0.25 ± 0.01 in the sulfate addition condition. The consistency between the experimental data and the

modeling results indicated a reliable estimation of the carbon and energy flows (Figure 2.5A, 2.5B).

R. cellulolyticum in the cultures was modeled by lactate fermentation and hydrogenic acetogenesis (Table S2.1). Sulfate addition stimulated the production of acetate and lactate in *R. cellulolyticum*. *D. vulgaris* was modeled to have three metabolic possibilities, lactate oxidation to acetate with proton reduction to hydrogen (hydrogenic lactate oxidation) (Figure 2.4F), lactate oxidation to acetate with sulfate reduction to sulfide (sulfidogenic lactate oxidation) (Figure 2.4G), and hydrogen oxidation to protons with sulfate reduction to sulfide (sulfidogenic hydrogen oxidation) (Figure 2.4G). As expected, sulfate addition increased the estimated flux through sulfate reduction from 0 to 3.09 ± 0.03 mmole (*p*-value <0.0001). The estimated flux of carbon and electrons through *D. vulgaris* was poorly constrained due to redundant pathways. However, the flux did increase within related possible flux distributions. For example, the maximum flux of hydrogen production by *D. vulgaris* increased from 3.16 ± 0.02 to 4.06 ± 0.02 mmole with the addition of sulfate, which agrees with the increased relative abundance of the *D. vulgaris* proteome in the community metaproteome (Figure 2.1B). *M. hungatei* and *M. concilii* were represented by hydrogenotrophic methanogenesis and acetoclastic methanogenesis, respectively. Compared to the control condition, the addition of sulfate halted hydrogenotrophic methanogenesis in *M. hungatei* and increased the flux through acetoclastic methanogenesis in *M. concilii* by 1.42-fold (*p*-value < 0.0001).

The model estimated the cross-feeding fluxes from *R. cellulolyticum* to the other microorganisms (Figure 2.5C). The fluxes of acetate and CO_2 from *R. cellulolyticum* to

M. concilii and *M. hungatei* were each 0.97 mmole in the control condition. In the sulfate addition condition, the flux of H_2 consumption by *M. hungatei* fully stopped, suggesting that substrate competition for H_2 by *D. vulgaris* was the main cause of the lower methane yields in the sulfate-amended quad-culture. Indeed, the H_2 consumption flux of *D. vulgaris* increased from 0 in the control condition to 3.09 mmole under the sulfate addition condition. For comparison, sulfate addition increased H_2 production by *R. cellulolyticum* from 3.16 to 4.63 mmole. Overall, this analysis demonstrates that sulfate addition deeply restructures carbon fluxes and metabolic hand-offs through the four-species synthetic community, ultimately affecting overall community metabolism.

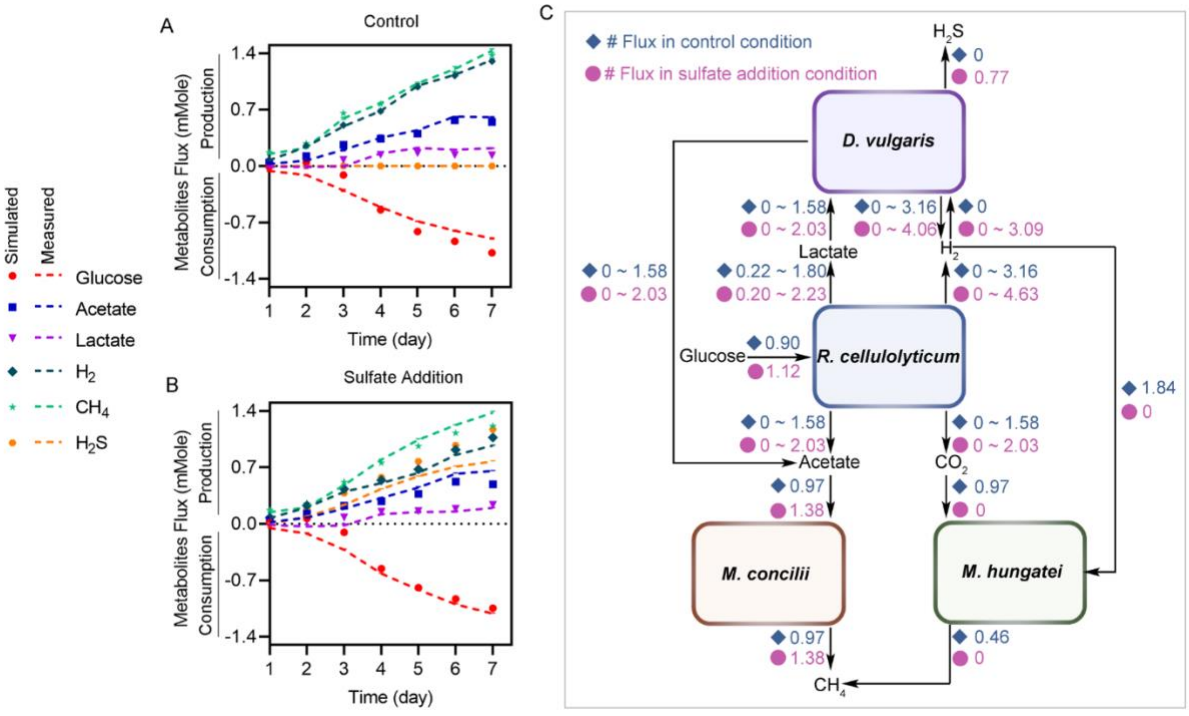

Figure 2.5 Community stoichiometric modeling. (A) Model fitting in the control condition. (B) Model fitting in sulfate addition condition. (C) Cross-feeding fluxes among the four species under the control condition and sulfate addition conditions.

2.5 Discussion

Synthetic communities have been shown to be a powerful approach to study the interactions among major microbial guilds in the degradation of cellulosic biomass to methane and CO_2. A bi-culture of *D. vulgaris* and *Methanococcus maripaludis* showed the requirement of hydrogen transfer for their syntrophic growth coupled to methane production [126]. Cellulose degradation by *Clostridium cellulovorans* was enhanced by co-culturing with *Methanosarcina barkeri* or *Methanosarcina mazei* [127]. Co-culturing *R. cellulolyticum* with *D. vulgaris* was also shown to accelerate cellulose degradation [128]. However, these bi-cultures can only reveal binary interactions between two organisms. By using a four-species synthetic community and comparing that to its constitutive parts, we investigated tertiary interactions (i.e., interactions of interactions) among four microorganisms involved in methanogenesis from cellulose. A tertiary interaction has positive synergy if the effect of combining three or more organisms on a phenotype of the community is greater than the addictive effects of combining two of these organisms separately. In contrast, a tertiary interaction has negative synergy when the effect of combining three or more organisms on a phenotype is less than the sum of the separate effects of combining the subsets. Here, we demonstrated that the bi-cultures of *R. cellulolyticum* with any of the other 3 species increased cellulose degradation relative to the *R. cellulolyticum* mono-culture. This provides a baseline to determine the type of the tertiary interactions. The quad-cultures further improved the cellulose degradation over any of the bi-cultures, but the increase of cellulose degradation by the quad-culture over the mono-culture (25.63 mg) was less than the sum of the increases by the 3 bi-cultures over the mono-culture (13.38 mg, 13.78 mg and 19.34 mg). Such a negative synergy suggests that the putative beneficial effects of

pH stabilization and cellulose colonization [127] provided by the methanogens and *D. vulgaris* may be antagonistic for cellulose degradation by *R. cellulolyticum* [129]. The methane production by the tri-culture of *R. cellulolyticum*, *M. concilii* and *M. hungatei* (0.62 ± 0.02 mmole) was approximately equal to the combined methane production by *R. cellulolyticum-M. concilii* bi-culture (0.18 ± 0.003 mmole) and *R. cellulolyticum-M. hungatei* bi-culture (0.42 ± 0.007 mmole), while the methane production of the quad-culture (1.37 ± 0.03 mmole) was higher than the combined methane production by the *R. cellulolyticum* and *M. hungatei* and *D. vulgaris* tri-culture (0.89 ± 0.02 mmole) and the *R. cellulolyticum* and *M. concilii* and *D. vulgaris* tri-culture (0.16 ± 0.001 mmole), hence indicating a positive synergy. Mechanistically, it may be that *D. vulgaris* enhances methanogenesis by producing the substrates, CO_2, acetate, and H_2, and removing lactate [130, 131]. The two methanogens can enhance each other's methanogenesis by also consuming the substrates. The whole of these positively synergistic effects was greater than the sum of the individual effects on methanogenesis.

Synthetic communities can be modeled to estimate their intracellular metabolic fluxes and cross-feeding fluxes, which can be used to infer competitive and cooperative interactions among the organisms. Genome-scale flux balance analysis (FBA) models of individual organisms have been combined to construct FBA models of their co-cultures [131-133]. However, genome-scale FBA is vastly under-parameterized and requires strong assumptions on the objective function for optimization of the fluxes in an organism [134], This is further complicated in a synthetic community with different organisms possibly requiring divergent objective functions to maximize the total fitness of the community. In addition, reliable FBA models require labor-intensive curation of the

genome-scale metabolic networks of all members of a synthetic community. As a result, the previous studies focused on the synthetic communities of microorganisms with pre-existing FBA models [135]. Alternatively, a kinetic model of anaerobic digestion, ADM1 [136], models the major metabolic processes in the degradation of complex biomass (e.g., cellulose) to methane and CO_2. However, the lack of knowledge of kinetic parameters in a study would limit the prediction accuracy of the ADM1 modeling [137]. Here, we constructed a simple stochiometric model for synthetic communities. Similar to ADM1, the stochiometric modeling approach considers only the major metabolic processes of the organisms, but enables quantifying metabolic fluxes without knowledge of substrate concentrations or kinetic parameters. Unlike a genome-scale FBA model, our simple stoichiometric model can be fitted just using the experimental data without assuming any objective function [138]. These complementary modeling approaches could be combined to build a multi-scale model for synthetic communities. Specifically, the organism-level boxes in a community-level stoichiometric model (Figure 2.5) can be expanded to individual genome-scale FBA models for selected organisms of interest. The estimated fluxes by the multi-scale flux balancing analyses can then be integrated with a parameterized kinetic model for each of the organisms to predict synthetic community dynamics and its responses to disturbances.

The stoichiometric model and metaproteomics analysis characterized the metabolic activities of microorganisms in two different ways, so we compared the fluxes through the modeled reactions with the protein abundances of marker enzymes in those reactions (Table S2.3). The stoichiometric model showed that sulfate addition zeroed out the flux through hydrogenotrophic methanogenesis. This change was also reflected

in the significantly decreased abundance of *M. hungatei* formate dehydrogenase, a marker enzyme for hydrogenotrophic methanogenesis. However, sulfate addition significantly increased the flux of acetoclastic methanogenesis in *M. concilii*, while the relative abundance of *M. concilii* methyl-coenzyme M reductase significantly decreased. In addition to the protein abundance of the corresponding enzyme, a reaction may also be regulated by a variety of other mechanisms, such as post-translational modifications and allosteric regulations [121]. Compared with the control condition, the accumulation of CH_4 was reduced by only 12% in the sulfate addition condition, while the flux of hydrogenotrophic methanogenesis decreased to 0 mmole, so a 1.42-fold increase in acetoclastic methanogenesis flux should be reasonable.

The quad-culture and its model were used to study the effects of increased sulfate availability on the microbial communities. Such a perturbation may occur to estuarine wetland soil communities as a result of more prevalent sulfate-laden seawater intrusion from rising seawater levels. The impact of seawater intrusion has been studied using natural wetland ecosystems [139, 140], demonstrating that seawater intrusion reduced the CH_4 and CO_2 fluxes from the wetland. However, it was not clear how microbial interactions responded to seawater intrusion because of the great complexity of natural communities. In this study, we showed that sulfate addition reduced CH_4 and CO_2 emission, consistent with results obtained with natural ecosystems [139, 141]. The main reason for decreased CH_4 production was the sharp decrease in H_2 available for the hydrogenotrophic methanogen. The competition for H_2 use between methanogens and sulfate reducers has been proposed to have a thermodynamic basis as hydrogenotrophic sulfate reduction is more energetically favorable than

hydrogenotrophic methanogenesis [142]. Therefore, such competitions exist in reactor systems and environments with transient sulfate [143, 144]. In addition, possible interactions can be estimated by modeling what is consumed and produced by the individual species. Our result demonstrated that sulfate addition increased both the production of acetate and lactate by *R. cellulolyticum* and their consumption by *M. concilii* and *D. vulgaris*. This suggested that sulfate addition intensified the carbon transfer from *R. cellulolyticum* to *M. concilii* and *D. vulgaris*. Although the flux of H_2 production by *R. cellulolyticum* increased, the flux of H_2 consumed to produce H_2S in *D. vulgaris* increased even more. This, in turn, further intensified the competitive interactions between *M. hungatei* and *D. vulgaris* for H_2 as substrate in the presence of sulfate.

Many syntrophic communities have been shown to develop around the exchange of H_2 and organic acids [100, 145]. In this study, our stoichiometric analysis was unable to constrain the possible exchange of lactic acid or H_2 between *R. cellulolyticum* and *D. vulgaris*, even in the absence of sulfate (Table S2.3). However, limited changes in hydrogenase abundance were observed in either *R. cellulolyticum* or *D. vulgaris*, indicating likely exchange of lactate or some other oxidizable carbon intermediate. While the oxidation of lactate to acetate and production of H_2 is expected to be unfavorable under the H_2 partial pressures studied, alternative organic compounds could be intermediates, including pyruvate or alanine, which have been demonstrated to produce H_2 in sulfate-reducing bacterium at high H_2 partial pressures [100]. Furthermore, *D. vulgaris* was observed in both the sulfate replete and deplete conditions, indicating growth under both conditions, and therefore, at least partial

exchange of lactate or another metabolite to support *D. vulgaris* growth. In the presence of sulfate, the lactate dehydrogenase in *R. cellulolyticum* also increased, indicating a possible increased participation of the lactate exchange in the flux distributions (Table S2.3). While *D. vulgaris* should out-compete *M. hungatei* for H_2 in the sulfate addition condition, the relative total protein abundance of *M. hungatei* remained at 3% in both conditions. This could be explained if *D. vulgaris* had a long lag phase in the quad-culture and *M. hungatei* entered the stationary phase before being out-competed by *D. vulgaris*. Alternatively, *M. hungatei* might employ direct electron transfer using its electrogenic pili [146] or utilize other compounds, such as formate [147], as the electron donor.

We anticipate this four-species community, as well as the future construction of additional multi-species synthetic communities, introduce the level of complexity needed to more realistically model carbon cycling in natural anaerobic communities. By combining metabolic profiling, metaproteomics and modeling, we observed many community behaviors as designed, especially the adaptive cross-feeding fluxes and the shifting substrate competitions under changing environments. More interestingly, the multi-species cultures also revealed some emergent properties of microbial communities, including synergistic epistasis and antagonistic epistasis of tertiary interactions. By quantifying the expected competitive/cooperative behaviors and revealing the emergent interaction properties, the synthetic communities may pave the way towards more accurate modeling of natural communities.

Chapter 3. Metabolic dependencies drive species interactions in a synthetic microbial community

3.1 Abstract

Anaerobic microbial communities play a critical role in biogeochemical cycles through complex networks of interactions that influence community structure, stability, and functionality. This study investigates the metabolic interactions within synthetic communities composed of a cellulolytic bacterium (*Ruminiclostridium cellulolyticum*), a hydrogenotrophic methanogen (*Methanospirillum hungatei*), an acetoclastic methanogen (*Methanosaeta concilii*), and a sulfate-reducing bacterium (*Desulfovibrio vulgaris*). Through proteogenomic analysis and metabolic modeling, we quantified the metabolic interaction potential (MIP) and metabolic resource overlap (MRO) across bi-, tri-, and quad-cultures. Our results revealed that the presence of *D. vulgaris* in the quad-culture reduced MRO by 76% and promoted balanced interactions, resulting in a 226% increase in methane production compared to tri-cultures. The low hydrogen partial pressure observed in multi-species interactions facilitates conditions for methanogenesis. However, cellulose degradation was negatively impacted in complex communities, with degradation rates 3-5% lower than additive effects from simpler configurations. Metaproteomics further revealed shifts in the abundance of key enzymes involved in hydrogen and lactate metabolism, suggesting a dynamic reorganization of metabolic pathways depending on community context. The higher-order interactions among multiple species led to emergent properties, such as enhanced methanogenic efficiency and reduced metabolic redundancy, which were not observed in pairwise interactions. These findings highlight the importance of considering higher-order

interactions for accurate prediction of microbial community behaviors and effective engineering of microbial consortia for environmental and industrial applications.

Key words: Cross-feeding interactions, Competitive interactions, Metaproteomics, Metabolic modeling

3.2 Introduction

Anaerobic microbial communities drive global geochemical cycles, colonize the animal and human guts, and are cultivated for many industrial applications [148-150]. In these communities, many species are assembled in complex networks of trophic interactions and other relationships [44, 45, 151, 152]. Within anaerobic ecosystems, tropic interactions form a cascade of cross-feeding processes. Complex organic matters, such as polysaccharides, are hydrolyzed to simple compounds by primary degrader. Secondary consumers subsequently process the byproducts of hydrolysis or the metabolic products of primary degraders[153, 154]. Cooperative and competitive interactions within these processes profoundly shape the community's structure, stability, and productivity, thereby influencing the community's capacity to perform essential functions for the environment or host organisms [5, 45, 155, 156].

Despite the importance of microbial interactions, understanding how microorganisms cooperate and compete remains a significant challenge[45, 157, 158]. Numerous omics studies have surveyed anaerobic microbial communities' gene and species content in diverse environments, such as animal guts, oceans, or soils [159-161]. However, a key challenge lies in translating the co-occurrences and abundance changes of these gene and species into metabolic or ecological interactions in complex natural communities [78, 162-164]. To overcome this challenge, microbiologists have used binary synthetic communities to study pair-wise interactions between two species. For example, a bi-culture of *Desulfovibrio vulgaris* and *Methanococcus maripaludis* has demonstrated the necessity of hydrogen transfer for their syntrophic growth and methane production [100]. The competitive dynamics between *Geobacter*

metallireducens and *Geobacter sulfurreducens* have been shown to significantly alter quorum sensing-regulated functions and surface motility [165]. Nevertheless, the interaction network among multiple organisms in a natural community is not a simple aggregation of all the binary interactions between two organisms, but contain tertiary interactions among three organisms or even higher-order interactions among four or more organisms. For example, the pair-wise interaction between two organisms can be modulated by a third organisms, which is a tertiary interaction likely prevalent in microbial communities [51, 59, 166]. Developing a more quantitative and predictive understanding of higher-order trophic network structures could enhance our ability to manipulate and manage communities, with broad implications for environmental conservation, as well as animal and human health [5, 45].

In a previous study, we constructed a series of synthetic communities, consisting of a cellulolyticum (*Ruminiclostridium cellulolyticum*), a hydrogenotrophic methanogen (*Methanospirillum hungatei*), an acetoclastic methanogen (*Methanosaeta concilii*) and a sulfate-reducing bacterium (*Desulfovibrio vulgaris*). These organisms are involved in the anaerobic conversion of cellulosic biomass to CO_2, CH_4, and other products in diverse anaerobic ecosystems, such as wetlands, the human gut, and waste treatment systems[166]. We observed positive synergistic interactions, as evidenced by a greater increase in CH_4 and CO_2 production in the quad-culture, compared to the sum of increase observed in the tri-culture. Conversely, negative synergy was observed where increased cellulose degradation in the quad-culture was lower than the additive effects observed in tri-cultures. However, a detailed insights into how the metabolic functions and activities of each organism change within different microbial configurations is still

lacking—an essential step towards elucidating the assembly and emergent features of microbial communities[167-169].

In this study, we extended our previous work on synthetic communities by incorporating proteogenomics and metabolic modeling for each microbial combination. Building upon geochemical observations, we investigated microbe-microbe interactions and metabolic capacities (Figure 1A). This study lays the groundwork for developing mechanistic metabolic models of anaerobic degradation, advancing our understanding of the behavior and functionality of anaerobic microbial ecosystems.

3.3 Materials and Methods

3.3.1 Genome-scale metabolic model building and Community simulation. The strains used in this study include *Ruminiclostridium cellulolyticum* H10 (ATCC 35319), *Desulfovibrio vulgaris* Hildenborough (ATCC 29579), *Methanospirillum hungatei* JF1 (txid323259) and *Methanosaeta concilii* (txid990316). The genomes and annotations of four species were downloaded from the National Center for Biotechnology Information (NCBI) database. These genomes were used to build genome-scale metabolic models with CarveMe [170], using the modified VM media composition to fill the gap. All community simulations were performed using the SMETANA tool [171]. The mathematical formulation, as well as the different scores, such as MIP, MRO, and SMETANA scores, are described in the original publication.

3.3.2 Protein Identification and Quantification. Samples from all the cultures at the end of cultivation were selected for full metaproteomic analysis. Protein extraction was carried out by a previously reported method [114, 115]. Briefly, harvested cell pellets were washed twice with nanopure water, cells were suspended in lysis buffer (containing 10 mM tris-HCl, 1% SDS, 0.1M DTT), and incubated at 60 °C for 1 h, and then the supernatant was collected after centrifugation. Proteins were then precipitated by trichloroacetic acid overnight at 4 °C and pelleted by centrifugation. Protein pellets were washed by ice-cold acetone three times and resuspended in guanidine buffer. Protein concentrations were quantified by Bicinchoninic Acid Assay [116].[116]. 20 mg samples of proteins were processed using filter-aided sample preparation and digested using Trypsin/LysC mixture. The digested peptides were labeled by TMTpro™ 16plex Label Reagent Set. TMT-labeled peptides were separated into 46 fractions on a 100 x

1.0 mm Acquity BEH C18 column (Waters) using an UltiMate 3000 UHPLC system (Thermo) with a 50 min gradient from 99:1 to 60:40 buffer A:B ratio under basic pH conditions, and then consolidated into 28 super-fractions. Each super-fraction was then further separated by reverse phase XSelect CSH C18 2.5 um resin (Waters) on an in-line 150 x 0.075 mm column using an UltiMate 3000 RSLCnano system (Thermo). Peptides were eluted using a 90 min gradient from 98:2 to 60:40 buffer A:B ratio. Eluted peptides were ionized by electrospray (2.4 kV) followed by mass spectrometric analysis on an Orbitrap Eclipse Tribrid mass spectrometer (Thermo) using multi-notch MS3 parameters. MS data were acquired using the FTMS analyzer in top-speed profile mode at a resolution of 120,000 over a range of 375 to 1500 m/z. Following CID activation with a normalized collision energy of 35.0, MS/MS data were acquired using the ion trap analyzer in centroid mode and normal mass range. Using synchronous precursor selection, up to 10 MS/MS precursors were selected for HCD activation with a normalized collision energy of 65.0, followed by the acquisition of MS3 and MS2 reporter ion data using the FTMS analyzer in profile mode at a resolution of 50,000 over a range of 100-500 m/z.

Protein identification and quantification followed established procedures. Briefly, mass spectrometry spectra were searched using Protein discovery software V3.1 with the SEQUEST algorism against a protein database constructed from the genome of four microorganisms. Raw search results were filtered to achieve 1% FDR (false discovery rate) at the peptide level, which was estimated using the target-decoy approach. Peptide identifications are assigned to protein or protein groups following the parsimonious rule. To avoid ambiguity in data analysis, protein groups were excluded

from biological analysis. Protein abundances were normalized against the average total of all data sets [172-174].

3.3.3 Construction of the stoichiometric model. A set of overall reactions depicting the documented metabolism of the individual species was fit to the measured amounts of metabolites in the constructed synthetic communities (Figure S1, Figure S2). The code used can be found on Github https://github.com/dywang0323/ProStoichiometric. The resulting fits provide a basis for quantifying metabolic contributions. Deviations between the inferred metabolic transformations and measured transformations indicate uncertainty in our understanding of the metabolic transformations or limitations in analytic capacity.

3.3.4 Statistical analysis. Metabolic measurement data were compared between different conditions using Student's t-test. The differences of protein abundance in metaproteome were analyzed by the Deseq R package [122] and the *p*-values were adjusted to *q*-values using the Benjamini and Hochberg method for multiple comparison correction [123]. Proteins with q-values < 0.05 were regarded as statistically significant.

3.3.5 Data availability. Proteomic data are available at the ProteomeXchange Consortium via the PRIDE (Proteomics Identification Database) partner repository with the dataset identifier PXD056517.

3.4 Results

3.4.1 Overview of metabolic cooperation and competition in microbial communities

Different subsets of *R cellulolyticum*, *M hungatei*, *M. concilii* and *D. vulgaris* were combined into one mono-culture, three bi-cultures, three tri-cultures, and one quad-culture, all grown in the same medium containing cellulose as the carbon substrate (Figure 3.1A). These synthetic communities were analyzed using the Species Metabolic Coupling Analysis (SMETANA) to generate the metabolic interaction potential (MIP) as a proxy measure for cooperative metabolism, and the metabolic resource overlap (MRO) to access the likelihood of resource competition (Figure 3.1B). In bi-cultures, an inverse relationship was observed between MIP and the MRO. The bi-culture of *R. cellulolyticum* and *M. concilii* showed a higher MIP, indicating more pronounced cooperative interaction. Conversely, the bi-culture of *R. cellulolyticum* with either *M. hungatei* or *D. vulgaris*, showed lower MIP and higher MRO, suggesting stronger competitive interactions (Figure 3.1B).

The complexity of tri-cultures (Figure 3.1B) altered the MIP-MRO relationship observed in bi-cultures. The MIP value of tri-cultures comprising *R. cellulolyticum*, *M. concilii,* and *M. hungatei*, was 60% higher than that of the bi-culture with *R. cellulolyticum* and *M. concilii*, and 300% higher than that of bi-culture with *R. cellulolyticum* with *M. hungatei* (Figure 3.1B). Additionally, the MRO of the tri-culture was 45% lower than the aggregate MRO of the two bi-cultures (Figure 3.1B), indicating that the concurrent presence of *M. concilii* and *M. hungatei* intensified cooperative interactions and mitigated competitive interactions within the community.

When all four species were integrated into a quad-culture, the MIP was 22% lower than the cumulative MIP of three bi-cultures, while the MRO was 76% lower than their cumulative MRO (Figure 3.1B and 3.1B). This suggested that integrating the four microbes into a quad-culture promoted a equilibrium between cooperative and competitive interactions compared to individual species pairings.

The primary metabolic products of synthetic communities were quantified in terms of carbon and electron molarity (Figure 3.1C). The bi-culture of *R. cellulolyticum* and *M. hungatei* transferred 0.42 ± 0.007 mmole carbon and 3.33 ± 0.06 mmole electron to CH_4. Introducing *D. vulgaris* to form a tri-culture resulted in a 112% increase in carbon and electrons transferred to CH_4. In the quad-culture, 1.37 ± 0.03 mmole carbon and 10.99 ± 0.21 mmole electron were transferred to CH_4, representing a 226% increase compared to the tri-culture of *R. cellulolyticum*, *M. concilii,* and *M. hungatei*, as well as compared to the cumulative transfers in the bi-culture of *R. cellulolyticum* with *M. concilii* or *M. hungatei*. This suggests that the presence of *D. vulgaris* enhanced the transfers of carbon and electrons to CH_4. Additionally, carbon and electrons transfer to acetate production was negatively correlated with MIP (r = -0.69, *p*-value = 0.002) and positively correlated with MRO (r = 0.76, *p*-value = 0.005), indicating that acetate production is highly responsive to shifts in resource cooperation and competition within these communities.

Metaproteomics identified a total of 1296 proteins across all eight cultures, based on unique peptide identifications assigned to individual proteins. The metabolic matrix from our previous stoichiometric model was refined in this study to include six reactions [166]: lactate fermentation, hydrogenic acetogenesis, mixed-acid fermentation,

hydrogenic lactate oxidation, hydrogenotrophic methanogenesis, and acetoclastic methanogenesis (Figure S3.1), along with ATP and biomass information. The contributions of each reaction were fitted to the accumulative measurements of lactate, acetate, ethanol, H_2, CO_2, CH_4 and biomass. The correlation co-efficient R^2, exceeded 0.9 in all cultures, and the normalized root mean square error (NRMSE) was 0.084 (Figure S3.1). The strong agreement between the experimental data and the modeling results confirmed plausible estimate of carbon and energy flow in the system. Flux calculations for two oxidized end products confirmed a positive synergistic effect on CO_2 and CH_4 production in more complex microbial communities, reinforcing findings from previous studies. Furthermore, the calculations indicated that different microbial assemblies predominantly influence acetoclastic methanogenesis, affecting both CO_2 and methane production (Figure 3.1D).

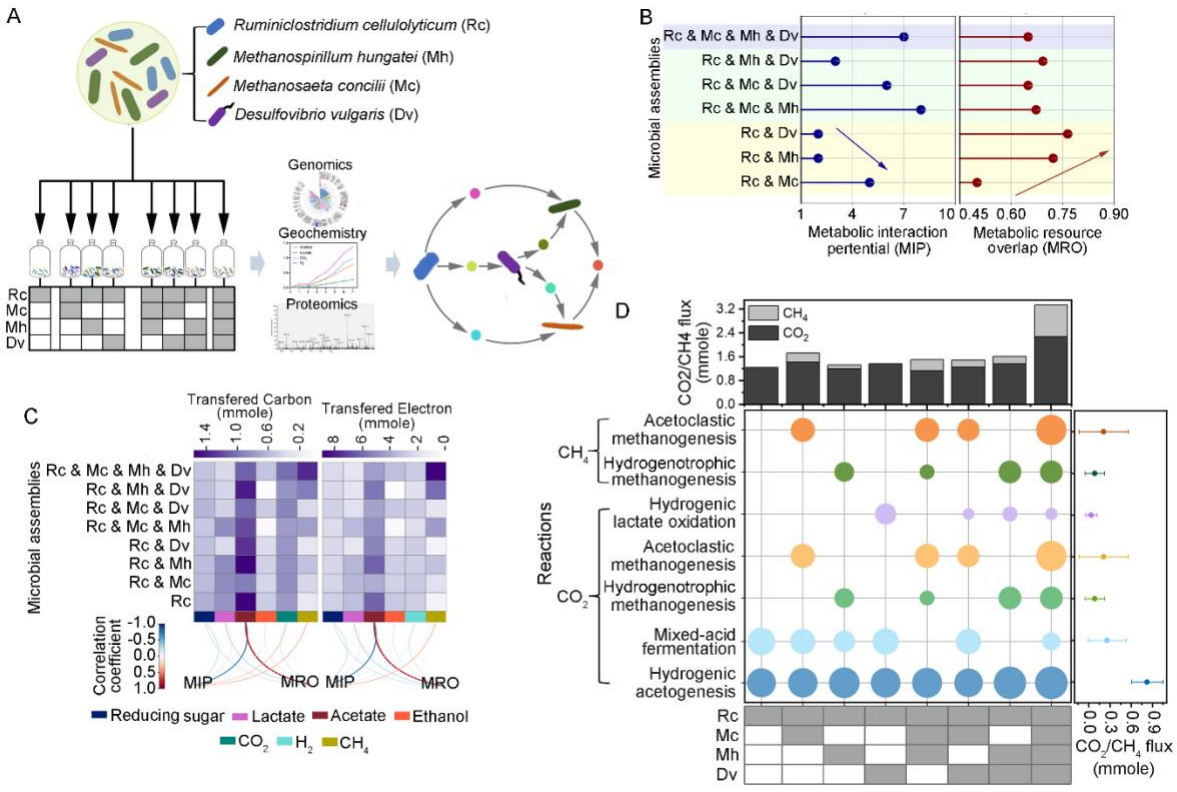

Figure 3.1 Synthetic community assembly. (A) Schematics of the combinatorial experimental setup. (B) Metabolic Interaction Potential (MIP) and Metabolic Resource Overlap (MRO) across seven synthetic microbial communities. (C) Cumulative production of fermentation products quantified by carbon molarity and electron molarity in different co-cultures, with correlations to MIP and MRO scores. (D) Fluxes of key metabolic reactions contributing to methane (CH_4) and carbon dioxide (CO_2) production. The cycles represent seven days of reaction fluxes, and error bars indicate the range of fluxes observed in CH_4 and CO_2 production across eight microbial assemblies. Rc: *Ruminiclostridium cellulolyticum,* the cycle represents the seven days' fluxes though reactions, and the error bar represent the range of fluxes producing CH_4 and CO_2 from each reaction across eight microbial assemblies. Mh: *Methanospirillum hungatei,* Mc: *Methanosaeta concilii*, Dv: *Desulfovibrio vulgaris.*

3.4.2 Enhanced cellulose degradation through multi-species metabolic interactions

Cellulose degradation by *R. cellulolyticum* was significantly enhanced when co-cultured with three other species (Figure 3.2A). This enhancement correlated with a higher abundance of cellulase in these co-cultures compared to mono-culture, as revealed by metaproteomics analysis (Figure 3.2C). Over 7 days of incubation, the *R. cellulolyticum* mono-culture degraded 184.4 ± 0.5 mg of cellulose. When co-cultured with *D. vulgaris*, cellulose degradation increased by up to 10.5% (*p*-value = 0.002). However, adding *M. concilii* to the bi-culture of *R. cellulolyticum* and *D. vulgaris* resulted in a 3% decrease in cellulose degradation (*p*-value = 0.03). No significant change was observed with adding *M. hungatei* to this bi-culture (*p*-value = 0.2). Incorporating both methanogens into the bi-culture of *R. cellulolyticum* and *D. vulgaris* to form a quad-culture, led to a 3% increase in cellulose degradation compared to the bi-culture (*p*-value = 0.008), and a 5% increase compared to tri-culture of *R. cellulolyticum*, *D.*

vulgaris, and either *M. concilii* (*p*-value = 0.003) or *M. hungatei* (*p*-value = 0.02). These observations suggest that the community structure and species interactions significantly influence the promotion of cellulose degradation by *R. cellulolyticum*.

SMETANA scores from community simulations using the SMETANA framework revealed a dynamic equilibrium between self-reliance and mutualistic cooperation among species [175] (Figure 3.2B). In microbial communities, an organism can function as a “receiver” or “donor”, based on the direction of metabolite transfer between a pair. In the bi-culture of *R. cellulolyticum* and *D. vulgaris*, the total SMETANA score was 2.12 when *R. cellulolyticum* acted as donor, and 2.46 when it was the receiver, indicating a mutualistic relationship. When *R. cellulolyticum*’s acted as donor in the bi-culture with *M. concilii* or *M. hungatei*, the SMETANA score was 4.60 and 4.85, respectively. However, when *R. cellulolyticum* was the receiver, the SMETANA score decreased by 47.8% in bi-culture with *M. concilii*, and decreased by 83.1% in the bi-culture with *M. hungatei*, suggesting reduced metabolic dependence of *R. cellulolyticum* on these two methanogens compared to its interaction with *D. vulgaris*. Additionally, in the tri-cultures and quad-culture, *R. cellulolyticum* functioned solely as a metabolic donor to the communities.

Metaproteomics identified key enzymes involved in the fermentation pathways of *R. cellulolyticum* across all eight cultures, including those for H_2, CO_2, lactate, acetate, and ethanol production (Figure 3.2C). Compared to the *R. cellulolyticum* mono-culture, the protein abundance of the sugar-related ABC transporter (Ats) remained unchanged in the bi-cultures, but significantly decreased in the tri-cultures and quad-culture (*p-adjust* < 0.0001). The protein abundance of NADH-fd reductase (Nhd) in H_2 production,

as well as acetaldehyde dehydrogenase (Aad) and alcohol dehydrogenase (His) in ethanol production, significantly increased in bi-cultures (*p-adjust* < 0.0001), but decreased in the tri-cultures and quad-culture (*p-adjust* < 0.0001). These differences suggest altered fermentation activities in *R. cellulolyticum* as it transitioned from pairwise interactions to high-order interactions with other three microbes. Additionally, compared to the mono-culture, the protein abundance of hydrogenase (Hyd) involved in H_2 production decreased up to 1.37-fold (*p-adjust* < 0.0001) in the bi-culture of *R. cellulolyticum* and *M. concilii*. In the tri-culture and quad-culture, this decreased was more than 30-fold (*p-adjust* < 0.0001), Suggesting that *R. cellulolyticum* maintained low hydrogen partial pressure by reducing H_2 production, thereby promoting syntrophic growth in the communities—a phenomenon that became more pronounced as community complexity increased.

Furthermore, the metabolic process of lactate fermentation, hydrogenic acetogenesis and mixed-acid fermentation in *R. cellulolyticum* were modeled across all cultures (Figure 3.2D). The fluxes of lactate fermentation and mixed-acid fermentation decreased when *R. cellulolyticum* was co-cultured with other species. In the bi-cultures and tri-cultures with *D. vulgaris*, the flux of lactate fermentation was lower than in cultures without *D. vulgaris*. Notably, in the quad-culture, the flux of lactate fermentation decreased by up to 88% (*p*-value < 0.0001). The flux of mixed-acid fermentation decreased more significantly in cultures containing *M. hungatei* compared to those without it. This was especially evident in the tri-culture of *R. cellulolyticum*, *M. hungatei* and *D. vulgaris*, where the flux of mixed-acid fermentation was longer detectable. Conversely, the flux through hydrogenic acetogenesis increased when *R. cellulolyticum*

was co-cultured with other species, particularly with *M. hungatei* and *D. vulgaris*. Compared to the mono-culture, the flux increased by 58.8% (*p*-value = 0.0004) in the tri-culture of *R. cellulolyticum*, *M. hungatei* and *D. vulgaris*, and by 61.8% (*p*-value = 0.0009) in the quad-culture. These observations suggest that the presence of *M. hungatei* and *D. vulgaris* significantly altered the metabolic pathways of *R. cellulolyticum* by reducing certain fermentation processes while enhancing others, depending on the specific microbial interactions in the community.

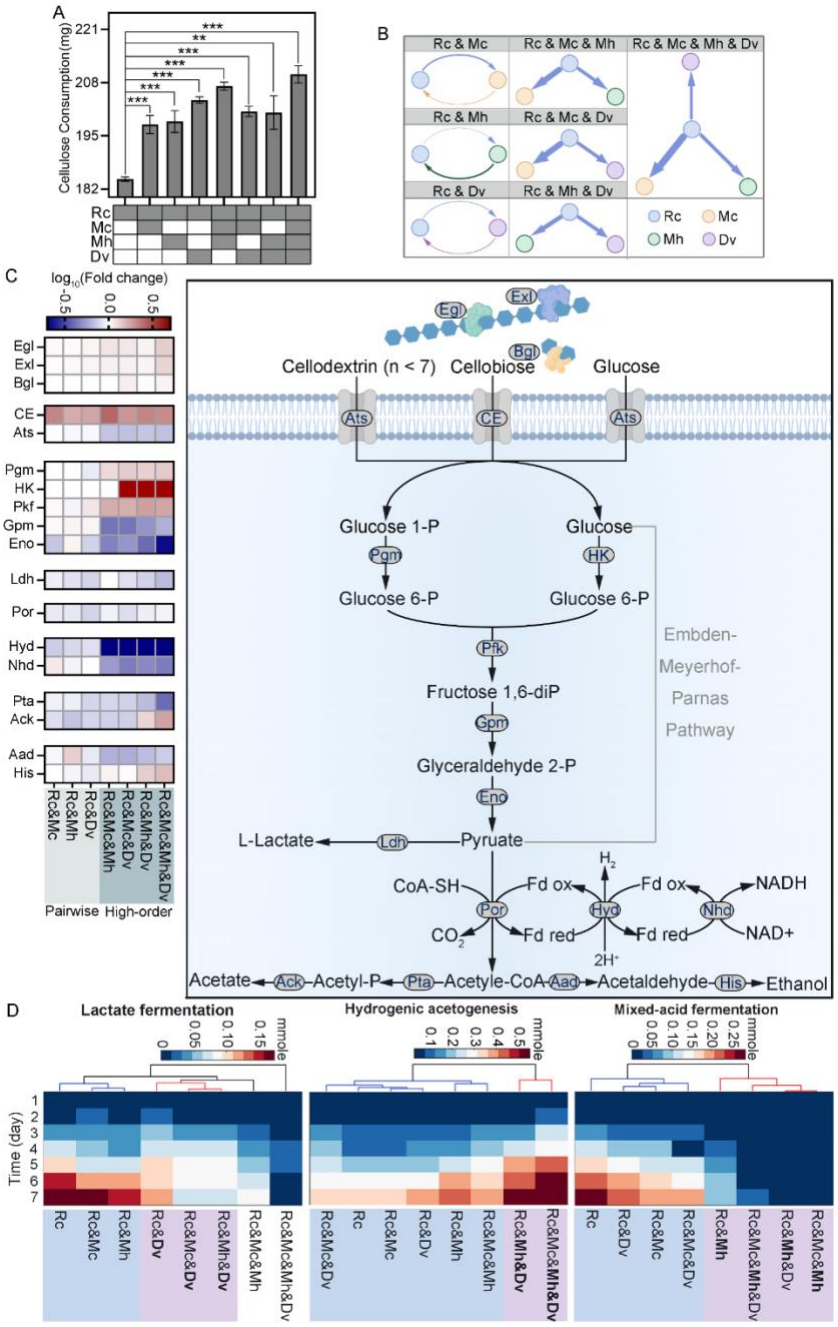

Figure 3.2 Metabolic activities of *R. cellulolyticum* in synthetic communities. (A)Comparison of cellulose consumption by *R. cellulolyticum* among different cultures. Significant differences with *p*-values determined using Student's t-test, and adjusted for the false discovery rate, are marked by * for *p*-value < 0.05, ** for *p*-value < 0.01 and *** for *p*-value < 0.001. The error bars are defined as standard deviation. (B) Cross-feeding interactions between *R. cellulolyticum* and other species in all the synthetic

communities. (C) Protein expression profile of the major carbon metabolism pathways in *R. cellulolyticum*. (D) Fluxes of the key reactions in *R. Cellulolyticum* modeled in all cultures. Rc: *Ruminiclostridium cellulolyticum,* Mh: *Methanospirillum hungatei,* Mc: *Methanosaeta concilii*, Dv: *Desulfovibrio vulgaris.*

3.4.3 Enhanced reliance and methanogenesis of *M. concilii* in complex communities

M. concilii showed increased dependency on other species in more complex synthetic communities. In both tri-cultures and quad-culture, *M. concilii* made no direct metabolic contributions, but showed greater reliance on the other three species. Compared to the bi-culture of *R. cellulolyticum* and *M. concilii*, the SMETANA score between these two species increased by 72.6% in the quad-culture (Figure 3.3A).

Metaproteomics identified four key enzymes in acetoclastic methanogenesis in *M. concilii*, including acetyl-CoA decarbonylase/synthase (CdhC), anaerobic carbon-monoxide dehydrogenase (CdhA), heterodisulfide reductase (Hdr) and methyl-coenzyme M reductase (Mcr) (Figure 3.3B). The abundances of these proteins significantly increased (q-value < 0.0001) in the tri-cultures and quad-culture compared to the bi-culture of *R. cellulolyticum* and *M. concilii*. This suggested that *M. concilii* enhances its methanogenic efficiency in more complex microbial environments.

The metabolic flux through acetoclastic methanogenesis was modeled in the *M.-concilii*-containing cultures (Figure 3.3C). In the bi-culture of *R. cellulolyticum* and *M. concilii*, the flux was 0.32 ± 0.03 mmole. Adding *M. hungatei* to this bi-culture did not significantly affect the flux (p-value = 0.87), while the addition of *D. vulgaris* decreased the flux by 28% (p-value = 0.005). However, In the quad-culture, the flux increased by

153% (*p*-value < 0.0001) compared to the tri-culture of *R. cellulolyticum*, *M. concilii* and *M. hungatei*. Moreover, it was 47% (*p*-value = 0.006) higher than the sum of flux in the bi-culture of *R. cellulolyticum* and *M. concilii* and the tri-culture of *R. cellulolyticum*, *M. concilii* and *D. vulgaris*. This suggests that *D. vulgaris* facilitates synergistic interactions between *R. cellulolyticum*, *M. concilii,* and *M. hungatei*, significantly enhancing the methanogenesis efficiency of *M. concilii* in complex microbial communities.

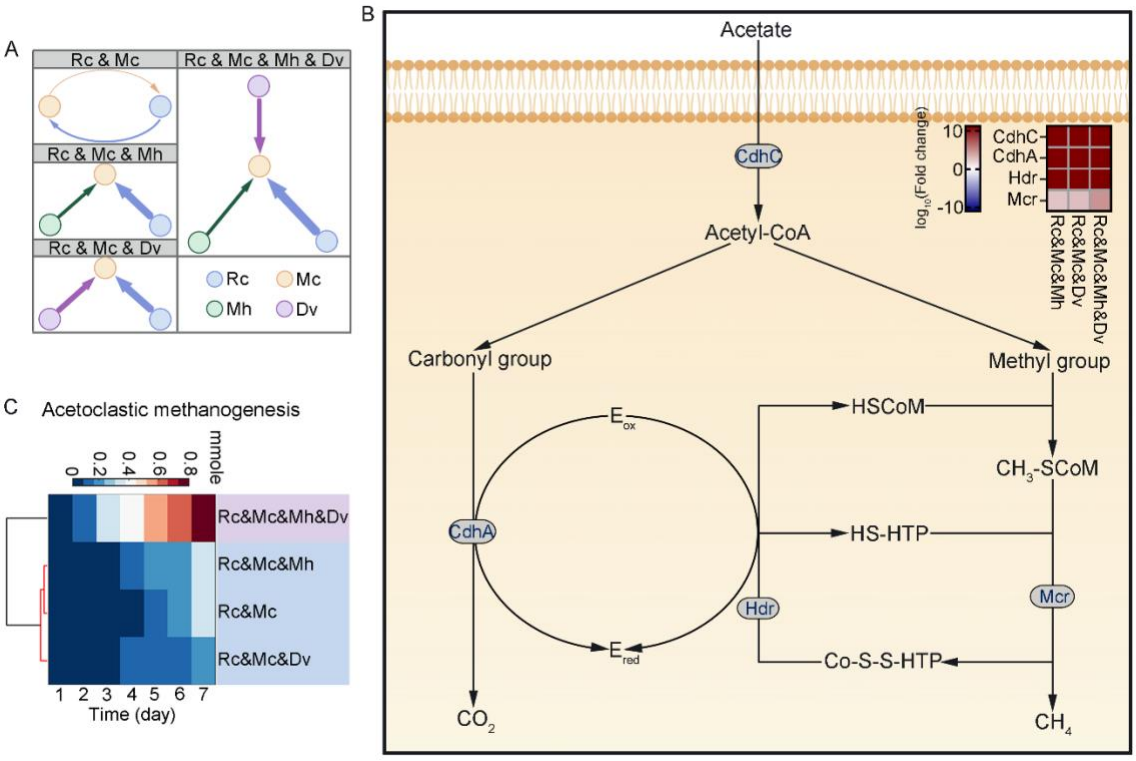

Figure 3.3 Metabolic activities of *M. concilii* in synthetic communities. (A) Cross-feeding interactions between *M. concilii* and other species in all synthetic communities. (B) Functional proteins profiling of acetoclastic methanogenesis. (C) Flux of acetoclastic methanogenesis modeled in *M. concilii*. Rc: *Ruminiclostridium cellulolyticum,* Mh: *Methanospirillum hungatei,* Mc: *Methanosaeta concilii*, Dv: *Desulfovibrio vulgaris.*

3.4.4 Reduced metabolic contribution of *M. hungatei* and enhanced methanogenesis

M. hungatei tends to have a smaller metabolic contribution when *D. vulgaris* is present in microbial communities (Figure 3.4A). In the bi-culture of *R. cellulolyticum* and *M. concilii*, where *M. hungatei* acted as the donor, the SMETANA score was 0.82. However, the addition of *D. vulgaris* resulted in *M. hungatei* ceasing to contribute metabolically. Similarly, in the tri-culture of *R. cellulolyticum*, *M. hungatei,* and *M. concilii*, where *M. hungatei* was the donor, the SMETANA score was 2.54. The introduction of *D. vulgaris* led to an 18.3% reduction in the score. Additionally, the presence of *M. concilii* reduced the metabolic reliance of *M. hungatei* within the community. When *M. hungatei* acted as the receiver in the bi-culture of *R. cellulolyticum* and *M. hungatei*, the SMETANA score was 4.85. Introducing *M. concilii* into this bi-culture caused the score to decrease by 11.5%. Likewise, when *M. concilii* was introduced to the tri-culture of *R. cellulolyticum*, *M. hungatei,* and *D. vulgaris*, forming a quad-culture, *M. hungatei's* SMETANA score as receiver decreased from 4.59 to 4.03.

Two key enzymes in hydrogenotrophic methanogenesis—formylmethanofuran dehydrogenase (Fmd) and formate dehydrogenase (Fdh)—were identified across these co-cultures (Figure 3.4B). Compared to the bi-culture of *R. cellulolyticum* and *M. hungatei*, the abundance of these functional proteins significantly increased in tri-cultures and quad-culture (fold change > 30, q-value < 0.0001), indicating enhanced methanogenesis activity due to more complex microbial interactions.

Furthermore, *D. vulgaris* was found to significantly enhance the metabolic efficiency of hydrogenotrophic methanogenesis (Figure 3.4C). Over seven days, the presence of *D. vulgaris* led to a 78.6% increase in the flux of hydrogenotrophic

methanogenesis (*p*-value = 0.01), compared to the bi-culture of *R. cellulolyticum* and *M. hungatei*. Similarly, compared to the tri-culture of *R. cellulolyticum*, *M. concilii* and *M. hungatei*, the flux through this reaction increased by 525% in the quad-culture (*p*-value < 0.0001).

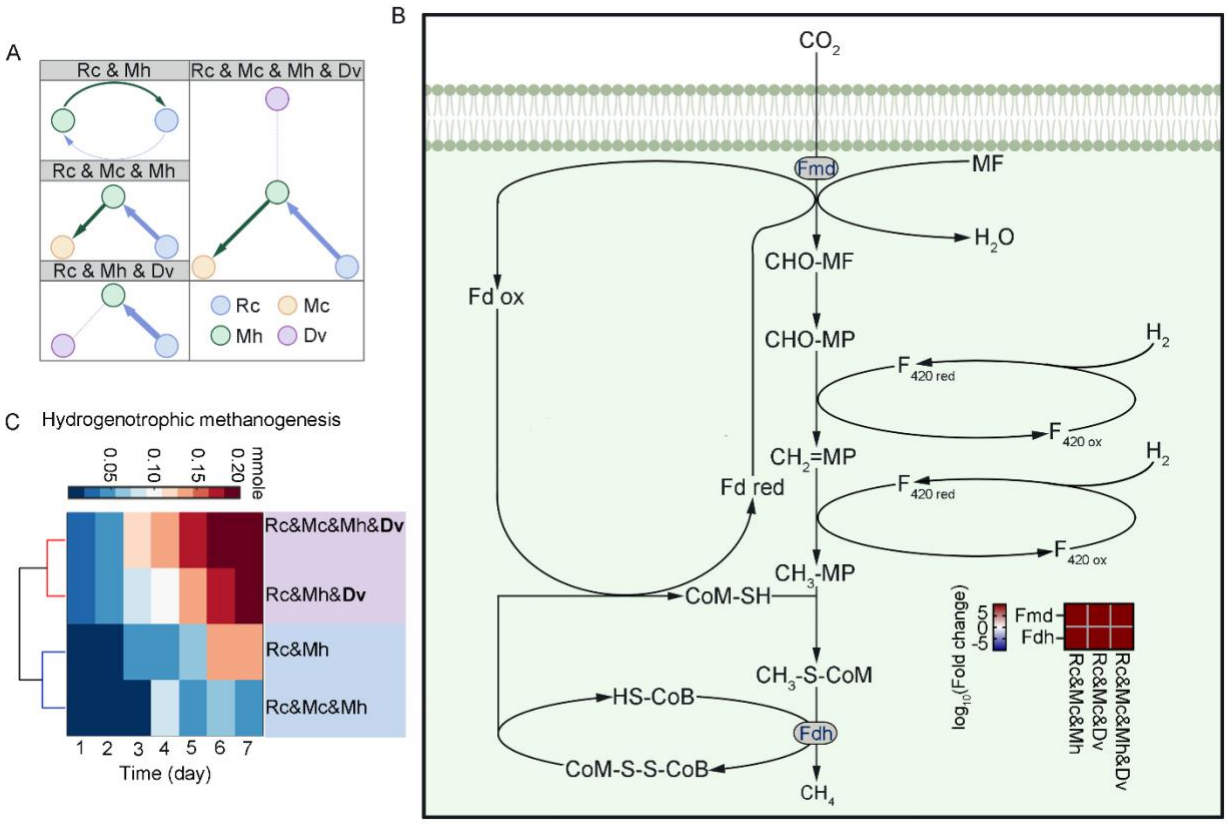

Figure 3.4 Metabolic activities of *M. hungatei* in synthetic communities. (A) Cross-feeding interactions between *M. hungatei* and other species in all synthetic communities. (B) Functional proteins profiling of hydrogenotrophic methanogenesis. (C) Flux of hydrogenotrophic methanogenesis modeled in *M. hungatei*. Rc: *Ruminiclostridium cellulolyticum,* Mh: *Methanospirillum hungatei,* Mc: *Methanosaeta concilii*, Dv: *Desulfovibrio vulgaris.*

3.4.5 Decreased lactate and hydrogen metabolism in multiple-species interactions

In the absence of sulfate, *D. vulgaris* can oxidize lactate to produce H_2. Compared to its interactions with *M. hungatei*, interactions between *D. vulgaris* and *M. concilii* result in a greater reduction in H_2 accumulation (Figure 3.5A). Introducing *M. hungatei* to the bi-culture of *R. cellulolyticum* and *D. vulgaris* resulted in a 13.2% decrease in H_2 accumulation (*p*-value = 0.005), a reduction comparable to that observed in the tri-culture of *R. cellulolyticum D. vulgaris* and *M. hungatei* compared to the mono-culture (13%, *p*-value = 0.0008). Additionally, adding *M. concilii* to the bi-culture of *R. cellulolyticum* and *D. vulgaris* led to a 14.5% decrease in H_2 accumulation (*p*-value < 0.0001). The subsequent addition of *M. hungatei* to this tri-culture did not produce any significant changes compared to the tri-culture baseline.

The presence of *M. concilii* or *M. hungatei* affected the metabolic contribution of *D. vulgaris* in contrasting ways—*M. concilii* increased the contribution, while *M. hungatei* decrease it (Figure 3.5B). When *D. vulgaris* acted as the metabolic donor, its SMETANA score increased by 114.6% after the *M. concilii* was introduced, compared to the bi-culture of *R. cellulolyticum* and *D. vulgaris*. In contrast, the addition of *M. hungatei* completely halted the metabolic contribution of *D. vulgaris*. Moreover, introducing *M. hungatei* to the tri-culture of *R. cellulolyticum*, *M. concilii* and *D. vulgaris*, led to a 21.4% decrease in SMETANA score of *D. vulgaris*. When *D. vulgaris* acted as receiver, *R. cellulolyticum* was its primary metabolic donor. Compared to the bi-culture of *R. cellulolyticum* and *D. vulgaris*, the SMETANA score of *D. vulgaris* increased by 34.0% with the addition of *M. concilii* , and by 102.4% with addition of *M. hungatei*. However, when both *M. concilii* and *M. hungatei* were added to form a quad-culture, the

SMETANA score of *D. vulgaris* increased by only 42.5%, compared to the bi-culture. This increase was lower than the combined effect of their separate addition, indicating a negative synergistic effect of *M. concilii* and *M. hungatei* on the metabolic dependency of *D. vulgaris*.

Metaproteomics identified six key enzymes in the hydrogenic lactate oxidation pathway of *D. vulgaris*: L-lactate permease (Lpe), L-lactate dehydrogenase (Ldh), Pyruvate:ferredoxin oxidoreductase (Por) and Phosphate acetyltransferase (Pat), periplasmic [NiFeSe] hydrogenase (Hyd), membrane-bound Coo hydrogenase (Coo) (Figure 3.5C). Compared to the bi-culture of *R. cellulolyticum* and *D. vulgaris*, the abundance of L-lactate permease, Pyruvate: ferredoxin oxidoreductase and Phosphate acetyltransferase—enzymes involved in lactate fermentation— significantly increased in co-cultures, correlating with decreased lactate accumulation. In contrast, the protein abundance of Periplasmic [NiFeSe] hydrogenase, involved in H_2 production, decreased by up to 92.3-fold (q-value < 0.0001) in the tri-culture of *R. cellulolyticum*, *M. concilii* and *D. vulgaris*, and decreased by 30-fold (q-value < 0.0001) in the tri-culture of *R. cellulolyticum*, *M. hungatei* and *D. vulgaris*, as well as in the quad-culture. These findings suggest an adaption by *D. vulgaris* aimed at reducing the H_2 pressure, facilitating syntrophic interactions with other microbes.

Hydrogenic lactate oxidation in *D. vulgaris* was modeled across all the co-cultures (Figure 3.5D). In the bi-culture of *R. cellulolyticum* and *D. vulgaris*, the flux was 0.18 ± 0.01mmole. This flux significantly decreased in the quad-culture and tri-cultures containing *D. vulgaris*, with a reduction of up to 89.9% observed in the quad-culture.

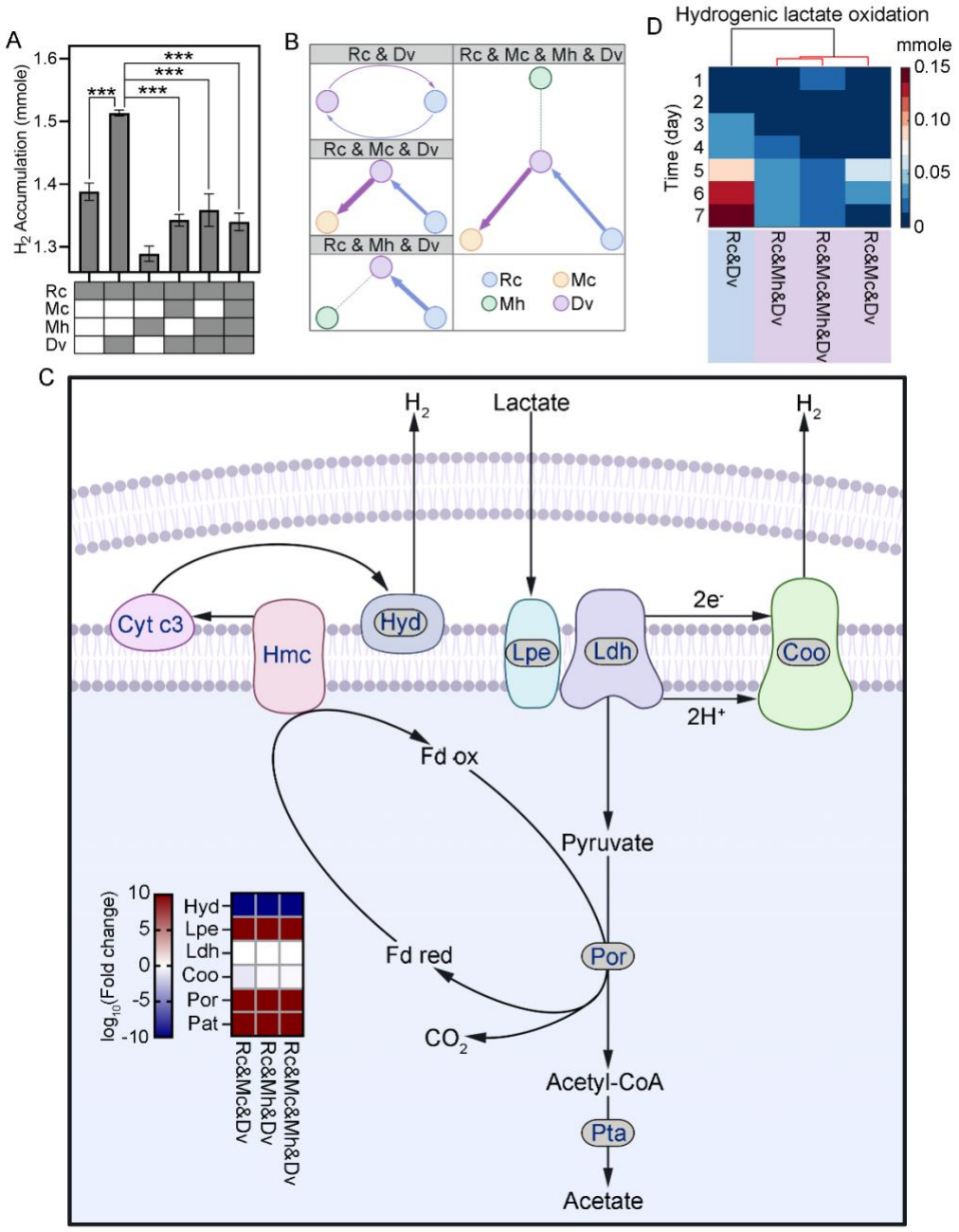

Figure 3.5 Metabolic activities of *D. vulgaris* in synthetic communities. (A) Comparison of H_2 accumulation in the co-cultures with *D. vulgaris*. (B) Cross-feeding interactions between *M. hungatei* and other species in all synthetic communities. (C) Functional proteins profiling of hydrogenic lactate oxidation. (D) Flux of hydrogenic lactate oxidation modeled in *D. vulgaris*. Rc: *Ruminiclostridium cellulolyticum,* Mh: *Methanospirillum hungatei,* Mc: *Methanosaeta concilii*, Dv: *Desulfovibrio vulgaris.*

3.4.6 Microbial interactions from modeling carbon and energy flow

The stoichiometric model estimated metabolic exchange fluxes, allowing the inference of interactions among microbial community members (Figure 3.6A). Specifically, the interactions between *R. cellulolyticum* and *M. concilii* were inferred from acetate-related fluxes, while the interactions between *R. cellulolyticum* and *M. hungatei* were deduced from fluxes associated with H_2 and CO_2. Interactions between *R. cellulolyticum* and *D. vulgaris* were determined from lactate-and H_2-related fluxes. Additionally, the model inferred interactions between *M. concilii* and *M. hungatei* from CO_2-related fluxes, *M. concilii* and *D. vulgaris* from acetate fluxes, and *M. hungatei* and *D. vulgaris* from fluxes associated with lactate and H_2. The variations in these metabolic pathways and efficiencies of the partner organisms likely contributed to the observed differences in interactions within the communities.

The strength of metabolic linkage varied significantly among the three bi-cultures (Figure 3.6B). The strongest interaction was observed between *R. cellulolyticum* and *M. hungatei,* with an exchange flux of 0.68 ± 0.003 mmole. This was followed by the exchange flux between *R. cellulolyticum* and *M. concilii* at 0.32 ± 0.03 mmole. The weakest interaction was between *R. cellulolyticum* and *D. vulgaris*, with an exchange flux of only 0.18 ± 0.001 mmole. These results suggest that the degree of metabolic exchange is highly dependent on the metabolic complementarity between the two organisms.

In more complex ternary and quaternary interactions, the nature of microbial relationships—such as cooperation, inhibition, or competition—and the intensity of these interactions were significantly altered, which impacted overall metabolic dynamics

and efficiency (Figure 3.6B). Compared to the bi-culture of *R. cellulolyticum* and *M. hungatei*, the addition of *M. concilii* decreased the exchange flux by 72.1% (*p*-value < 0.0001). However, the addition of *D. vulgaris* increased the exchange flux by 72.1% (*p*-value = 0.006). When *M. concilii* was subsequently added to this tri-culture, no significant change in the exchange flux was observed (*p*-value = 0.76), suggesting that *M. concilii* weakened the interaction between *R. cellulolyticum* and *M. hungatei* in the presence of *D. vulgaris*. This pointed to a dynamic equilibrium between *R. cellulolyticum* and *M. hungatei* in quaternary interactions. Compared to the bi-culture of *R. cellulolyticum* and *M. concilii*, the exchange flux between *R. cellulolyticum* and *M. concilii* remained unchanged after the addition of *M. hungatei* (*p*-value = 0.87). However, the addition of *D. vulgaris* decreased the exchange flux by 31.2% (*p*-value = 0.004). When *M. hungatei* was added to this tri-culture, the exchange flux increased by 146.9% (*p*-value < 0.0001), suggesting that in the quaternary interactions, *M. hungatei* significantly enhanced microbial interactions, counteracting the inhibitory effect of *D. vulgaris* on the interaction of *R. cellulolyticum* and *M. concilii*. Similarly, compared to the bi-culture of *R. cellulolyticum* and *D. vulgaris*, the presence of *M. concilii* decreased the exchange flux by 88.9% (*p*-value < 0.0001), and the addition of *M. hungatei* reduced the exchange flux by 61% (*p*-value = 0.005). However, the addition of both *M. concilii* and *M. hungatei* increased the exchange flux by 83.3% (p-value < 0.0001), suggesting that the presence of both *M. concilii* and *M. hungatei* can overcome each other's inhibitory effects on the interaction of *R. cellulolyticum* and *D. vulgaris*, leading to a synergistic enhancement of microbial interactions in the quaternary culture.

In addition to common exchange fluxes observed in the bi-cultures, three emergent fluxes were identified in the tri-cultures and the quad-culture. The flux between *M. concilii* and *M. hungatei* in the tri-culture was 0.012 ± 0.001 mmole. The flux between *M. concilii* and *D. vulgaris* in the tri-culture was 0.005 ± 0.001 mmole, both of which increased by 75% to 88% (*p*-value < 0.0001) in the quad-culture. The flux between *M. hungatei* and *D. vulgaris* in the tri-culture was 0.07 ± 0.02 mmole, which remains unchanged in the quad-culture (*p*-value = 0.78). These observations suggest that the presence of multiple microbial species in the quad-culture can significantly alter the metabolic interactions compared to simpler bi- or tri-cultures. The emergence of new metabolic fluxes and the dramatic interactions observed in multi-species communities highlight the complexity that should be considered in models aiming to predict and understand microbial behavior in natural and engineered environments.

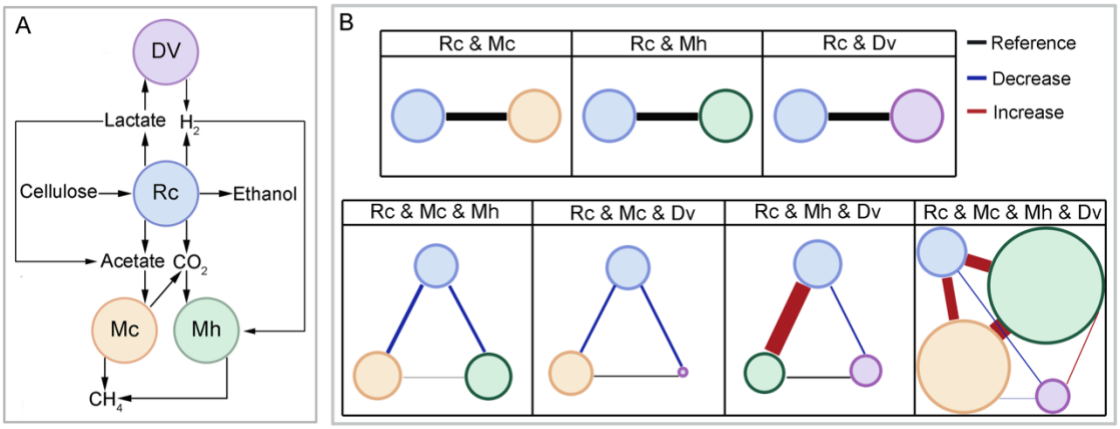

Figure 3.6 Stoichiometric modeling of synthetic communities. (A) Conceptual metabolic network among four microbial species in the synthetic community. (B) Exchanging fluxes estimating the metabolic interactions between species. The edges represent the exchange flux, and the circles represent the biomass. Rc: *Ruminiclostridium cellulolyticum,* Mh: *Methanospirillum hungatei,* Mc: *Methanosaeta concilii*, Dv: *Desulfovibrio vulgaris.*

3.5 Discussion

In our previous study [166], we observed both positive and negative synergies in the quad-culture. Methane production was enhanced due to cooperative cross-feeding, while cellulose degradation was suppressed due to increased competition and negative synergy. Additionally, we highlighted the role of sulfate in modulating community interactions, showing that sulfate addition altered metabolic exchanges and intensified substrate competition [166]. However, our previous analyses were limited to proteomic profiling and metabolic modeling of only the quad-culture. The metabolic model developed in that study was based on a stoichiometric matrix, where each reaction was sequentially excluded to access redundancy. As a results, we identified multiple possible flux distributions for quad-culture under both control and sulfate-enrich conditions. While this approach provided qualitative insights into metabolic flexibility, it introduces uncertainties, since several reaction fluxes were represented as ranges rather fixed values. This limitation hindered a comprehensive understanding of individual reactions' contributions to overall microbial metabolism.

In the present study, we addressed these limitations by refining the metabolic matrix composition and incorporating energy constraints, allowing for the determination of fixed values for all metabolic fluxes. Additionally, we expanded the scope of analysis from the quad-culture to the three bi-cultures and three tri-culture. By integrating experimental proteogenomic data with stoichiometric modeling across eight combinations of the four organisms, we obtained a deeper understanding of how microbial species cooperate and compete through binary, tertiary, and quaternary

interactions. The emergence of high-order interactions was revealed by the impact of a third or a fourth organisms on the metabolic interactions between two organisms.

Cooperative interactions, as indicated by higher MIP, were more significant in tri-cultures, particularly when *M. hungatei* and *D. vulgaris* were present. This observation suggests that syntrophic cooperation between methanogens and sulfate-reducing bacteria (SRB) modulates electron flow and stabilize community structure [169, 176, 177]. In tri-cultures containing *M. hungatei* and *M. concilii*, the presence of both methanogens further strength cooperative interactions, as demonstrated by increased MIP and reduced MRO. The reduction in MRO observed in tri-cultures compared to bi-cultures indicates that having multiple species reduces competition for shared resources, leading to a more balanced community metabolism. These findings are consistent with previous studies showing that methanogens can engage in competitive yet cooperative behaviors to optimize resource utilization and maintain stable methane production [178-180].

Our proteogenomic analysis further revealed that key metabolic pathways, such as hydrogenic acetogenesis, lactate fermentation, and methanogenesis, are highly sensitive to the community context. For instance, in the quad-culture, *R. cellulolyticum* significantly downregulated hydrogen production pathways, creating more favorable conditions for methanogens. This regulation was less significant in tri-cultures, suggesting that the presence of both *M. concilii* and *M. hungatei* in the quad-culture facilitates a more coordinated metabolic response, through cross-feeding or competitive exclusion mechanisms. Additionally, we observed that *R. cellulolyticum* downregulated cellulase expression in both tri-cultures and quad-cultures compared to bi-cultures,

potentially explaining the reduced cellulose degradation efficiency. These results indicated that as community complexity increases, competition for electron donors (e.g., hydrogen) and carbon sources becomes more intense, resulting in decreased cellulose degradation rates despite increased metabolic activity of individual species [181, 182].

Proteogenomic and metabolic modeling analyses revealed that higher-order interactions observed in the quad-culture are not simply a sum of pairwise interactions but are modulated by the presence of multiple species. For instance, *R. cellulolyticum* shifted its fermentation pathways from lactate to acetate production depending on the presence of methanogens or *D. vulgaris*. This adaptive strategy reduced hydrogen accumulation and promoted syntrophic growth with hydrogenotrophic methanogens. Such context-dependent shifts in metabolic pathways were not observed in simpler bi-cultures, indicating that microbial communities self-organize to optimize energy flow and minimize competition in more complex environments. Moreover, the role of *M. hungatei* as a hydrogen sink was influenced by the presence of *D. vulgaris*, demonstrating that higher-order interactions can either stabilize or destabilize key metabolic functions. These findings expanded on our previous observations by illustrating how the inclusion of additional species can either enhance or mitigate the competitive dynamics observed between *M. hungatei* and *D. vulgaris*, depending on the community context. Conventional studies focusing on pairwise species interactions may overlook the modulating effects of additional species on community cooperation and competition [100, 165, 183]. Our findings provide a more comprehensive understanding of anaerobic microbial ecosystems and pave the way for manipulating these communities

to optimize their functionality in diverse environments, from natural ecosystems to industrial applications.

Overall, our study demonstrated that microbial interactions in communities are highly context-dependent and shaped by the specific metabolic capabilities and ecological roles of individual species. The emergent properties observed in this study highlight the importance of considering community-level interactions rather than isolated pairwise interactions when studying microbial consortia. By expanding our analysis from mono- and bi-cultures to more complex tri- and quad-cultures, we provide a deeper understanding of the mechanisms that underpin microbial community assembly, stability, and functionality. These insights have broad implications for the management and engineering of microbial communities in various environmental and industrial applications, such as bioremediation, waste treatment, and the maintenance of gut health.

Chapter 4. Metaproteomics-informed stoichiometric modeling reveals the responses of wetland microbial communities to oxygen and sulfate exposure

4.1 Abstract

Climate changes significantly impact greenhouse gas emissions from wetland soil. Specifically, wetland soil may be exposed to oxygen (O_2) during droughts, or to sulfate (SO_4^{2-}) as a result of sea level rise. How these stressors – separately and together – impact microbial food webs driving carbon cycling in the wetlands is still not understood. To investigate this, we integrated geochemical analysis, proteogenomics, and stoichiometric modeling to characterize the impact of elevated SO_4^{2-} and O_2 levels on microbial methane (CH_4) and carbon dioxide (CO_2) emissions. The results uncovered the adaptive responses of this community to changes in SO_4^{2-} and O_2 availability and identified altered microbial guilds and metabolic processes driving CH_4 and CO_2 emissions. Elevated SO_4^{2-} reduced CH_4 emissions, with hydrogenotrophic methanogenesis more suppressed than acetoclastic. Elevated O_2 shifted the greenhouse gas emissions from CH_4 to CO_2. The metabolic effects of combined SO_4^{2-} and O_2 exposures on CH_4 and CO_2 emissions were similar to those of O_2 exposure alone. The reduction in CH_4 emission by increased SO_4^{2-} and O_2 was much greater than the concomitant increase in CO_2 emission. Thus, greater SO_4^{2-} and O_2 exposure in wetlands is expected to reduce the aggregate warming effect of CH_4 and CO_2. Metaproteomics and stoichiometric modeling revealed a unique subnetwork involving carbon metabolism that converts lactate and SO_4^{2-} to produce acetate, H_2S, and CO_2 when SO_4^{2-} is elevated under oxic conditions. This study provides greater quantitative resolution of key metabolic processes necessary for the prediction of CH_4 and CO_2 emissions from wetlands under future climate scenarios.

Keywords: Wetlands; Microbiome; Seawater intrusion; drought; Sulfate; Oxygen; Greenhouse gas; Proteogenomics; Stoichiometric modeling

4.2 Introduction

Wetlands store approximately one-third of global soil organic carbon (SOC) and play important roles in regulating and stabilizing global climate [184-186]. CH_4 and CO_2, the two greatest contributors to the greenhouse effect, are the dominant gaseous end-products from the mineralization of organic carbon in wetland ecosystems [187, 188]. Carbon fluxes in a wetland ecosystem are closely linked to its hydrological features [189]. Climate changes may introduce specific hydrology-related stressors. For instance, freshwater wetlands are increasingly vulnerable to drought events, which lower water tables and introduce O_2 into wetland soils. This leads to more frequent exposure of soil organic matter to O_2, thereby affecting the organic carbon balance [190]. In addition, freshwater wetlands face perturbations as a result of seawater intrusions. As the sea level rises, the inundation of wetlands by seawater brings a high concentration of sulfate ions (SO_4^{2-}), substantially altering the sediment chemistry [185, 191, 192]. These stressors can change the production patterns of CH_4 and CO_2, resulting in feedback that is poorly characterized qualitatively in terms of the direction of the changes and quantitatively in terms of the magnitudes of the changes. Understanding how environmental disturbances affect the dynamic of metabolic processes and the succession of ecological communities is critical for accurately modeling changes in greenhouse gas emissions from wetland ecosystems in future climate scenarios.

Microbial interactions are vital in modulating organic matter decomposition and greenhouse gas emissions within wetland ecosystems [193, 194]. These interactions are driven by fermentation and respiration, coupling the oxidation of organic compounds

by electron transfer to electron acceptors [166, 195, 196]. In the absence of disturbance by droughts and seawater intrusions, obligatory anaerobic fermenters become dominant [197]. Syntrophic interactions among these diverse anaerobic microorganisms facilitate the stepwise breakdown of complex organic substrates into simpler, chemically stable compounds, ultimately resulting in the production of CH_4 and CO_2 [198]. However, O_2 exposure introduced during drought can promote aerobic microbial respiration of carbon stocks, with CO_2 as the primary product [181]. The introduction of SO_4^{2-} from seawater inundation as an alternative electronic acceptor leads to sulfate-reducing bacteria (SRB) to produce more H_2S, utilizing H_2 and/ or organic acids as electron donors. The competition from SRBs for H_2 and organic acids may reduce methane production by methanogens [199, 200]. Characterizing these metabolic interactions provides insight into biochemical transformations within the community under changing redox conditions, and allows for investigations into how changes in these conditions, induced by climate change, will affect the microbial metabolic networks that control carbon cycling in wetland ecosystems.

Carbon cycling and gas emissions in wetlands have been studied extensively in both field and laboratory conditions [201-204]. Elevated CO_2 levels, reduced carbon accumulation, and decreased CH_4 emissions have been observed when introducing O_2 into previously anoxic wetland soil [203, 205]. Previous studies have also demonstrated lower CH_4 emissions to the atmosphere from lacustrine wetlands following seawater intrusion [21-23]. However, few studies have characterized how the critical syntrophic interactions controlling CH_4 and CO_2 productions respond to environmental redox

perturbations, such as increased O_2 from periods of drought or SO_4^{2-} from seawater intrusion.

Establishing a clear connection between environmental disturbance and microbial adaptions remains a challenge, due to the complex and dynamic nature of microbial communities [44, 206]. In this study, we set up laboratory microcosms to investigate the effects of SO_4^{2-} exposure and O_2 exposure alone or in combination on microbial activities and interactions, as well as the resulting fate of carbon within wetland soil (Fig. 1). We used proteogenomics to characterize the biochemical and physiological responses of microbial communities to individual perturbations and their combined effects. Stoichiometric models were employed to deconvolute carbon exchanges among the main functional guilds. By integrating geochemical, metaproteomic, and stoichiometric analyses, we aimed to develop a molecular understanding of how climate change-induced stressors modulate wetland microbial communities and greenhouse gas fluxes.

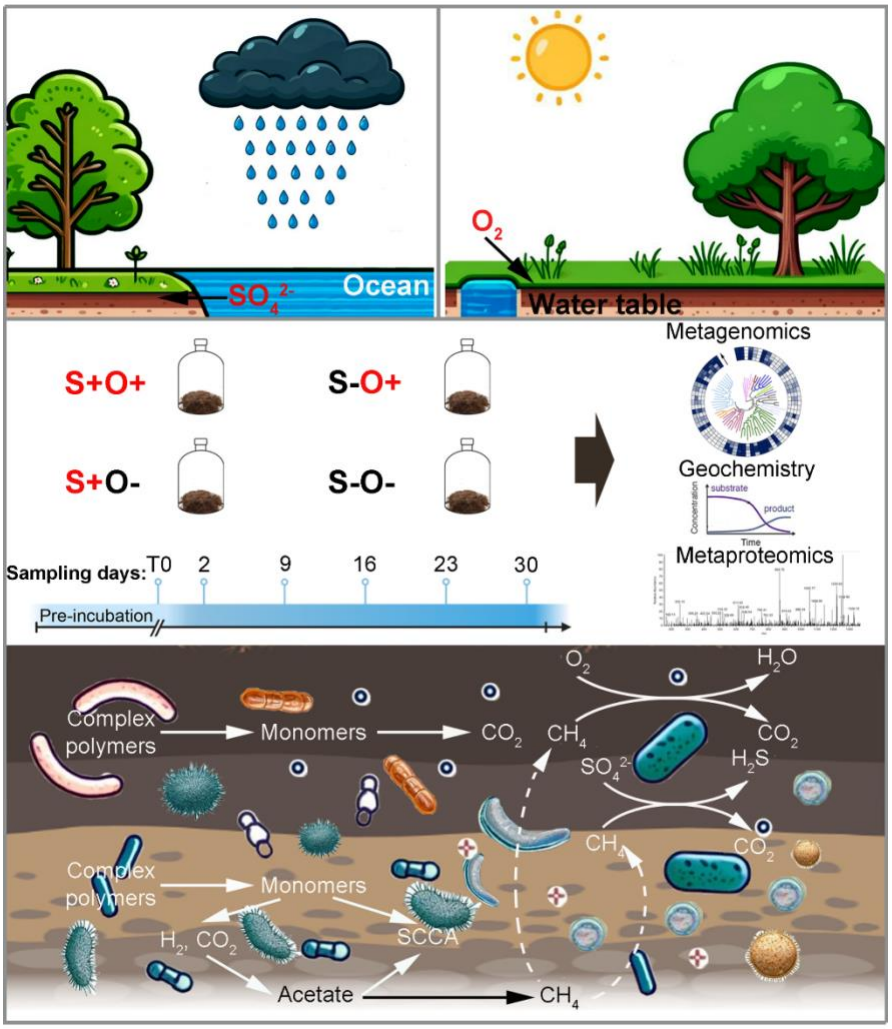

Figure 4.1 Schematic diagram of study design. Emissions of methane and carbon dioxide from wetland ecosystems can be severely perturbed by climate-change-induced stressors, such as seawater intrusions and droughts. To investigate this, we constructed laboratory microcosms using freshwater wetland soils under four incubation conditions, including anoxic non-sulfate addition (S-O-), anoxic sulfate-addition (S+O-), oxic non-sulfate addition (S-O+) and oxic sulfate-addition conditions. The soil communities were characterized by integrating geochemical analysis, metagenomics, metaproteomics and stoichiometric modeling. The results uncovered the molecular mechanism on how wetland microbial communities modulate greenhouse gas fluxes under future climate scenarios.

4.3 Materials and Methods

4.3.1 Sampling and soil microcosm set up. Triplicate soil samples were collected from a seasonally flooded urban freshwater wetland connected to Lake Washington in Seattle, WA, USA (Coordinates: 47.642196° N, -122.296236° W) in May 2022 using a soil core sampler with 2" x 6" plastic liners (AMS, Inc., American Falls, ID). The core sampler was forced approximately 60 cm into the sediment bed with a slide hammer to cut roots and other plant material. The three replicate soil cores were collected approximately one meter apart from each other, avoiding large tree branches or roots. The broader location was selected based on its variably submerged nature, with the water table generally being below the surface during the spring and summer months and above the surface during the spring and summer months. At the time of sampling, the water table was above the soil surface and the soil was completely saturated with water. The cores were sealed air-tight upon removal from the natural habitat, to protect the redox state of samples. Samples were then transported to the lab on ice, for immediate processing.

Microcosms were set up by filling 160 mL bottles with 40 g fresh sediment soil slurry in an anaerobic chamber. The chamber gas contained N_2 : H_2 (97:3). All bottles were preincubated for five days at room temperature and then incubated at 30 °C for 30 days. Soil microcosms were divided into four groups, with each group receiving specific treatments every two days: anoxic non-sulfate-addition, anoxic sulfate-addition (resulting in a final SO_4^{2-} concentration of approximately 7.2 mM), oxic non-sulfate-addition (where half of the gas phase was replaced by sterile air), and oxic sulfate-addition, which was treated with both SO_4^{2-} and sterile air. Sampling was conducted on

days 2, 9, 16, 23, and 30, with each group sacrificing three bottles for sampling at the indicated time points. During sampling, 10 mL of gas phase products were collected in vacuumed Labco exetainer gas vails for later analysis. Then 10 ml of PBS buffer was injected into the bottle, and shaken at 200 rpm for 10 min, after which 10 ml of well-shaken culture liquid was sampled, and stored at -80 °C for subsequent analysis.

4.3.2 Chemical analysis. Headspace pressure was measured using a pressure gauge (Cole Parmer SK-68900-24) before sampling. pH measurements were taken immediately after sampling. Analysis of H_2, CO_2 and CH_4 was carried out using a gas chromatograph (GC-8A, Shimadzu, Japan). H_2S in the gas phase was measured by an H_2S monitor (Forensics, FD-103-H2S, US), the H_2S dissolved in slurry was calculated based on the pH and the amount of H_2S in the gas phase. Absolute gas composition was calculated with the ideal gas law. The soluble sugars (glucose, xylose, mannose and galacturonic acid) and fermentation products (acetate, lactate, and butyrate) in the slurry were analyzed by high-performance liquid chromatography (HPLC) as reported previously [113]. The metabolic measurements were standardized using the gram of dry soil at the endpoint, which constitutes 22.9 ± 0.1 % of soil slurry.

4.3.3 DNA extraction and metagenomic sequencing. Only the initial soils from the field were sequenced using metagenomic analysis. The total DNA in the triplicate field soil samples was extracted using the PowerMaxSoil DNA isolation kit as described previously [207]. Metagenomic library preparation and DNA sequencing were performed at the Joint Genome Institute. The metagenomic libraries were prepared for sequencing using 2X151-bp lanes on the Illumina NovaSeq S4 platform. A total of 404,050,411 ± 23,970,278 sequence reads were obtained.

4.3.4 Metagenomic data processing. Metagenomic reads were preprocessed using BBTools for removing adaptors, trimming reads, and sequencing error correction [208]. The pre-processed reads from three replicates were co-assembled into a combined metagenome with SPAdes v3.15.5 [209], A total of 857,101 scaffolds with a length > 1kbp were retained. The total length and L50 of the assembly were 1,939,450,947 bp and 2420 bp, respectively. The percentage of sequencing reads mapped onto the scaffolds is 87%. Genes were called from these retained scaffolds using the Prodigal algorithm [210]. A total of 26,768,938 genes were identified. Gene functions were annotated using Kofamscan [211]. Taxonomic classification was carried out at the scaffold level using Kaiju, based on reference species in the NCBI RefSeq [212]. Metagenome-assembled genomes (MAGs) were obtained using MetaBAT v2.12.1 with default parameters [213]. The quality of MAGs was estimated using CheckM v1.1.2. The MAGs obtained were classified into high-quality MAGs with completeness > = 50% and contamination < 5%. The taxonomy classifications of high-quality MAGs were inferred using GTDB-Tk v2.3.2 [214].

4.3.5 Metaproteomics measurement. Soil cultures at the end of the experiment were analyzed by metaproteomics. Proteins were extracted as described previously. Briefly, soil samples were suspended in lysis buffer (containing 10 mM tris-HCl, 4% SDS and 10mm dithiothreitol), boiled for 5 min and further disrupted by sonication for a 2 min 10% pulse 5 times. The supernatant was collected by centrifugation at 14000g for 10 min. Proteins were then precipitated by TCA (trichloroacetic acid) overnight and pelleted by centrifugation. Protein pellets were washed with ice-cold acetone three times and resuspended in guanidine buffer. Protein concentrations were quantified by

Bicinchoninic Acid Assay. Twenty mg samples of proteins were processed using FASP (filter-aided sample preparation) and digested by Trypsin/LysC mixture. Each sample was analyzed using 2D-LC-MS/MS (two-dimensional liquid chromatography-tandem mass spectrometry) on an Orbitrap Fusion Tribrid mass spectrometer (Thermo Fisher Scientific, USA) at the IDeA National Resource for Quantitative Proteomics. Tryptic peptides were separated into 46 fractions on a 100 x 1.0 mm Acquity BEH C18 column (Waters) using an UltiMate 3000 UHPLC system (Thermo) with a 50 min gradient from 99:1 to 60:40 buffer A:B ratio under basic pH conditions, then consolidated into 12 super-fractions. Each super-fraction was then separated by reverse phase XSelect CSH C18 2.5 um resin (Waters) on an in-line 120 x 0.075 mm column using an UltiMate 3000 RSLCnano system (Thermo). Peptides were eluted using a 60 min gradient from 98:2 to 65:35 buffer A:B ratio. Eluted peptides were ionized by electrospray (2.4 kV) followed by mass spectrometric analysis on an Orbitrap Fusion Tribrid mass spectrometer (Thermo). MS data were acquired using the FTMS analyzer in profile mode at a resolution of 240,000 over a range of 375 to 1500 m/z. Following HCD activation, MS/MS data were acquired using the ion trap analyzer in centroid mode and normal mass range with normalized collision energy of 28-31% depending on charge state and precursor selection range. Protein identification and quantification followed established procedures. Briefly, mass spectrometry spectra were searched using Sipros Ensemble against a protein database constructed from the metagenome. Raw search results were filtered to achieve 1% FDR (false discovery rate) at the peptide level, which was estimated using the target-decoy approach. Peptide identifications are assigned to protein or protein groups in accordance with the parsimonious rule. To avoid ambiguity

in data analysis, protein groups were excluded from biological analysis. Protein quantification was achieved through Intensity-based label-free analysis using ProRata [215]. Protein abundances were quantified by the total peak height of all quantified peptides from a protein, normalized against the average total of all data sets [172-174].

Following previously described methods [216-218], the taxonomic annotations were assigned to the identified peptides based on the matched corresponding scaffold's taxonomic annotation information, which had a length greater than 1000bp. The relative abundance of a species is expressed as the sum of the abundances of all proteins detected that belong to this species. If a protein was identified in more than one species, its abundance was equally divided among these identified species. The richness and evenness of the communities were calculated using the vegan R package, based on the total protein abundance of species [219].

4.3.6 Construction of the stoichiometric model. A set of overall reactions depicting the documented metabolism of major functional populations was fit to the measured amounts of metabolites in the microcosms (Supplementary Fig. 3, Supplementary Fig. 4). The code used in fitting can be found on the Github https://github.com/thepanlab/WetlandSoil. The resulting fits provide a basis for quantifying metabolic contributions. Deviations between the inferred metabolic transformations and measured transformations indicate uncertainty in our understanding of the metabolic transformations or limitations in analytic capacity.

4.3.7 Statistical analysis. Pairwise comparisons for metabolic measurement data were carried out using Student's t-test, while metabolic fluxes from modeling were analyzed using Wald type II χ^2 tests. One-way or two-way ANOVA was used for comparisons

among groups of more than two. Differences in protein abundance in the metaproteome were analyzed by Deseq2 R package, which is based on a model using the negative binomial distribution to account for variance and mean linkage through local regression [220-222]. The *p*-values were adjusted to *q*-values using the Benjamini and Hochberg method for multiple comparison correction [123]. Differences with q-value < 0.05 were regarded as statistically significant.

4.3.8 Data availability. The metagenome data was deposited in NCBI under the accession code PRJNA1112840. Proteomic data are available at the ProteomeXchange Consortium via the PRIDE (Proteomics Identification Database) partner repository with the dataset identifier PXD047453. The rest generated or analyzed data during this study are included in this published article and Supplementary Table 4.1-4.3.

4.4 Results

4.4.1 SO_4^{2-} and O_2 additions changed community structure and activities

Laboratory microcosms were constructed using lacustrine wetland soils and incubated under four conditions: anoxic non-sulfate-addition (S-O-), anoxic sulfate-addition (S+O-), oxic non-sulfate-addition (S-O+), and oxic sulfate-addition (S+O+) (Figure 4.1). Sterile air was introduced under S-O+ and S+O+ conditions. The final concentration of SO_4^{2-} following addition under the S+O- and S+O+ conditions was approximately 7.2 mM, falling within the range of natural seawater concentration [223].

Metaproteomic analysis identified a total of 10598 proteins based on assignments of unique peptide identifications to individual proteins. These proteins originated from 807 microbial species and 50 phyla, with *Pseudomonadota* (~51% of total proteome abundance) and *Euryarchaeota* (~33% of total proteome abundance) being the dominant phyla (Figure 4.2A and Table S4.2). All experimental treatments resulted in an increase of *Pseudomonadota* in proteome abundance compared to the S-O- condition. However, the increase under dual exposure (S+O+, 82%, *p*-value < 0.000, t-test) was more than the addictive effect of the increase observed under the S+O- condition (45%, *p*-value = 0.001, t-test) and S-O+ condition (7%, *p*-value = 0.5, t-test). This suggests a synergistic interaction between the effects of SO_4^{2-} and O_2 on the proteome abundance of *Pseudomonadota*, where their combined impact on microbial communities is greater than the sum of their individual effects. Conversely, *Euryarchaeota* consistently decreased in proteome abundance upon stress exposure, although this reduction was less under dual exposure (S+O+, 52%, *p*-value = 0.0006, t-test) than the sum of the decreases under S+O- condition (29%, *p*-value = 0.008, t-test) and S-O+ condition (41%, *p*-value = 0.001, t-test) (Figure 4.2A). This suggests an

antagonistic interaction between the effects of SO_4^{2-} and O_2 on the proteome abundance of *Euryarchaeota*, where their combined impact on microbial communities is less than the sum of their individual effects.

Compared to the S-O- condition, the metaproteome abundances of active communities showed increased richness under both the S+O- (28%, *p*-value = 0.02, t-test) and S-O+ conditions (36%, *p*-value = 0.0009, t-test). There was also an increase in evenness under S+O- (5%, *p*-value = 0.04, t-test) condition, S-O+ condition (8%, *p*-value < 0.002, t-test), and S+O+ condition (9%, *p*-value = 0.001, t-test) (Figure 4.2B, 4.2c). This suggests that SO_4^{2-} and O_2 exposures contributed to the proliferation of low-abundance microbial species. Moreover, we found a negative correlation between the increased richness and evenness of the active community and the accumulation of CH_4 and a positive correlation with CO_2 accumulation (Figure 4.2D).

The primary metabolic products in the microcosm system were quantified by carbon (Figure 4.2E) and electron molarity (Figure 4.2F). Under the S-O- condition, the soil carbon was fermented into 0.32 ± 0.03 mmole/g dry soil of organic acids, 0.44 ± 0.02 mmole/g dry soil of CO_2, and 0.29 ± 0.01 mmole/g dry soil of CH_4 over seven days of incubation. Compared to S-O-, the SO_4^{2-} addition increased the carbon transfer to organic acids by 94% (*p*-value = 0.0003, t-test) and decreased the CH_4 production by 73% (*p*-value < 0.0001, t-test), and the O_2 exposure decreased the carbon transfer to organic acids by 76% (*p*-value = 0.0002, t-test), increased that to CO_2 by 70% (*p*-value < 0.0001, t-test), and eliminated the CH_4 production. Under the S-O- condition, 1.36 ± 0.13 mmole/g dry soil of electrons was transferred to organic acids, 0.19 ± 0.01 mmole/g dry soil to H_2, and 2.32 ± 0.63 mmole/g dry soil to CH_4. In comparison, the

SO_4^{2-} addition diverted 1.44 ± 0.07 mmole/g dry soil of electrons to H_2S and decreased the electron transfer to H_2 by 40% (*p*-value = 0.0004, t-test), and the O_2 exposure decreased the electron transfer to H_2 by 55% (*p*-value = 0.001, t-test). The effects of the combined exposure to both SO_4^{2-} and O_2 on the carbon and electron transfers were similar to the effects of the O_2 exposure only.

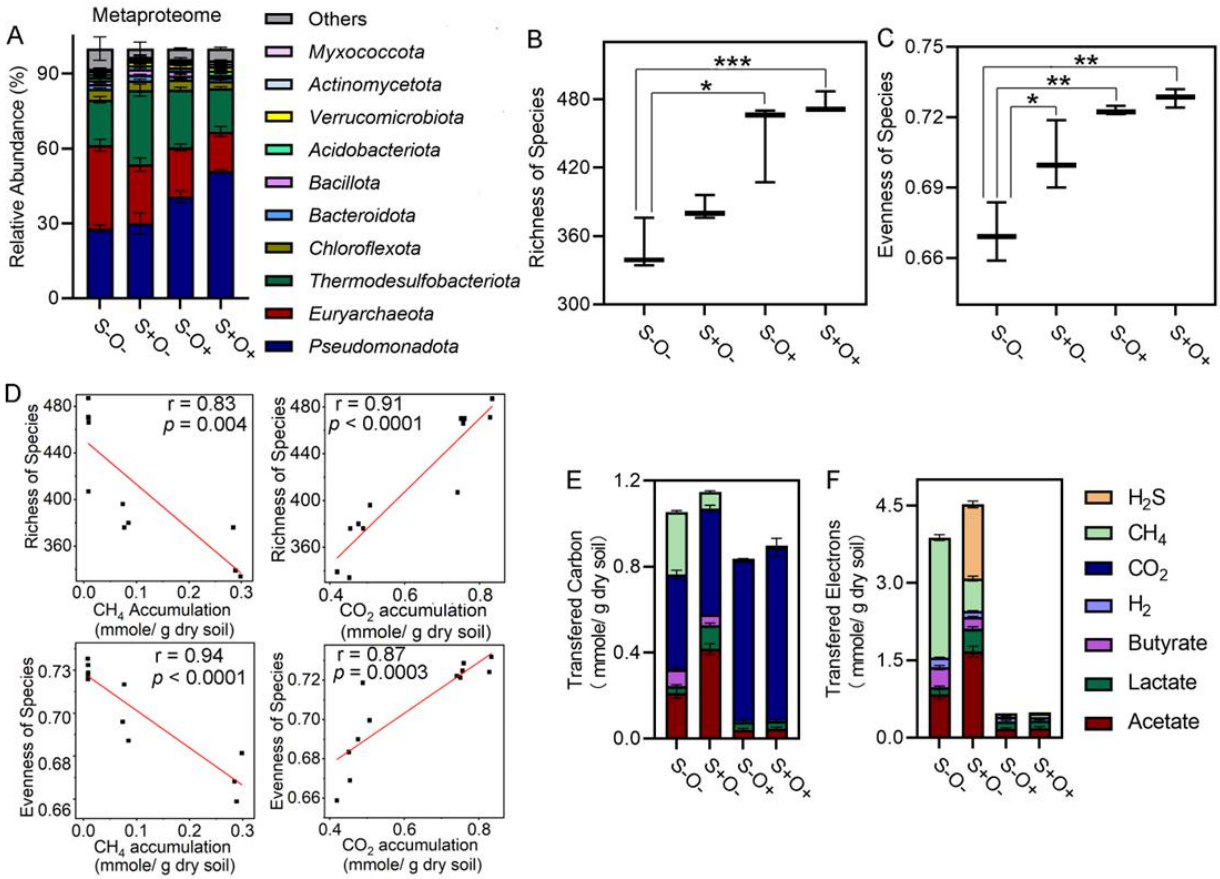

Figure 4.2 Effects of SO_4^{2-} and O_2 exposures on microbial community composition and activities. (A) Relative proteomic abundance of microbial phyla under four treatment scenarios. The relative proteomic abundance is expressed as the proportion of total proteins attributable to each microbial species. (B-C) Community species diversity indices, with (B) showing the richness and (C) the evenness across the four experimental conditions. Significant differences with p-values determined using Student's t-test and adjusted for the false discovery rate, are marked by * for *p*-value <

0.05, ** for *p*-value < 0.01 and *** for *p*-value < 0.001. (D) Correlation between microbial species diversity and the accumulations of CH_4 and CO_2, where each dot represents an experimental measurement (X-axis for geochemical measurements, Y-axis for metaproteomic measurements) from the four conditions with three replicates, and the red line displays best linear fit. r is the Pearson correlation coefficient, and p values were determined by t-statistic. (E-F) Cumulative amounts of fermentation products are measured by carbon molarity (E) and electron molarity (F) within the microcosms. The error bars are defined as standard deviation.

4.4.2 SO_4^{2-} and O_2 additions altered depolymerization of plant polysaccharides

The formation of hydrolysis products derived from plant polysaccharides, such as glucose, xylose, mannose, and galacturonic acid, was affected by exposure to SO_4^{2-} and O_2 over time (Figure S4.1A – 4.1D). Under both anoxic and oxic conditions, the addition of SO_4^{2-} slowed down the accumulation of glucose. This resulted in a 12% lower accumulation under anoxic conditions (*p*-value = 0.04, t-test) and a 14% reduced glucose accumulation (*p*-value = 0.02, t-test) under oxic conditions (Figure S4.1). Xylose reached its peak accumulation later under anoxic conditions compared to oxic conditions. The highest accumulation of xylose was observed under the S-O- condition, while its accumulation was relatively similar under the other three conditions. Mannose and galacturonic acid continuously accumulated under anoxic conditions. Their accumulation peaked between 16 to 23 days and then decreased under oxic conditions.

The metaproteomic analysis identified five key enzymes from species involved in the degradation of plant polysaccharides. These species had the highest proteome abundance under anoxic conditions. Pairwise comparisons of proteome richness and evenness of these species, between the S-O- condition and the S-O+ condition, as well

as between the S+O+ condition and the S+O+ condition, revealed no significant changes under different oxic conditions, which suggests that the actual species composition remained relatively stable across four conditions. A strong negative correlation (r = -0.70, *p*-value = 0.01, t-test) was observed between the total proteome abundance of plant polysaccharide-degrading microbes and the accumulation of CO_2 (Figure 4.3A). Conversely, a weak positive correlation was observed between the total proteome abundance of these microbes and the accumulation of CH_4 (Figure 4.3A).

The identified carbohydrate-active enzymes (CAZymes), including pectate lyase, beta-glucosidase, xylosidase, beta-galactosidase, and starch phosphorylase, showed the highest total abundance under the S-O- condition, and the lowest abundance under the S+O+ condition (Figure 4.3B). This indicates that elevated SO_4^{2-} and O_2 levels suppressed the activities of plant polysaccharide degradation.

Among the identified CAZymes, beta-glucosidase was detected across all conditions, with the highest abundance observed under the S+O- condition (fold change > 4.0, *q*-value < 0.007). Xylosidase, involved in xylan degradation, showed higher abundance under the S+O- condition (fold change > 3.2, *q*-value < 0.0001) (Table S4.3), indicating enhanced cellulose and xylan degradation capacity under this condition. Beta-galactosidase was only detected under the S+O+ condition (Table S4.3). This enzyme can release galactose from hemicellulose, which enters the glycolysis pathway after conversion into glucose 1-phosphate by glucuronate isomerase (UXA). The highest abundance of UXA proteins was detected under the S+O+ condition (fold change > 1.7, *q*-value < 0.0001) (Table S4.3), suggesting enhanced hemicellulose utilization under this condition. These observations collectively demonstrate that

changes in SO_4^{2-} and O_2 levels altered the preference of the microbial community in degrading plant polysaccharides. Specifically, the enzymes enriched under oxic conditions use more complex structural substrates (e.g., hemicellulose) compared to those enriched under anoxic conditions (e.g., cellulose).

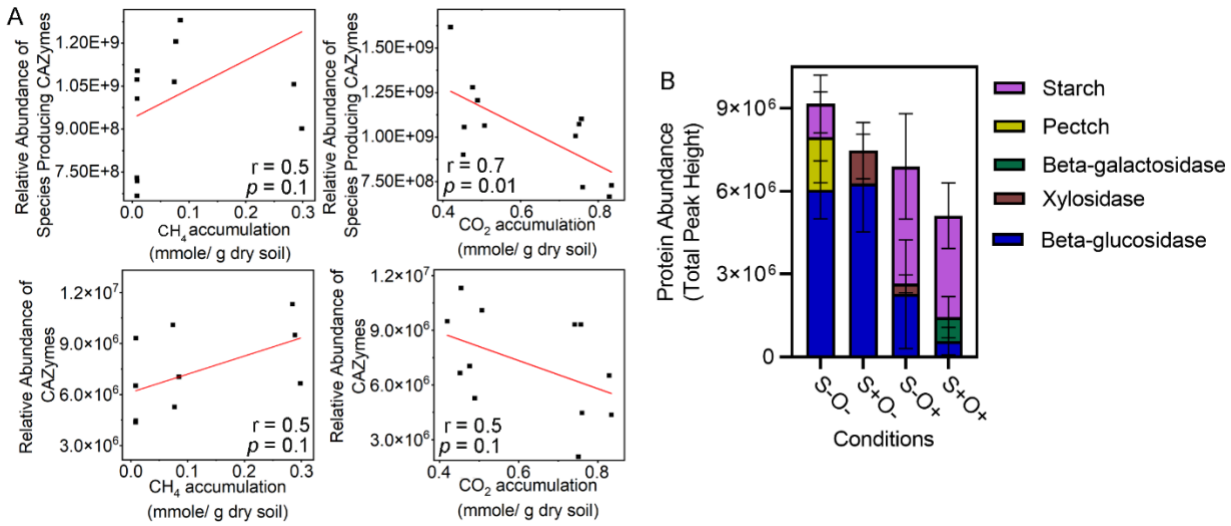

Figure 4.3 Effects of SO_4^{2-} and O_2 exposures on plant polysaccharide degradation. (A) Correlation analysis between the relative abundances of plant polymer degradation species and CAZymes with the accumulation of CH_4 and CO_2, where each dot represents experimental measurements (X-axis for geochemical measurements, Y-axis for metaproteomic measurements) from four conditions with three replicates, and the red line is the result of linear fitting. r is the Pearson correlation coefficient, and *p*-values were determined by t-test. (B) Protein abundances of CAZyme under the four conditions. The error bars are defined as standard deviation.

Table 4.1 Accumulation of metabolic products in the microcosms under the four incubation conditions.

Conditions / Metabolite	S-O-	S+O-	S-O+	S+O+
Glucose	0.023 ± 0.003	0.02 ± 0.002	0.02 ± 0.001	0.016 ± 0.001
Xylose	0.033 ± 0.001	0.023 ± 0.004	0.02 ± 0.002	0.02 ± 0.001
Mannose	0.008 ± 0.001	0.008 ± 0.001	0.011 ± 0.001	0.011 ± 0.001
Galacturonic acid	0.015 ± 0.003	0.016 ± 0.002	0.019 ± 0.001	0.015 ± 0.001
H_2	0.096 ± 0.005	0.058 ± 0.003	0.044 ± 0.009	0.037 ± 0.001
CO_2	0.44 ± 0.02	0.49 ± 0.02	0.75 ± 0.008	0.81 ± 0.04
CH_4	0.29 ± 0.007	0.079 ± 0.006	0.009 ± 0.001	0.008 ± 0.001
H_2S	0	0.18 ± 0.008	0	0.003 ± 0.001
Acetate	0.11 ± 0.012	0.21 ± 0.013	0.021 ± 0.002	0.022 ± 0.004
Lactate	0.01 ± 0.002	0.037 ± 0.004	0.012 ± 0.002	0.013 ± 0.002
Butyrate	0.02 ± 0.002	0.012 ± 0.004	0	0

4.4.3 SO_4^{2-} and O_2 decreased methanogenesis and promoted methane oxidation

Under the S-O- condition, the microbial community continuously produced CH_4 (0.29 ± 0.007 mmole/g dry soil) and CO_2 (0.44 ± 0.02 mmole/g dry soil) throughout the experiment (Figure 4.4A, 4.4B). The two-way ANOVA indicated a significant interaction between SO_4^{2-} and O_2 on CH_4 accumulation ($F(1,8) = 1590$, p-value < 0.0001). CH_4 release was reduced by 73% (p-value < 0.0001, t-test) under the S+O- condition, and by 97% (p-value < 0.000, t-test) under the S-O+ condition (Figure 4.4A and Table 4.1), highlighting the higher sensitivity of CH_4 accumulation to O_2 than to SO_4^{2-}. However, the same analysis showed no significant interaction between SO_4^{2-} and O_2 ($F(1, 8) = 0.1$, p-value = 0.75). The main effects were observed, CO_2 accumulation increased by 11% higher under the S+O- condition (p-value = 0.03, t-test), by 70% higher under the S-O+ condition (p-value < 0.0001, t-test), and by 83% higher under the S+O+ condition (p-

value = 0.0002, t-test), compared to the S-O- condition (Figure 4.4B), suggesting an addictive effect of SO_4^{2-} and O_2 on CO_2 accumulations.

Metaproteomic analysis identified 634 proteins from methanogens (Table S4.1). These methanogens showed the highest proteome abundance under the S-O- condition, constituting 22% of the total metaproteome (Table S4.1). The addition of SO_4^{2-} and O_2, either individually or in combination, led to a reduction in the proteome abundance (*p*-value < 0.0001, one-way ANOVA), richness (*p*-value = 0.005, one-way ANOVA), and evenness (*p*-value = 0.008, one-way ANOVA) of methanogenic populations (Figure 4.4C, 4.4D and 4.4E). Furthermore, strong positive correlations were observed between the CH_4 accumulation and the proteome abundance (r = 0.9, *p*-value < 0.0001, t-test), richness (r = 0.9, *p*-value = 0.0001, t-test), as well as evenness (r = 0.8, *p*-value = 0.002, t-test) of methanogens (Figure S4.2). In summary, the observed relationships among SO_4^{2-} and O_2 availability, CH_4 accumulation, and the composition of methanogen populations could serve as diagnostics for more predictive climate modeling.

Metaproteomics revealed significant suppression of both hydrogenotrophic and acetoclastic methanogenesis by SO_4^{2-} and O_2. Many marker proteins involved in methanogenesis, including methyl-coenzyme M reductase (Mcr), 5,10-methylenetetrahydromethanopterin reductase (Mer), tetrahydromethanopterin S-methyltransferase (Mtr), acetyl-CoA decarbonylase/synthetase (CdhA) and methylenetetrahydromethanopterin dehydrogenase (Mtd) were most abundant under S-O- condition (Figure 4.4F and Table 4.2). The addition of SO_4^{2-} and O_2, either individually or in combination, led to a significant decrease in the abundance of these

proteins (Figure 4.4F). This decrease coincided with the decrease in CH_4 emissions observed when exposed to SO_4^{2-} and O_2 stressors (Figure 4.4A).

Furthermore, the SO_4^{2-} and O_2 exposures suppressed hydrogenotrophic methanogenesis much more than acetoclastic methanogenesis. Specifically, after SO_4^{2-} addition to the anoxic sediment, the abundance of acetyl-CoA decarbonylase/synthetase essential for acetoclastic methanogenesis, decreased by 1.2-fold (*q*-value = 0.0001). And there was a more pronounced decrease in proteins for hydrogenotrophic methanogenesis (Figure 4.4F, Table 4.2), including a 3.4-fold decrease of the 5,10-methylenetetrahydromethanopterin reductase (*q*-value = 0.003) and a 5.8-fold decrease of the tetrahydromethanopterin S-methyltransferase (*q*-value < 0.0001). This indicated a stronger suppression of hydrogenotrophic methanogenesis by SO_4^{2-}. Under S-O+ condition, we observed a decrease in proteins for both the acetoclastic and hydrogenotrophic pathways of methanogenesis when compared to S-O- condition. In the acetoclastic pathway, there was a 2.6-fold decrease in acetyl-CoA synthetase (Acs) (*q*-value = 0.01) and a 2.1-fold decrease in methyl-coenzyme M reductase (*q*-value < 0.0001) (Figure 4.4F, Table 4.2). In the hydrogenotrophic pathway, there was a 7.0-fold decrease in the methylenetetrahydromethanopterin dehydrogenase (*q*-value < 0.0001) and a 3.1-fold decrease in methyl-coenzyme M reductase (*q*-value = 0.02). Similarly, under S+O+ condition, compared to the S+O- condition, there was a more substantial decrease in key enzymes associated with hydrogenotrophic methanogenesis, including a 9.2-fold decrease in 5,10-methylenetetrahydromethanopterin reductase (*q*-value < 0.0001) and a 5.0-fold decrease in tetrahydromethanopterin S-methyltransferase (*q*-value < 0.01), compared to

a 1.5-fold decrease in acetyl-CoA decarbonylase/synthetase (*q*-value = 0.006). These results highlight that O_2 had a greater suppression of hydrogenotrophic methanogenesis than acetoclastic methanogenesis. Moreover, compared to the S-O- condition, under S+O+ condition, the abundance of methyl-coenzyme M reductase decreased by 1.7-fold (*q*-value = 0.01), and the abundance of tetrahydromethanopterin S-methyltransferase decreased by 8.7-fold (*q*-value < 0.0001). This suggests that the combined addition of SO_4^{2-} and O_2 had a more significant impact on hydrogenotrophic methanogenesis compared to acetoclastic methanogenesis.

In addition, metaproteomics identified 208 proteins from methanotrophs (Table S1). Under the S+O+ condition, methanotrophs showed the highest richness (*p*-value = 0.0001, one-way ANOVA), and evenness (*p*-value = 0.0004, one-way ANOVA) (Figure 4.4c – 4.4e). Moreover, significant negative correlations were found among the CH_4 accumulation and proteome abundance (r = -0.7, *p*-value = 0.02, t-test), richness (r = -0.9, *p*-value < 0.0001, t-test), and evenness (r = -0.8, *p*-value = 0.002, t-test) of active methanotrophs (Figure S4.2).

Key enzymes involved in methane oxidation, including methane/ammonia monooxygenase (Pmo) and lanthanide-dependent methanol dehydrogenase (XoxF), showed distinct responses to elevated SO_4^{2-} and O_2 (Figure 4.4F and Table 4.2). Under the anoxic condition, SO_4^{2-} addition increased the abundance of methane/ammonia monooxygenase and lanthanide-dependent methanol dehydrogenase by 2.3-fold (*q*-value < 0.0001) and 1.4-fold (*q*-value = 0.0002), respectively. However, under the oxic conditions, SO_4^{2-} addition decreased the abundance of lanthanide-dependent methanol dehydrogenase by 1.7-fold (*q*-value = 0.005). Oxygen addition led to an increase in the

abundance of methane/ammonia monooxygenase and lanthanide-dependent methanol dehydrogenase by 3.9-fold (q-value < 0.0001) and 2.5-fold (q-value = 0.006), respectively, under the non-sulfate-addition condition. Under the sulfate-addition condition, their abundance increased by 1.7-fold (q-value = 0.005) and 3.0-fold (q-value < 0.0001), respectively. Furthermore, when compared to S-O- condition, the abundance of methane/ammonia monooxygenase and lanthanide-dependent methanol dehydrogenase increased by 4.2-fold (q-value < 0.0001) and by 3.9-fold (q-value = 0.001) under S+O+ condition (Figure 4.4F, Table 4.2).

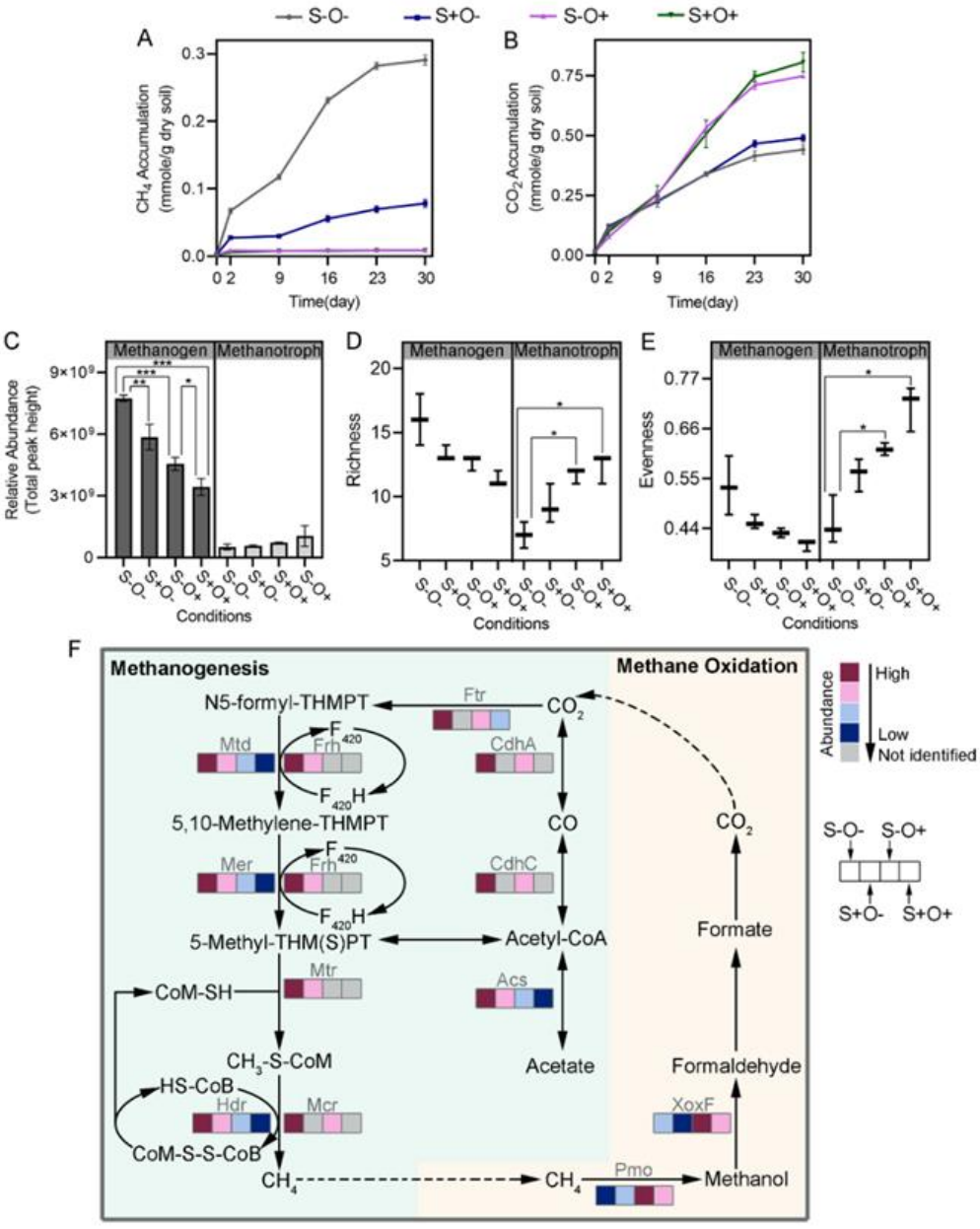

Figure 4.4 Modulation of methane metabolism by SO42- and O2 exposures. (A-B) Changes in molar mass of CH4 (A) and CO2 (B) under the four conditions, over a 30-day incubation. (C-E) Comparison of methanogens and methanotrophs in terms of relative abundance (C), richness (D) and evenness (E) under the four conditions. Relative abundance is quantified as the aggregate of protein abundances attributable to a specific species. (F) Schematic representation of methane metabolic pathways. The boxes in the pathway map, arranged from left to right, correspond to the S-O-, S+O-, S-

O+ and S+O+ conditions. The color gradient from red to blue represents the relative abundance ranking of proteins among the four conditions, with red indicating the highest ranked relative abundance and blue the lowest. The grey color indicates proteins not detected by LC-MS/MS. Significant differences with *p*-values determined using Student's t-test, and adjusted for the false discovery rate, are marked by * for *p*-value < 0.05, ** for *p*-value < 0.01 and *** for *p*-value < 0.001. The error bars are defined as standard deviation.

Table 4.2 Proteins in methane metabolism and sulfate reduction pathway.

Processes	Enzymes	Symbol	Comparison				
			S-O- vs. S+O-	S-O+vs. S+O+	S-O- vs. S-O+	S+O- vs. S+O+	S-O- vs. S+O+
			Fold Change (*padj*)	Fold Change (*padj*)	Fold Change (*padj*)	Fold Change (*padj*)	Fold Change (*padj*)
Hydrogenotrophic Methanogenesis	methyl-coenzyme M reductase	Mcr	-	-	3.1 (*) ▼	-	-
	5,10-methylenetetrahydromethanopterin reductase	Mer	3.4 (**) ▼	-	-	9.2 (***) ▼	-
	tetrahydromethanopterin S-methyltransferase	Mtr	5.8 (***) ▼	-	-	5.0 (*) ▼	8.7 (***) ▼
	methylenetetrahydromethanopterin dehydrogenase	Mtd	-	-	7.0 (***) ▼	-	-
Acetoclastic Methanogenesis	acetyl-CoA decarbonylase/synthetase	CdhA	1.2 (***) ▼	-			
	acetyl-CoA synthetase	Acs	-	-	2.6 (*) ▼	1.5 (**) ▼	-
	methyl-coenzyme M reductase	Mcr	-	-	2.1 (***) ▼	-	1.7 (*) ▼
Methane Oxidation	methane/ammonia monooxygenase	Pmo	2.3 (***) ▲	-	3.9 (***) ▲	1.7 (**) ▲	3.9 (**) ▲
	lanthanide-dependent methanol dehydrogenase	XoxF	1.4 (***) ▲	1.7 (**) ▲	2.5 (**) ▲	3.0 (***) ▲	4.2 (***) ▲
Sulfate Reduction	pyruvate ferredoxin oxidoreductase	Por	8.0 (***) ▲	1.8 (**) ▲	1.4 (***) ▼		5.7 (***)
	acetyl-CoA synthetase	Acs	5.3 (***) ▲	2.4 (***) ▲	3.2 (***) ▼	2.0 (***) ▼	-
	sulfate adenylyltransferase	Sat	1.4 (**) ▲	2.8 (***) ▲	2.3 (**) ▼	1.2 (*) ▼	1.2 (***) ▼
	adenylylsulfate reductase	Apr	1.8 (***) ▲	-	1.3 (**) ▼	1.5 (**) ▼	1.2 (**) ▼
	dissimilatory sulfite reductase	Dsr	1.5 (**) ▲	1.6 (***) ▲	1.4 (***) ▼	-	-

▲ significant increase, ▼ significant decrease, - no significant changes were observed.

4.4.4 SO_4^{2-} and O_2 additions changed metabolic behaviors of sulfate-reducing bacteria

Under the sulfate-limited conditions, some sulfate-reducing bacteria (SRB) function as syntrophic oxidizers, metabolizing lactate to produce acetate, H_2, and CO_2. With added SO_4^{2-}, SRB may oxidize lactate to acetate and CO_2 and concurrently reduce SO_4^{2-} to H_2S [224]. Two-way ANOVA indicated a significant interaction between SO_4^{2-} and O_2 on lactate accumulation ($F(1,8) = 66.51$, p-value < 0.0001), with significant main effects of SO_4^{2-} ($F(1, 8) = 55.4$, p-value < 0.0001) and O_2 ($F(1, 8) = 74.76$, p-value < 0.0001). Under the S-O- condition, lactate substantially accumulated, reaching its peak of 0.033 ± 0.004 mmole/g dry soil on day 9, and then decreased to 0.018 ± 0.002 mmole/g dry soil over the next 7 days. Under the S+O- condition, lactate accumulation continually increased, reaching 0.037 ± 0.004 mmole/g dry soil at the end of incubation. Under oxic conditions, lactate accumulation remained consistently low at less than 0.012 ± 0.004 mmole/g dry soil over 30 days (Figure 4.5A). Similarly, the two-way ANOVA for H_2S accumulation revealed a significant interaction between SO_4^{2-} and O_2 ($F(1, 8) = 1222$, p-value < 0.0001), with significant main effects for both SO_4^{2-} and O_2. Specifically, a substantial accumulation of H_2S (0.18 ± 0.008 mmole/g dry soil) was observed under the S+O- condition, while only trace amounts of H_2S (0.003 ± 0.0002 mmole/g dry soil) were detected under the S+O+ condition (Figure 4.5B).

Metaproteomics identified a total of 145 proteins from SRB species, with the highest SRB proteome abundance observed under S+O- condition (fold change > 1.3, p-value < 0.006, t-test) (Figure 4.5C, Table S4.1). SO_4^{2-} addition enhanced the activities of both lactate oxidation and dissimilatory sulfate reduction within this community (Figure 4.5D – 4.5F and Table 4.2). In the lactate oxidation pathway, SO_4^{2-} addition

resulted in an 8.0-fold increase in the abundance of pyruvate ferredoxin oxidoreductase (Por) (*q*-value < 0.0001) and a 5.3-fold increase in acetyl-CoA synthetase (*q*-value < 0.0001). In the dissimilatory sulfate reduction pathway, the abundance of adenylylsulfate reductase (Apr) increased by 1.8-fold (*q*-value < 0.0001), sulfate adenylyltransferase (Sat) increased by 1.4-fold (*q*-value = 0.002), and dissimilatory sulfate reductase (Dsr) increased by 1.5-fold (*q*-value = 0.005) following SO_4^{2-} addition (Figure 4.5F, Table 4.2).

Oxygen addition significantly suppressed the activities of lactate oxidation and dissimilatory sulfate reduction. The response of key proteins in both pathways to O_2 varied with the availability of SO_4^{2-}. In the lactate oxidation pathway, the reduction in the abundance of acetyl-CoA synthetase was more significant when comparing S-O- to S-O+ condition (2.6- fold decrease, *q*-value = 0.01), than when comparing S+O- to the S+O+ condition (1.5-fold decrease, *q*-value = 0.006). A 1.4-fold reduction (*q*-value < 0.0001) in pyruvate ferredoxin oxidoreductase was observed only when comparing S-O- to S-O+ condition, suggesting that O_2 showed a stronger suppressive effect under the sulfate-sufficient condition. Conversely, in the dissimilatory sulfate reduction pathway, the suppressive effect of O_2 was intensified under sulfate-limited conditions, as indicated by a larger decrease in the abundance of sulfate adenylyltransferase when comparing S-O- to S-O+ condition (2.3-fold decrease, *q*-value = 0.007), than when comparing S+O- to S+O+ condition (1.2-fold decrease, *q*-value = 0.01). Additionally, a 1.4-fold (*q*-value = 0.0001) decrease in the abundance of dissimilatory sulfate reductase was only observed when comparing S-O- to S-O+ condition (Figure 4.5F, Table 4.2) and no significant change when comparing S+O- to S+O+ condition.

Furthermore, metaproteomics analysis identified a total of 779 proteins from sulfide/sulfur-oxidizing bacteria (SOB), with the highest SOB proteome abundance observed under S+O+ condition (Figure 4.5C and Table S4.1). The proteome abundance of SOBs was negatively correlated with the CH_4 accumulation (r = -0.7, *p*-value = 0.01, t-test), while the evenness of SOBs showed a positive correlation with the CH_4 accumulation (r = 0.8, *p*-value = 0.0006, t-test) (Figure S4.2).

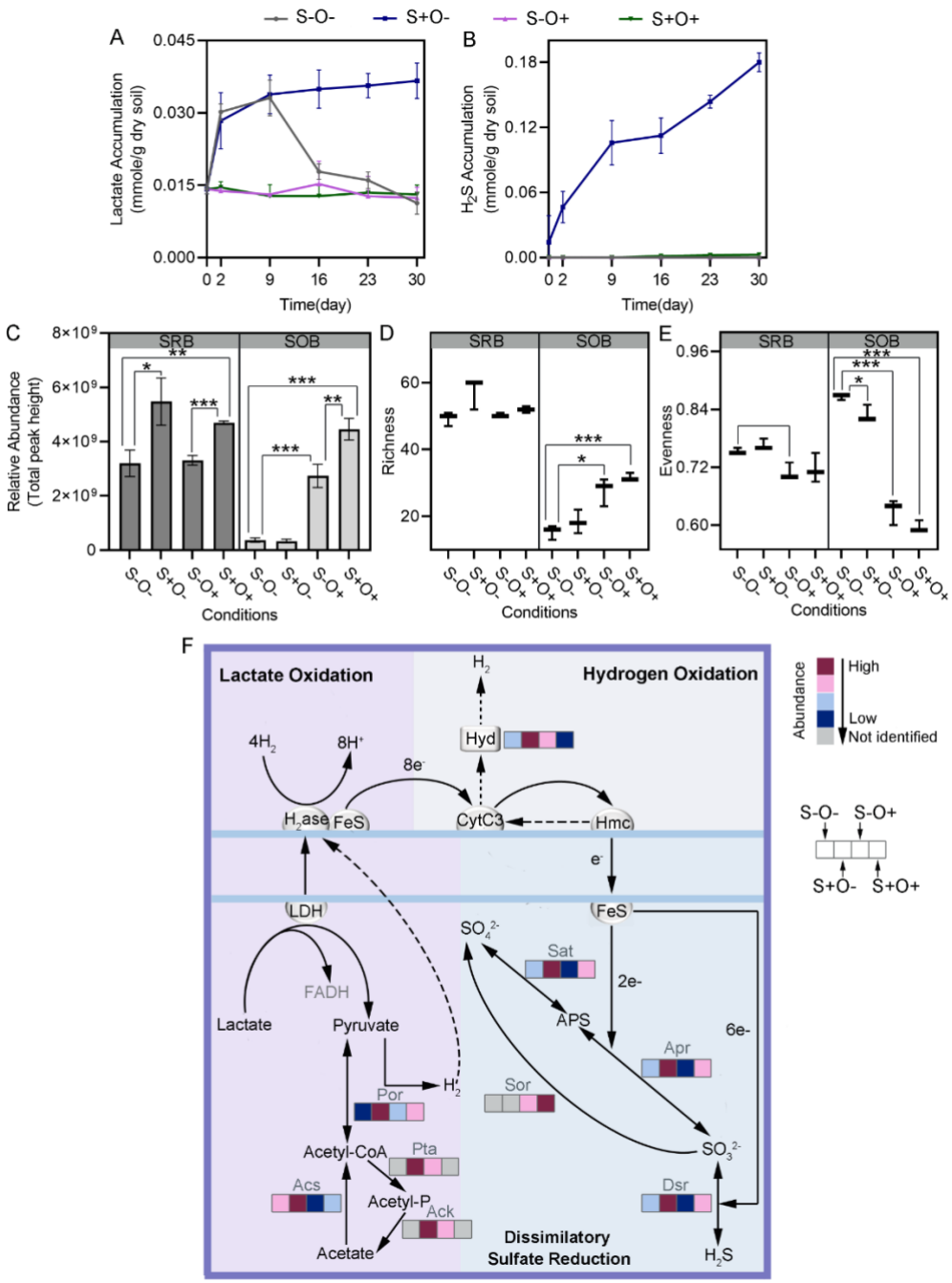

Figure 4.5 Effects of SO42- and O2 exposures on sulfate reduction and sulfite/sulfide oxidation processes. (A-B) Changes in molar mass of lactate (A) and H2S (B) over the 30 days of incubation. (C-E) Relative abundances (C), richness (D) and evenness (E) of sulfate-reducing bacteria (SRB) and sulfide/sulfur-oxidizing bacteria (SOB). Significant differences with p-values determined using Student's t-test, and adjusted for the false discovery rate, are marked by * for *p*-value < 0.05, ** for *p*-

value < 0.01 and *** for *p*-value < 0.001. (F) Sulfur metabolism pathways. The boxes in the pathway map, arranged from left to right, correspond to the S-O-, S+O-, S-O+ and S+O+ conditions. The color gradient from red to blue represents the relative abundance ranking of proteins among the four conditions, with red indicating the highest ranked relative abundance and blue the lowest. The grey color indicates proteins not detected by LC-MS/MS. The error bars are defined as standard deviation.

4.4.5 Modeling of Carbon and Energy Flow Through the Microbial Communities

A stoichiometric model was constructed to model the fluxes through the primary carbon metabolism and energy conservation pathways among the predominant microbial guilds in the wetland communities. The overall model comprised nine reactions, including aerobic heterotrophic, lactate fermentation, hydrogenic acetogenesis, sulfidogenic lactate oxidation, sulfidogenic hydrogen oxidation, hydrogenotrophic methanogenesis, acetoclastic methanogenesis, methane oxidation, and butyrate production (Figure S4.3). The fluxes of these reactions were fitted to the cumulative amounts of acetate, lactate, butyrate, H_2, CO_2, CH_4, and H_2S produced or consumed over the 30 days of incubation. The correlation coefficient R^2, exceeded 0.9 in all four conditions (Figure S4.4). The consistency between the experimental data and the modeling results indicated a plausible estimation of the carbon and energy flows.

Under the S-O- condition, the primary reactions involved were hydrogenic acetogenesis, hydrogenotrophic methanogenesis, and acetoclastic methanogenesis. SO_4^{2-} addition significantly increased the flux from 0 to 0.33 $\pm$ 0.005 mmole/g dry soil through sulfidogenic hydrogen oxidation (Figure 4.6A, 4.6B). This observation was consistent with the increased abundance of functional proteins, including sulfate

adenylyltransferase (1.4-fold, *q*-value = 0.002), adenylylsulfate reductase (1.8-fold, *q*-value < 0.001) and dissimilatory sulfate reductase (1.5-fold, *q*-value = 0.001) in the dissimilatory sulfate reduction pathway (Figure 4.5C). Furthermore, SO_4^{2-} addition halted hydrogenotrophic methanogenesis and significantly reduced the flux by 1.7- folds through acetoclastic methanogenesis (*p-value* = 0.0014, Wald type II χ^2 tests) (Figure 4.6B). These reductions were supported by the fact that the abundance of functional proteins for hydrogenotrophic methanogenesis decreased much more than for acetoclastic methanogens. Under the two oxic conditions, the dominant reaction shifted to aerobic heterotrophy. The fluxes through dominant reactions observed under anoxic conditions were consistently lower than oxic conditions, such as hydrogenic acetogenesis (fold change > 3.9, *p*-value = 0.000, Wald type II χ^2 tests), hydrogenotrophic methanogenesis (fold change = 6.0, *p*-value = 0.004, Wald type II χ^2 tests), and acetoclastic methanogenesis (fold change > 35.4, *p*-value = 0.0003, Wald type II χ^2 tests). Moreover, O_2 also eliminated sulfidogenic hydrogen oxidation and butyrate production (Figure 4.6C, 4.6D). Under S+O+ condition, sulfidogenic lactate oxidation replaced sulfidogenic hydrogen oxidation for sulfate reduction compared to S+O- condition (Figure 4.6B, 4.6D). These findings indicate that the addition of SO_4^{2-} and O_2 restructured the carbon flows across the metabolic network of the wetland community.

The models estimated the contributions of each reaction to the CO_2 and CH_4 accumulations. Under S-O- condition – where CO_2 accumulation was lowest – it was estimated 51% of CO_2 was derived from hydrogenic acetogenesis (0.28 ± 0.01 mmole/g dry soil), 32% from acetoclastic methanogenesis (0.18 ± 0.002 mmole/g dry soil), and

17% from butyrate production (0.091 ± 0.01 mmole/g dry soil). Additionally, 0.14 ± 0.008 mmole/g dry soil CO_2 was used for hydrogenotrophic methanogenesis to produce CH_4. SO_4^{2-} addition reduced the contributions of butyrate production (0.064 ± 0.014 mmole/g dry soil) and acetoclastic methanogenesis (0.099 ± 0.002 mmole/g dry soil) to CO_2 accumulation by 31% and 45%, respectively. However, the contribution of CO_2 accumulation from hydrogenotrophic acetogenesis increased by 13%, and no flux was detected from hydrogenotrophic methanogenesis using CO_2 to produce CH_4. These overall changes resulted in a 16% increase in total CO_2 accumulation. The highest CH_4 accumulation was observed under S-O- condition, with acetoclastic methanogenesis contributing 56.6% (0.18 ± 0.002 mmole/g dry soil) and hydrogenotrophic methanogenesis contributing 43.4% (0.14 ± 0.008 mmole/g dry soil) (Figure 4.6E). Under the S+O- condition, only acetoclastic methanogenesis contributed to CH_4 accumulation, and the total CH_4 accumulation decreased by 69% compared to the S-O- condition (Figure 4.6F). Under the two oxic conditions, aerobic heterotrophs contributed 94% and 96% of the CO_2 produced under non-sulfate addition and sulfate addition conditions, respectively (Figure 4.6G, 4.6H).

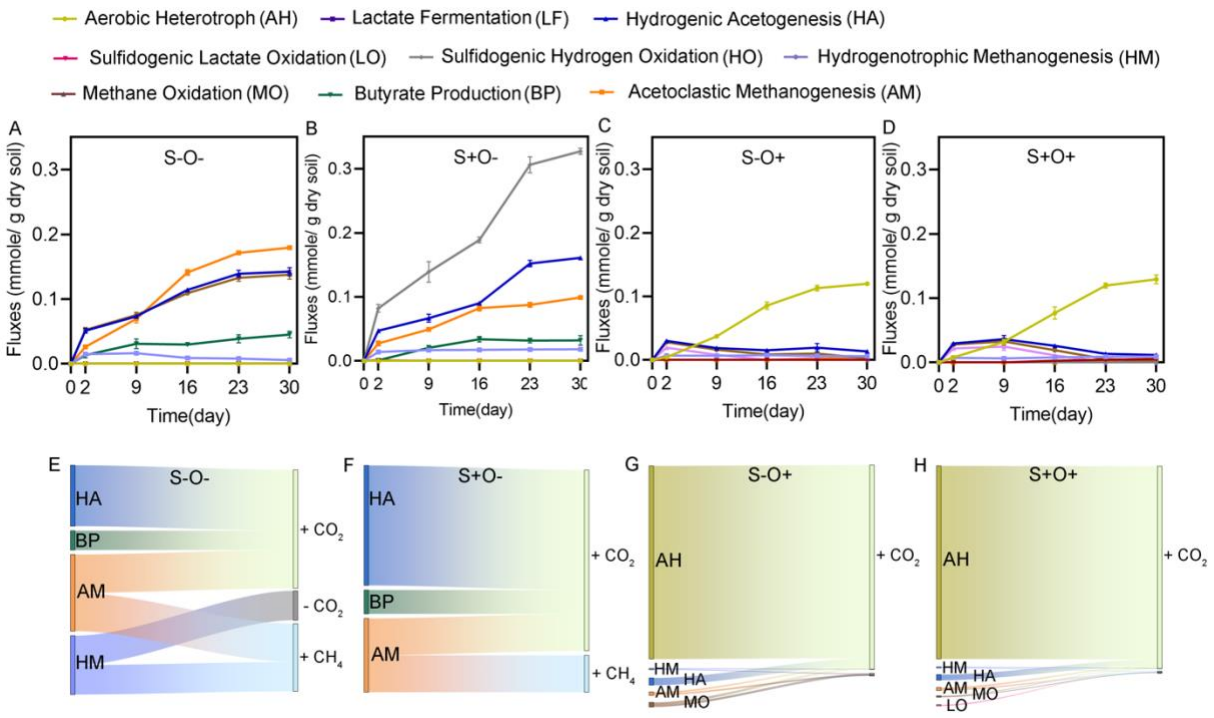

Figure 4.6 Stoichiometric modeling of the wetland microbial community. (A-D) fluxes of the key reactions under four experimental conditions. (E-F) Production (+) and consumption (-) of CO2 and CH4 by these reactions. The error bars are defined as standar.

4.5 Discussion

Climate change will result in increased hydrological challenges to wetlands, including seawater intrusion and changing regional regimes of drought and flooding. These stressors lead to recurrent perturbations in wetland microbial communities, primarily due to elevated O_2 during periods of drought and elevated SO_{4z}^{2-} from seawater intrusion [203, 225]. Our findings demonstrated that the addition of SO_4^{2-} and O_2 diminished CH_4 emissions and increased CO_2 emissions, which is consistent with observations in natural wetland ecosystems exposed to increased seawater and O_2 [184, 226, 227]. However, it remains challenging in natural wetland soil to determine how SO_4^{2-} and O_2 shape microbial processes that ultimately impact CH_4 and CO_2 emissions [228, 229]. In this study, we developed a conceptual food web connecting the metabolic activities of key microbial populations to CH_4 and CO_2 emissions, under the perturbation of elevated SO_4^{2-} and O_2 (Figure 4.7). Our findings indicated that elevated availabilities of SO_4^{2-} and O_2 changed the compositions of functional guilds and their metabolic activities, including plant polymer breakdown, methane production and oxidation, as well as sulfide/sulfur oxidation. Elevated SO_4^{2-} reduced CH_4 emission by 3.7-fold and increased CO_2 emission by 1.1-fold. Exposure to O_2 resulted in a 33.3-fold decrease in CH_4 emission and only a 1.7-fold increase in CO_2 emission. Because the warming effect of CH_4 is approximately 28-36 times greater than that of CO_2 [230], the elevated SO_4^{2-} and O_2 exposures may reduce the overall warming effect of gas emissions from wetlands.

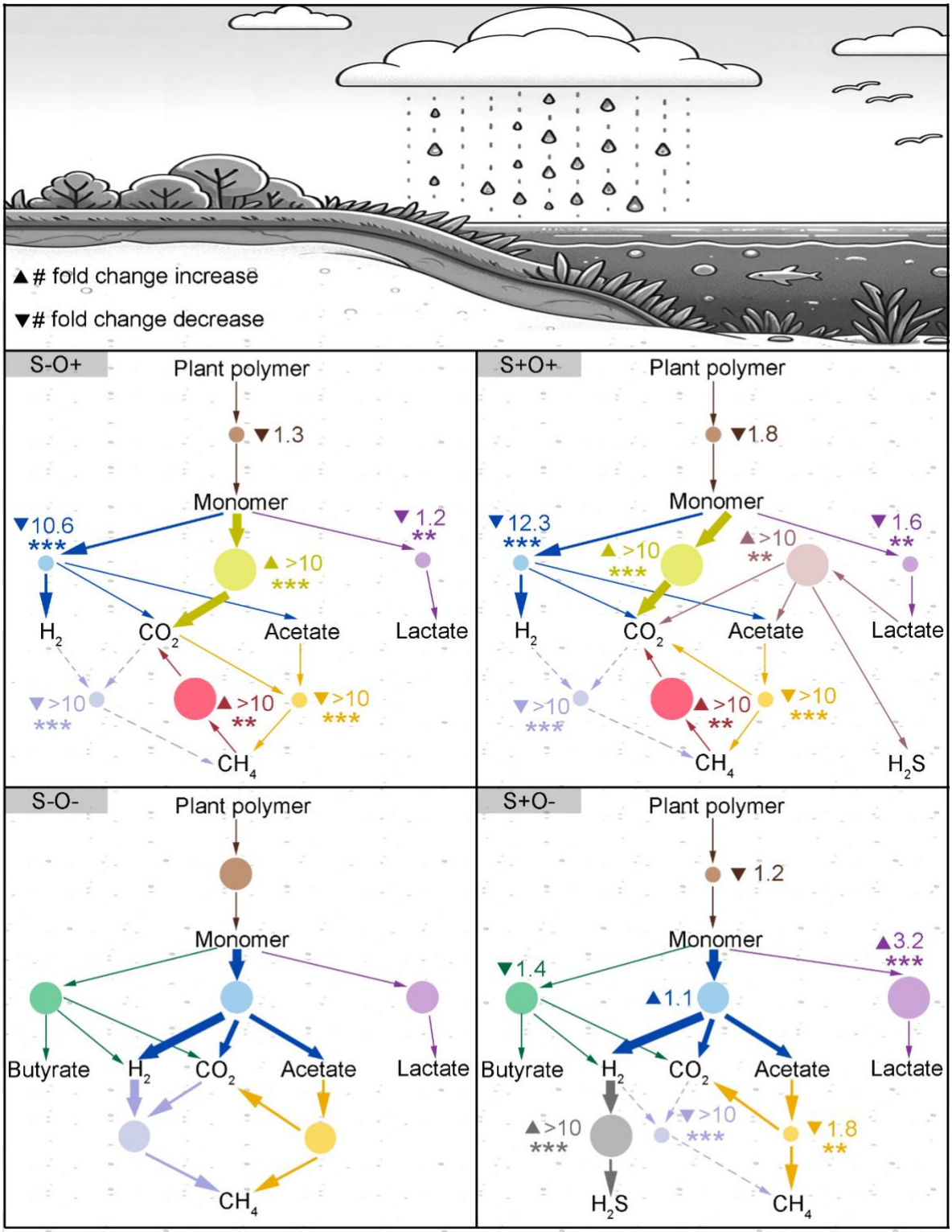
▲# fold change increase
▼# fold change decrease
S-O+
Plant polymer
▼1.3
Monomer
▼10.6
***
▼1.2
**
▲>10
***
H2
CO2
Acetate
Lactate
▼>10
***
▲>10
**
▼>10
***
CH4
S+O+
Plant polymer
▼1.8
Monomer
▼12.3
***
▲>10
***
▲>10
**
▼1.6
**
H2
CO2
Acetate
Lactate
▼>10
***
▲>10
**
▼>10
***
CH4
H2S
S-O-
Plant polymer
Monomer
Butyrate
H2
CO2
Acetate
Lactate
CH4
S+O-
Plant polymer
▼1.2
Monomer
▲3.2
***
▼1.4
▲1.1
Butyrate
H2
CO2
Acetate
Lactate
▲>10
***
▼>10
***
▼1.8
**
H2S
CH4
Hydrolysis
Hydrogenic acetogenesis
Butyrate production
Aerobic heterotroph
Lactate fermentation
Sulfidogenic lactate oxidation
Hydrogenotrophic methanogenesis
Methane oxidation
Acetoclastic methanogenesis
Sulfidogenic hydrogen oxidation

Figure 4.7 Conceptual food web responding to SO42- and O2 perturbations. The S-O- condition serves as the baseline. Circle size corresponds to the relative abundance of marker proteins within the reaction, with larger circles indicating higher abundance, and smaller circles denoting lower abundance. Numbers alongside circles indicate the fold change in metabolic fluxes as inferred from stoichiometric models relative to the control. Edge thickness represents the magnitude of fluxes that consume or produce metabolites. Dashed lines indicate fluxes for nearly eliminated hydrogenotrophic methanogenesis post-treatment. Statistical significance was assessed by Wald type II χ^2 tests, with *p*-values adjusted for the false discovery rate indicated by: *** $p < 0.001$, ** $p < 0.01$, * $p < 0.05$.

The reduction in the CH_4 production by SO_4^{2-} exposure was attributed primarily to the sharp decrease in H_2 available for hydrogenotrophic methanogenesis and acetate needed for acetoclastic methanogenesis. Notably, hydrogenotrophic methanogenesis appeared to be more sensitive to elevated SO_4^{2-} compared to acetoclastic methanogenesis. This sensitivity is rooted in the thermodynamic basis of competition for H_2 and carbon by methanogenic consortia and SRB, as hydrogenotrophic sulfate reduction is more energetically favorable than either hydrogenotrophic methanogenesis or acetoclastic methanogenesis [203, 231, 232]. Even under oxic conditions, SO_4^{2-} addition facilitated the co-existence of SOB and SRB. Oxygen consumed by sulfide-oxidizing SOB fosters the growth of anaerobic sulfide-generating SRB. In contrast, acetoclastic methanogens do not directly compete with SRB, as most SRBs have an incomplete TCA cycle, which prevents them from completing the oxidation of acetate to CO_2 [233, 234]. In addition, our results indicated that a key factor contributing to the increase in CO_2 emission due to the addition of SO_4^{2-} is the inhibition of hydrogenotrophic methanogenesis, which consumes CO_2. SO_4^{2-} addition reorganized

carbon fluxes through the community due to SRB outcompeting hydrogenotrophic methanogens, in turn driving accumulation of short-chain fatty acids and increasing CO_2 emissions.

O_2 suppressed both hydrogenotrophic methanogenesis and acetoclastic methanogenesis. In the absence of SO_4^{2-}, elevated O_2 suppressed reactions that produce H_2, such as hydrogenic acetogenesis. The decreased H_2 production constrained the hydrogenotrophic methanogenesis [235]. Under the sulfate addition conditions, the introduction of O_2 was found to enhance the consumption of H_2S by SOB. Consequently, this promoted H_2 uptake by sulfate reduction and intensified the competition between hydrogenotrophic methanogens and SRB [234]. The proteomic abundances of carbohydrate degradation enzymes also indicated that O_2 altered the preference for the degradation of plant polysaccharides. Exposure to O_2 favored microbial communities that hydrolyze polysaccharides with more complex structures. Upon recovery from oxic conditions, this may lead to prolonged release of CO_2 [205].

Approximately 80% of the studies investigating the impact of anthropogenic pressures on ecosystem functions have primarily focused on analyzing the effect of individual stressors in isolation [3, 236]. However, climate change may introduce many co-occurring stressors, which need to be investigated in combination. In this study, we found an antagonistic interaction between the effects of sulfate and O_2 on CH_4, and CO_2 emissions, where the reduction in CH_4 accumulation and the increase in CO_2 resulting from the combined treatment of SO_4^{2-} and O_2 was less pronounced compared to the sum of individual effects. This non-addictive effect can be attributed to the high functional redundancy stemming from extraordinarily diverse functional guilds in soils

[236-238]. Furthermore, both SO_4^{2-} and O_2 affect certain metabolic processes in a similar manner. For instance, elevated levels of either SO_4^{2-} or O_2 nearly completely halted hydrogenotrophic methanogenesis, resulting in a reduction in CH_4 accumulation. Therefore, when SO_4^{2-} and O_2 exposures are combined, the observed methanogenesis decrease is not addictive.

In this study, we generated a functional understanding of the decreased CH_4 and increased CO_2 emissions in wetland microcosms subjected to SO_4^{2-} and O_2 pressure by integrating geochemical analysis, proteogenomics, and stoichiometric modeling. The geochemical analysis quantified the end-products' accumulation levels and the intermediates' standing levels in the metabolic network, which were used by the stoichiometric modeling to estimate the flux rates across key metabolic processes under different conditions. Many of the changes in the estimated flux rates were supported by the concordant changes in the protein abundances of enzymes involved in those metabolic processes. The obtained results may enable climate models to better estimate greenhouse gas emissions under changing environmental conditions.

Chapter 5. Maternal Complex Carbohydrates Diet Enhances Taxonomic Diversity and Metabolic Activities of the Microbiome in Gestational Diabetes and in Their Infants

5.1 Abstract

Gestational diabetes mellitus (GDM) is a prevalent pregnancy complication linked to significant disruptions in the maternal gut microbiome, potentially affecting both maternal and infant health. Dietary management is the cornerstone of GDM treatment, yet the influence of maternal diet on the gut microbiome and its long-term health implications remains poorly understood. This study investigates the taxonomic composition and metabolic capacity of the maternal and infant gut microbiomes to determine the effects of dietary interventions on microbial function and subsequent health outcomes. Stool samples were collected from a randomized controlled trial involving diet-managed women with GDM. Eighteen women followed the CHOICE diet, consisting of 60% complex carbohydrates, 25% fat, and 15% protein, while sixteen women adhered to the CONV diet, comprising 40% complex carbohydrates, 45% fat, and 15% protein. Dietary regimens were followed from the 30th week of gestation until delivery. Maternal stool samples were collected at 31 and 37 weeks of gestation, and infant stool samples were collected at 2 weeks, 2 months, and 4-5 months of age. Shotgun metagenomics and high-resolution metaproteomics were employed to assess the taxonomic diversity and metabolic capacity of the fecal microbiomes. The results demonstrated that maternal dietary interventions significantly altered microbiome diversity. In the maternal microbiome, alpha diversity increased by 9.6% in the CHOICE diet. Despite identifying numerous mother-to-infant species and gene transmission events, no significant differences were found between the CONV and CHOICE diets in these events. However, the CHOICE diet led to substantial shifts in the microbial

community, particularly in the enhancement of short-chain fatty acid production. This study provides valuable insights into the role of targeted dietary interventions in modulating gut microbiome composition and metabolic activity, with potential implications for precision medicine and disease prevention.

Key words: Gestational Diabetes Mellitus, Gut Microbiome, Dietary Intervention, Microbial Diversity, Functional dynamics

5.2 Introduction

Gestational diabetes mellitus (GDM), defined as glucose intolerance that first manifests during pregnancy, has become increasingly prevalent worldwide, affecting up to 20% of pregnancies depending on the diagnostic criteria used. This metabolic disorder presents serious risks for both mothers and their infants [239, 240]. Women with GDM face heightened risks of preeclampsia, cesarean section delivery, and preterm birth, and nearly half of these women go on to develop type 2 diabetes within a decade [241]. For infants, maternal GDM raises the likelihood of developing obesity, type 2 diabetes, and other chronic conditions later in life, highlighting the urgent need for more effective management strategies [242].

Dietary intervention is the primary method for controlling GDM, aimed at stabilizing blood glucose levels and mitigating associated health risks [243-245]. However, growing evidence suggests that the impact of maternal diet extends beyond glycemic control, influencing the composition and functionality of the gut microbiome—an ecosystem of trillions of microorganisms that play essential roles in metabolic health, immune function, and inflammation regulation [246, 247]. The gut microbiome undergoes significant changes during pregnancy, and these changes are particularly pronounced in women with GDM, where shifts toward an overrepresentation of pathogenic bacteria, such as those from the *Enterobacteriaceae* family, are commonly observed. At the same time, beneficial microbes like *Bifidobacterium* and *Lachnospiraceae*, which produce anti-inflammatory short-chain fatty acids (SCFAs), are often depleted [248, 249]. These microbial imbalances may contribute to metabolic dysfunction, inflammation, and insulin resistance, exacerbating the risks posed by GDM [250].

Beyond the maternal microbiome, these dietary and microbial interactions are likely to have important implications for infant health [251-254]. Maternal gut microbes are among the first to colonize the infant gut, influencing the development of the infant's microbiome and potentially predisposing the child to conditions like obesity and diabetes later in life. Research indicates that infants born to mothers with GDM tend to have lower microbial diversity and altered gut composition, and while studies have explored the neonatal microbiome in the early weeks after birth, few have examined how the maternal diet affects infant microbiome development during the crucial first few months of life [255, 256]. Since this period is critical for immune and metabolic programming, understanding how maternal dietary interventions shape both maternal and infant microbiomes could have far-reaching implications for long-term health.

In this study, we conducted a randomized controlled trial (RCT) to investigate the effects of two distinct dietary interventions in women with GDM: a conventional high-fat (CONV) diet and a CHOICE diet that emphasizes complex carbohydrates. This rigorous study design, which provided all meals to participants, allowed us to control for potential confounders such as gestational weight gain and ensure that any observed differences in microbial composition or health outcomes were directly attributable to the dietary intervention. While prior studies have explored maternal diet’s effects on the microbiome, few have offered such a highly controlled comparison, and none to date have assessed the specific effects of these diets on both maternal and infant microbiomes in a GDM context [257, 258].

To better understand how these dietary interventions impact the microbiome at both taxonomic and functional levels, we employed shotgun metagenomics and high-

resolution metaproteomics. Metagenomics enabled us to explore the microbial diversity present in maternal and infant gut samples, while metaproteomics provided an in-depth look at the proteins expressed by the microbiota, revealing critical insights into the functional activities of these microbial communities. By using metaproteomics, we moved beyond simply identifying microbial species to understanding how they function in response to dietary changes—particularly in terms of key metabolic processes like the production of SCFAs, which play a vital role in regulating inflammation and maintaining gut health.

We explore how different maternal diets influence microbial diversity and metabolic function. We hypothesized that the CHOICE diet, rich in complex carbohydrates, would increase beneficial bacterial populations and enhance SCFA production in both mothers and infants compared to the conventional high-fat diet. We also aimed to understand how these dietary interventions impact the transmission of microbial species from mother to infant and whether shifts in the infant microbiome, particularly during the first few months of life, are associated with beneficial metabolic outcomes. Furthermore, this study investigates the possibility that the functional capacities of these microbial communities—such as their ability to produce key metabolites—are more important than taxonomic diversity alone in shaping health outcomes for both mother and child. Through this multi-omics approach, we provide a comprehensive picture of how maternal dietary choices modulate gut microbial composition and function during and after pregnancy. Our findings have the potential to inform precision nutrition strategies for women with GDM, offering new ways to optimize maternal and infant health through targeted microbiome modulation. By exploring not just the microbiome's composition but also its metabolic activities, this

study contributes critical insights into the broader understanding of how maternal health interventions can have lasting effects on both maternal and infant well-being.

5.3 Materials and Methods

5.3.1 Assembly-Based Data Analysis

Metagenomic reads were preprocessed using BBTools for adaptor removal, trimming, filtering, and sequencing error correction [208]. The preprocessed reads from three samples were co-assembled into a combined metagenome using MetaSPAdes [209]. Scaffolds longer than 2 kb were used to bin metagenome-assembled genomes (MAGs) using MetaBAT with default parameters [213]. The quality of the MAGs was assessed using CheckM v1.1.2, which classified the MAGs into high-quality (completeness > 90% and contamination < 5%) and medium-quality (completeness ≥ 50% and contamination < 10%) [259].

Taxonomic classification of high-quality MAGs was performed using GTDB-Tk [214]. A phylogenetic tree of 73 species was constructed based on their MAGs using PhyloPhlAn 3.0 and visualized using the iTOL tool [260, 261]. Richness and taxonomic α-diversity indices, including the Shannon index, inverse Simpson index, and Pielou's evenness, were calculated using the vegan package in R. Genes and proteins were predicted from scaffolds longer than 1 kb using Prodigal [210], and protein functions were annotated using KofamScan with KEGG Orthology (KO) terms [211].

5.3.2 Core Protein Family Construction, Annotation, and Clustering

Proteins were predicted from scaffolds greater than 1 kb assembled from subjects with at least four metagenome samples using Prodigal v2.6.3 (–p meta option). A total of 158,247,178 proteins were generated with a minimum length of 50 amino acids. These proteins were clustered hierarchically using CD-HIT v4.8.1 at 90%, 65%, and 40% identity thresholds [262]. Full-length and fragmented open reading frames (ORFs) were clustered separately, with alignment coverage requirements of 90% on

both long and short sequences for full-length ORFs. Results from full-length and fragmented ORFs were then merged at each identity level, generating 288,586 protein families.

5.3.3 Metaproteomics Measurement

At the conclusion of the experiment, fecal samples were analyzed using metaproteomics to profile protein abundances and functions. Protein extraction followed previously described protocols with slight modifications [169]. Briefly, fecal samples were suspended in lysis buffer containing 10 mM Tris-HCl, 4% SDS, and 10 mM dithiothreitol. The samples were boiled for 5 minutes, followed by disruption via sonication (10% pulse, 5 times, 2-minute duration). The supernatant was collected after centrifugation at 14,000Xg for 10 minutes. Proteins were precipitated overnight using trichloroacetic acid (TCA) with the final concentration of 25%, pelleted by centrifugation, washed three times with ice-cold acetone, and resuspended in guanidine buffer. Protein concentrations were quantified using the Bicinchoninic Acid Assay (BCA).

For downstream analysis, 20 mg of protein from each sample was processed using filter-aided sample preparation (FASP) and digested with a Trypsin/LysC mixture. The resulting peptides were analyzed by two-dimensional liquid chromatography-tandem mass spectrometry (2D-LC-MS/MS) on an Orbitrap Fusion Tribrid mass spectrometer (Thermo Fisher Scientific, USA) at the IDeA National Resource for Quantitative Proteomics.

Peptides were first separated into 46 fractions using a 100 x 1.0 mm Acquity BEH C18 column (Waters) on an UltiMate 3000 UHPLC system (Thermo) under basic pH conditions with a 50-minute gradient (99:1 to 60:40 buffer A ratio). The fractions were

consolidated into 12 super-fractions. Each super-fraction was further separated on an in-line 120 x 0.075 mm column using reverse-phase XSelect CSH C18 resin (2.5 µm, Waters) on an UltiMate 3000 RSLCnano system (Thermo), with a 60-minute gradient (98:2 to 65:35 buffer A ratio). Eluted peptides were ionized by electrospray (2.4 kV) and subjected to mass spectrometric analysis on an Orbitrap Fusion Tribrid Mass spectrometry (MS) data were acquired in profile mode using the Fourier transform mass spectrometer (FTMS) analyzer at a resolution of 240,000 across a mass range of 375 to 1500 m/z. Following higher-energy collisional dissociation (HCD) activation, MS/MS data were collected in centroid mode using the ion trap analyzer, with a normalized collision energy of 28–31%, depending on precursor charge state and selection range.

Protein identification and quantification followed established protocols. MS spectra were searched using Sipros Ensemble against a protein database constructed from the metagenome [117]. Raw search results were filtered to achieve a 1% false discovery rate (FDR) at the peptide level, estimated using a target-decoy approach. Peptide identifications were assigned to proteins or protein groups following the parsimonious rule. To avoid ambiguity in downstream analysis, protein groups were excluded from biological interpretation. Protein quantification was performed using intensity-based label-free analysis via ProRata, where protein abundance was quantified by summing the total peak height of all peptides associated with a protein, normalized against the average total of all datasets [119].

Following previously described methods, taxonomic annotations were assigned to identified peptides based on the corresponding scaffold's taxonomic annotation information (scaffolds longer than 1 kb). The relative abundance of each species was

determined by summing the abundances of all proteins detected for that species. In cases where a protein was identified in multiple species, its abundance was equally divided among those species.

5.4 Results

5.4.1 Diet-Induced Differences in Microbial Species and Functional Diversity

Principal coordinate analysis (PCoA) was conducted to assess microbial species composition and functional activity in subjects consuming the conventional (CONV) and CHOICE diets, using both metagenomic and metaproteomic data. The PCoA of species composition from metagenomic data (Figure 5.1A) revealed no significant separation between the CONV and CHOICE diet groups (*p*-value = 0.13), suggesting that the overall taxonomic makeup of the microbiomes did not differ substantially between the two diets at the DNA level. However, when analyzing species composition based on metaproteomic data (Figure 5.1A), a significant difference was observed between the groups (*p*-value = 0.002). This result indicates that while the species present may be similar between the two diets, their functional activities, as reflected by protein expression, differ significantly.

Further investigation of functional differences in the microbiomes was performed using PCoA of functional profiles derived from both metagenomic and metaproteomic data (Figure 5.1B). The functional potential, as represented by metagenomic data (Figure 5.1B, left panel), showed no significant difference between the two dietary groups (*p*-value = 0.35), indicating comparable genetic potential for microbial functionality. However, the metaproteomic analysis (Figure 5.1B) revealed a significant separation between the CONV and CHOICE groups (*p*-value = 0.001). This finding suggests that although the functional potential encoded in the genomes may be similar, the actual metabolic activity, as evidenced by protein expression, differs substantially between the two diets.

Microbial diversity was further evaluated within the CONV and CHOICE diet groups using the Shannon diversity index (Figure 5.1C), which assesses species-level

diversity and functional richness. Consistent with the PCoA results, metagenomic data showed no significant difference in microbial diversity between the CONV and CHOICE diets (*p*-value = 0.49), indicating similar species richness across the two groups. However, metaproteomic data revealed significantly higher microbial diversity in the CHOICE group compared to the CONV group (*p*-value = 0.01). This suggests that while the overall taxonomic composition remains stable across diets, the CHOICE diet promotes greater functional diversity at the protein level, reflecting more varied metabolic activities within the microbiome.

To further investigate functional richness, Rao's Quadratic Entropy—a measure of functional diversity—was assessed (Figure 5.1D). In the metagenomic data (Figure 5.1D), no significant difference in functional diversity was observed between the two groups (*p*-value = 0.13), reinforcing the conclusion that the genetic potential for functionality is similar across diets. In contrast, the metaproteomic data (Figure 5.1D) showed a significant increase in functional diversity in the CHOICE group compared to the CONV group (*p*-value = 0.04). This indicates that the CHOICE diet not only influences the metabolic activity of the microbiome but also enhances functional diversity, suggesting that the microbial community in the CHOICE group may have a greater capacity to perform a wider range of metabolic functions.

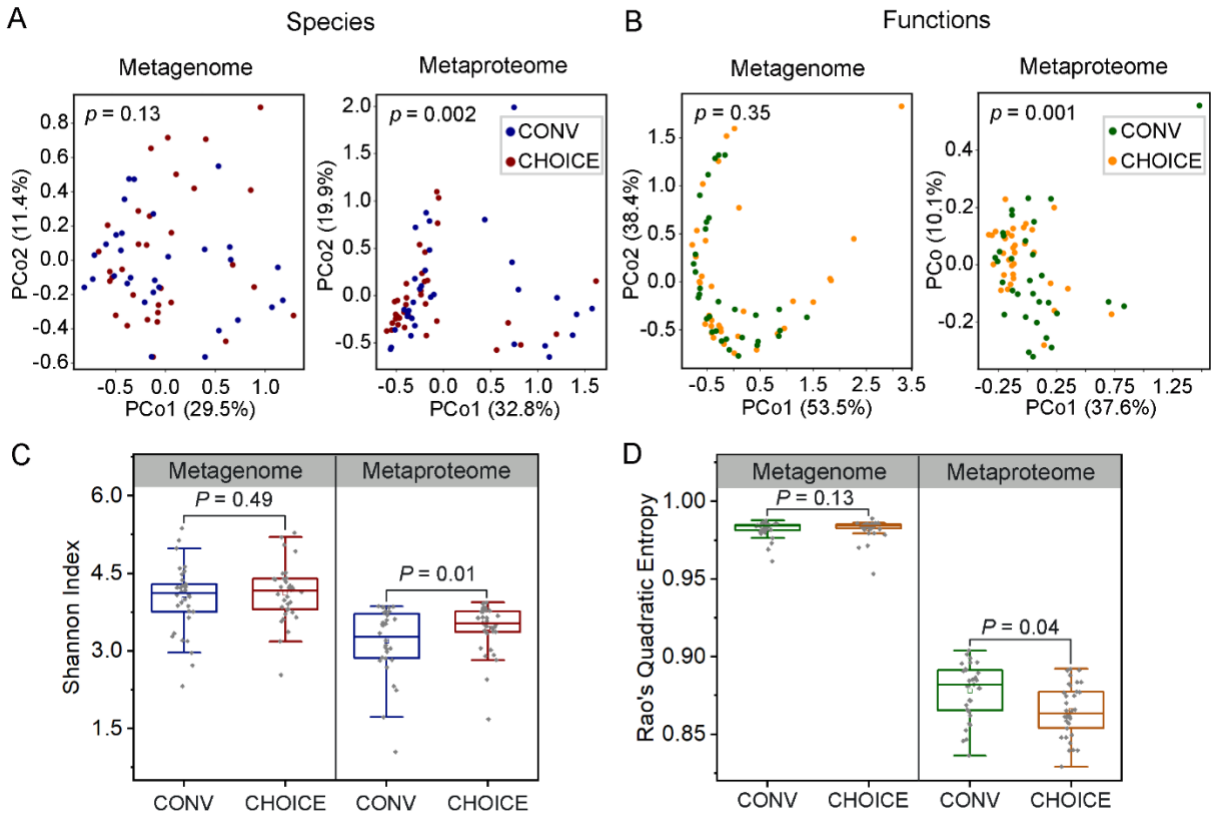

Figure 5.1 Comparison of species composition and functional diversity between CONV and CHOICE samples. (A) Comparing species diversity between conventional (CONV) and CHOICE treatments based on metagenome and metaproteome data. (B) Comparing functional diversity between CONV and CHOICE samples based on metagenome and metaproteome data. *P*-values indicate the statistical significance of the differences in function between the two treatments, as evaluated by PERMANOVA. (C) Shannon Index comparing the alpha diversity of species in the metagenome and metaproteome datasets between CONV and CHOICE groups. (D) Rao's Quadratic Entropy, a measure of functional diversity, showing differences between CONV and CHOICE treatments in both the metagenome and metaproteome datasets.

5.4.2 Species Composition Changes in the Microbiomes of Mother and Infant

Metagenomic and metaproteomic analyses were performed to investigate the species composition changes in the microbiomes of both the mother and the infant. Significant alterations in microbial species abundance were observed, with distinct patterns emerging for the mother and infant cohorts (Figure 5.2).

The metagenomic analysis revealed significant shifts in the microbial composition within the mother's microbiome (Figure 5.2A). Several species exhibited a marked increase in relative abundance. Notably, *Aminobacterium mobile* and *Blautia faecis* demonstrated the largest positive effect sizes, indicating a significant enrichment in the mother's microbiota. *Shigella boydii* and *Mitsuokella multacida* were among the species that showed substantial decreases, with negative effect sizes suggesting their depletion.

The changes observed in the mother's microbiome were corroborated by the metaproteomic data (Figure 5.2A), which reflected similar trends in species composition. Species such as *Ruminococcus bromii* and *Clostridium isatidis* displayed prominent increases in abundance. In contrast, species like *Neglectibacter timonensis* and *Clostridium merdae* were significantly reduced. The congruence between the metagenomic and metaproteomic analyses suggests that these shifts in microbial composition may represent robust changes in the mother's microbiota at the species level, likely driven by environmental or physiological factors.

In the infant microbiome, species composition changes were primarily observed at the metagenomic level (Figure 5.2B). A significant increase in the relative abundance of *Bifidobacterium catenulatum* was detected, with a fold change exceeding 100, making it one of the most dominant species in the infant's microbiota. Other species

such as *Holdemania filiformis* and *Clostridium cadaveris* also exhibited positive effect sizes, indicating an increase in their relative abundance. Conversely, *Shigella sonnei*, *Streptococcus equi*, and *Stenotrophomonas maltophilia* were significantly reduced, as indicated by their negative effect sizes, suggesting a decline in their presence within the infant's microbiome.

Unlike the mother, no substantial species composition changes were detected in the metaproteomic analysis for the infant. The absence of significant shifts at the metaproteome level suggests that while certain species are becoming established in the infant's gut, they may not yet be metabolically active or contributing significantly to functional pathways at this early developmental stage. This finding highlights a potential lag between species colonization and their functional integration into the infant's microbiome.

Overall, these results indicate significant species composition changes in both the mother and infant microbiomes, albeit with distinct patterns. The mother's microbiome displayed shifts in species abundance across both metagenomic and metaproteomic levels, suggesting a more mature and metabolically active microbial community. In contrast, the infant's microbiome exhibited substantial changes at the metagenomic level, with key species like *Bifidobacterium catenulatum* dominating, but with no corresponding changes in the metaproteome, implying that the functional activity of the infant microbiome may still be developing.

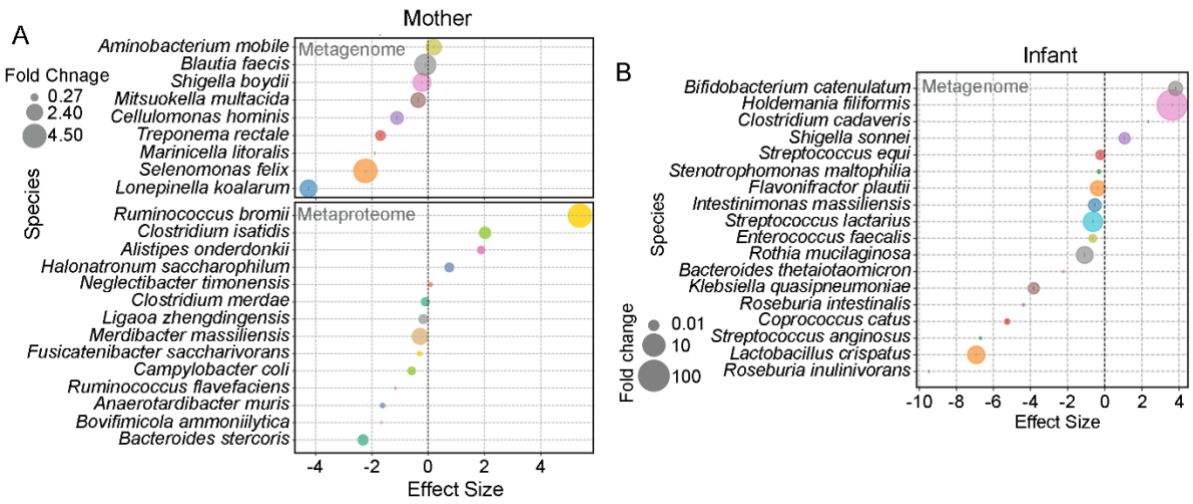

Figure 5.2 Species composition changes in the microbiomes of mother and infant. (A) the species composition changes in the mother's microbiome at the metagenomic and metaproteomic levels. (B) Species composition changes in the infant's microbiome at the metagenomic and metaproteomic levels. Each point represents a bacterial species, the size of the points indicating fold change. Positive effect sizes represent species that increased in abundance, while negative effect sizes represent species that decreased.

5.4.3 Functional Metabolic Pathway Shifts in the Microbiomes of Mother and Infant

Metagenomic and metaproteomic analyses revealed significant changes in microbial metabolic pathways in both the mother and infant, with notable differences in the extent of functional shifts between the two groups (Figure 5.3). In the mother, alterations were observed at both the metagenomic and metaproteomic levels, while in the infant, significant changes were only detected in the metagenome.

In the mother's microbiome, metagenomic analysis indicated significant enrichment in several metabolic pathways (Figure 5.3A). Pathways related to energy metabolism, such as oxidative phosphorylation, methane metabolism, and nitrogen

metabolism, exhibited marked increases, with oxidative phosphorylation showing the highest positive effect size. Carbohydrate metabolism pathways, including glycolysis/gluconeogenesis, the citrate cycle (TCA cycle), and pentose phosphate pathway, were also significantly enriched. In addition, pathways involved in amino acid metabolism, such as alanine, aspartate, and glutamate metabolism and valine, leucine, and isoleucine degradation, demonstrated increased abundance.

Metaproteomic analysis (Figure 5.3A) corroborated some of these findings, though fewer pathways showed significant shifts at the protein level compared to the metagenome. Notably, oxidative phosphorylation and methane metabolism exhibited slight increases in protein expression, suggesting active microbial processes in these pathways. However, most other metabolic pathways showed little to no change at the metaproteome level, indicating that while these pathways are genomically enriched, their functional activity may be limited or undetected in the current proteomic snapshot.

Infant:

In the infant's microbiome, significant shifts were observed exclusively at the metagenomic level (Figure 5.3B), with no corresponding changes detected in the metaproteome (Figure 5.3B). Metagenomic analysis revealed substantial alterations in pathways related to energy metabolism, including oxidative phosphorylation, which displayed a large positive effect size, and methane metabolism. Pathways associated with carbohydrate metabolism, such as starch and sucrose metabolism, pentose/glucuronate interconversions, and glycolysis/gluconeogenesis, were also significantly enriched, indicating active microbial contributions to carbohydrate processing in the infant's gut.

In addition to energy and carbohydrate metabolism, several pathways involved in amino acid metabolism, such as alanine, aspartate, and glutamate metabolism and valine, leucine, and isoleucine degradation, exhibited positive effect sizes, suggesting an increasing role of microbial amino acid metabolism in the developing infant microbiome. Interestingly, pathways related to lipid metabolism, such as fatty acid degradation and glycerophospholipid metabolism, showed significant decreases, with negative effect sizes indicating reduced potential for lipid metabolism in the infant gut.

No significant changes were observed in the infant's metaproteomic data, suggesting that while metagenomic analysis reveals a high potential for metabolic activity, these pathways may not yet be actively expressed at the proteomic level in the infant microbiome, or that functional expression is still developing.

The results demonstrate distinct patterns of microbial metabolic activity in the mother and infant microbiomes. In the mother, both metagenomic and metaproteomic analyses revealed enrichment in energy, carbohydrate, and amino acid metabolism pathways, with certain pathways, such as oxidative phosphorylation, showing functional expression at the protein level. In contrast, the infant microbiome exhibited significant shifts in metagenomic pathways, particularly in energy and carbohydrate metabolism, but no significant changes at the metaproteomic level, indicating a developing functional capacity in early infancy.

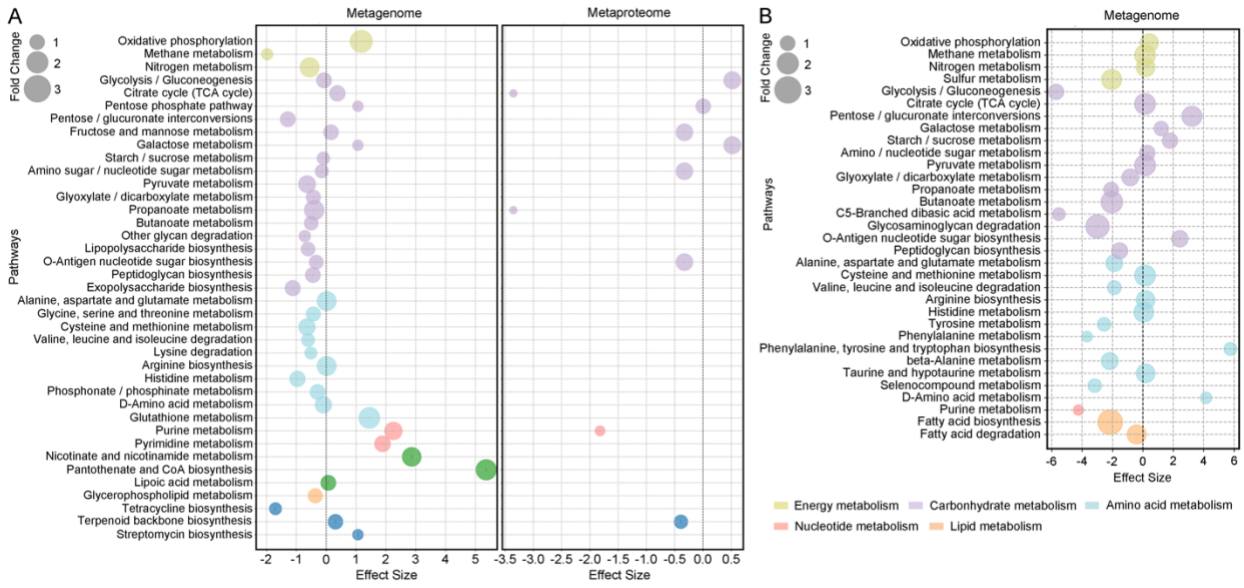

Figure 5.3 Changes in functional metabolic pathways in the microbiomes of mother and infant. (A) Metagenomic and metaproteomic analyses of the mother's microbiome. (B) Metagenomic analysis of the infant's microbiome. Pathways are categorized into functional groups: energy metabolism, carbohydrate metabolism, nucleotide metabolism, amino acid metabolism, and lipid metabolism. Circle size corresponds to fold change, with larger circles indicating greater fold changes. Positive effect sizes indicate an increase in the relative abundance of the pathway, while negative effect sizes represent a decrease.

5.4.4 Species-Specific Alterations in Metabolic Functions in the Mother's Microbiome

The combined metagenomic and metaproteomic analyses of the mother's microbiome revealed substantial species-specific shifts in metabolic pathways, with significant changes observed across pathways related to energy metabolism, carbohydrate metabolism, and amino acid metabolism (Figure 5.4). The functional contributions of individual species were characterized by both genomic potential and protein expression, highlighting differential activity across key metabolic functions.

Metagenomic analysis revealed pronounced changes in pathways related to energy metabolism, with significant enrichment in oxidative phosphorylation and methane metabolism. The species *Bifidobacterium pseudocatenulatum*, *Flavonifractor plautii*, and *Eubacterium ventriosum* exhibited the highest positive effect sizes, indicating enhanced genomic potential for these energy-producing pathways. In addition, pathways such as sulfur metabolism and nitrogen metabolism were enriched in species like *Gallibacterium anatis* and *Subdoligranulum variabile*, suggesting diverse microbial contributions to energy metabolism.

The metaproteomic data supported these findings, with several species, including *Bifidobacterium breve* and *Subdoligranulum variabile*, displaying increased protein expression in energy metabolism pathways. Notably, the proteomic data confirmed the functional realization of oxidative phosphorylation in a subset of these species. However, compared to the metagenomic data, fewer species showed significant protein-level activity, suggesting that not all species with genomic enrichment are actively engaged in energy metabolism under the conditions sampled.

Carbohydrate metabolism pathways demonstrated broad species-specific enrichment across the metagenome, particularly in pathways such as starch and sucrose metabolism, fructose and mannose metabolism, and pentose phosphate pathway. Species such as *Ruminococcus albus*, *Anaerostipes hadrus*, and *Roseburia inulinivorans* showed significant genomic enrichment, reflecting their capacity to degrade complex carbohydrates. These species are known for their role in short-chain fatty acid (SCFA) production, which is critical for host health and energy balance.

The metaproteomic analysis provided further evidence of active carbohydrate metabolism, with protein expression detected in species like *Ruminococcus albus* and *Roseburia inulinivorans*. The concordance between metagenomic potential and metaproteomic expression in these species highlights their active involvement in carbohydrate metabolism. However, in some cases, such as *Anaerostipes hadrus*, genomic potential for carbohydrate metabolism did not correspond to substantial protein expression, indicating possible regulation or delayed metabolic activity.

Species involved in amino acid metabolism pathways exhibited distinct contributions at both the genomic and proteomic levels. Metagenomic analysis showed significant enrichment in pathways such as arginine and proline metabolism, glycine, serine, and threonine metabolism, and cysteine and methionine metabolism. Species such as *Parabacteroides distasonis*, *Blautia faecis*, and *Bifidobacterium longum* displayed high effect sizes, indicating their important roles in amino acid turnover and biosynthesis.

Metaproteomic data corroborated the involvement of several of these species in active amino acid metabolism, with significant protein expression detected in *Parabacteroides distasonis* and *Blautia faecis*, confirming their functional roles in these pathways. However, for other species, such as *Faecalibacterium prausnitzii* and *Bacteroides vulgatus*, a discrepancy was observed between their genomic enrichment and lower levels of protein expression, suggesting that their functional activity in amino acid metabolism may be context-dependent or not fully realized at the time of sampling.

The integration of metagenomic and metaproteomic data reveals distinct species-specific shifts in the mother's microbiome across multiple metabolic functions. Energy metabolism pathways, particularly oxidative phosphorylation and methane

metabolism were driven by a select group of species, with some demonstrating both genomic potential and active protein expression. Carbohydrate metabolism was characterized by the involvement of key species capable of polysaccharide degradation and SCFA production, with active protein expression confirming their functional roles. Amino acid metabolism exhibited enrichment in pathways essential for amino acid turnover, with several species showing concordant metagenomic and proteomic activity. These findings underscore the functional complexity of the mother's microbiome and its critical role in nutrient metabolism, with species-specific contributions that reflect both genomic capacity and actualized metabolic function.

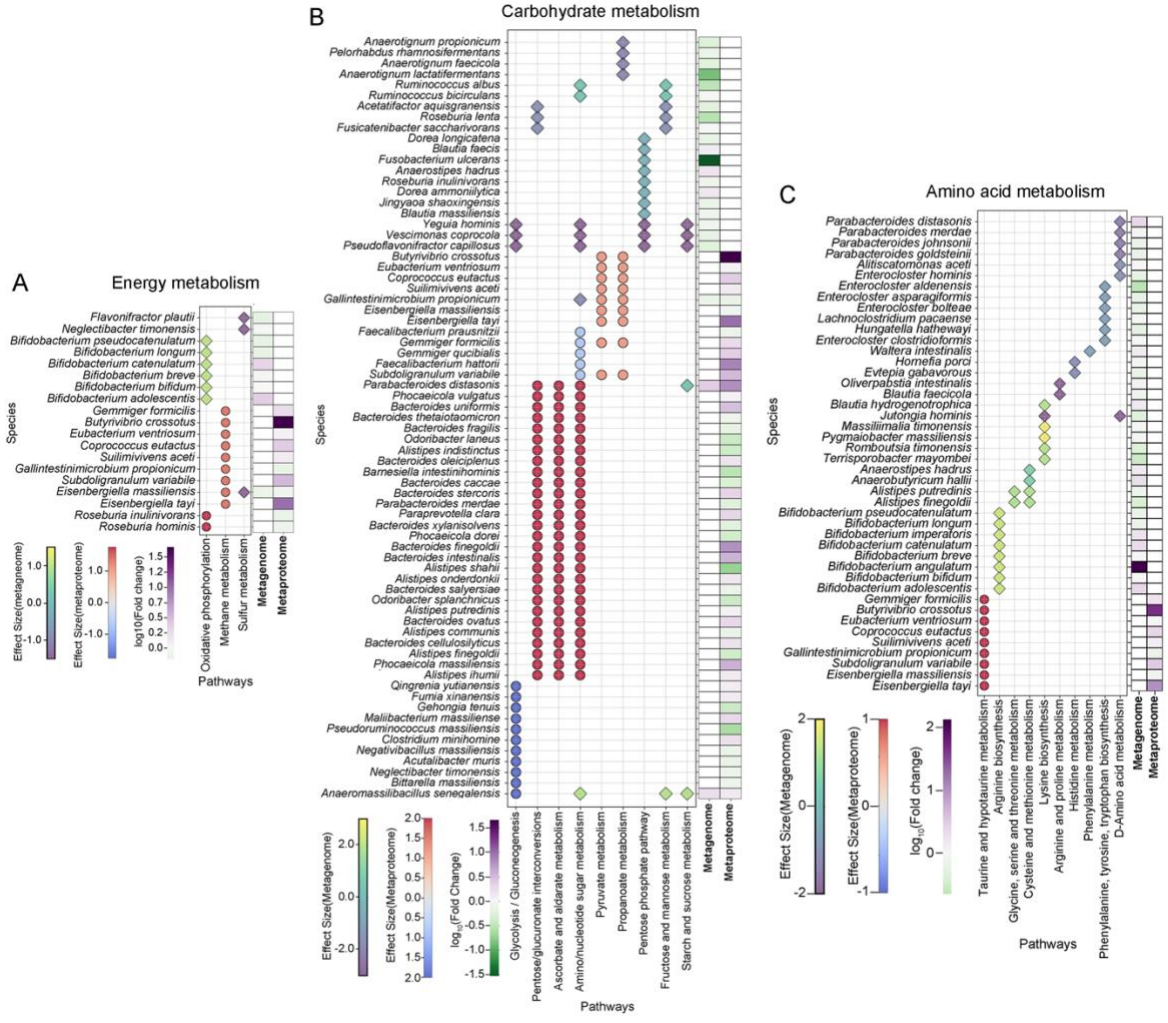

Figure 5.4 Species-specific changes in key metabolic pathways in the mother's microbiome. (A) Energy metabolism. (B) Carbohydrate metabolism. (C) Amino acid metabolism. Circle colors correspond to effect sizes (as shown in the color bar), and circle size indicate the magnitude of the fold change in pathway enrichment for each species. Metagenomic data reflect the genomic potential for functional activity, while metaproteomic data indicate active protein expression in these pathways.

5.4.5 Species-Specific Metabolic Function Changes in the Infant's Microbiome

Metagenomic and metaproteomic analyses revealed significant alterations in the infant's microbiome, particularly within pathways related to energy metabolism, carbohydrate metabolism, and amino acid metabolism. These changes were primarily observed at the metagenomic level, with limited corresponding functional activity detected in the metaproteomic data, reflecting the early developmental stage of the infant gut microbiome (Figure 5.5).

The metagenomic analysis showed significant enrichment in key energy metabolism pathways, particularly oxidative phosphorylation, methane metabolism, and sulfur metabolism. Species such as *Bifidobacterium breve* and *Bifidobacterium longum* were highly enriched in these pathways, indicating their potential roles in microbial energy production within the infant gut. However, despite strong genomic signals for these energy-related pathways, minimal protein expression was detected in the metaproteomic data, suggesting that these pathways are not yet functionally active or that the microbiome is still in the early stages of functional establishment.

Carbohydrate metabolism pathways exhibited significant species-specific enrichment in the infant’s microbiome at the metagenomic level. Pathways involved in the metabolism of starch and sucrose, fructose and mannose, and the pentose

phosphate pathway were particularly prominent. Species such as *Bacteroides vulgatus* and *Bifidobacterium longum* showed the highest effect sizes in these pathways, reflecting their capacity to degrade complex carbohydrates and contribute to short-chain fatty acid production—key processes for gut health and energy balance in infants. Similar to energy metabolism, these species displayed minimal protein expression in carbohydrate pathways, indicating that while the genomic potential for carbohydrate metabolism is present, functional activity may be delayed or not fully expressed at this developmental stage.

The metagenomic data also revealed significant enrichment in amino acid metabolism pathways, including glycine, serine, and threonine metabolism, arginine and proline metabolism, and cysteine and methionine metabolism. Species such as *Bifidobacterium longum*, *Parabacteroides distasonis*, and *Blautia faecis* exhibited substantial genomic contributions to these pathways, suggesting active roles in amino acid biosynthesis and degradation. However, similar to the energy and carbohydrate pathways, metaproteomic analysis showed limited protein expression, indicating that these metabolic functions may not yet be fully realized in the infant’s microbiome or may be subject to regulatory processes during early development.

The infant's microbiome exhibited significant species-specific enrichment across energy, carbohydrate, and amino acid metabolism pathways, predominantly at the metagenomic level. Species such as *Bifidobacterium longum*, *Bacteroides vulgatus*, and *Parabacteroides distasonis* were identified as key contributors to these metabolic processes. However, the limited protein expression observed in the metaproteomic data suggests a developmental lag between genomic potential and functional metabolic

activity, consistent with the early maturation of the infant gut microbiome. These findings highlight the dynamic nature of microbiome establishment in early life, with microbial species poised to fulfill essential metabolic roles as the microbiome continues to develop.

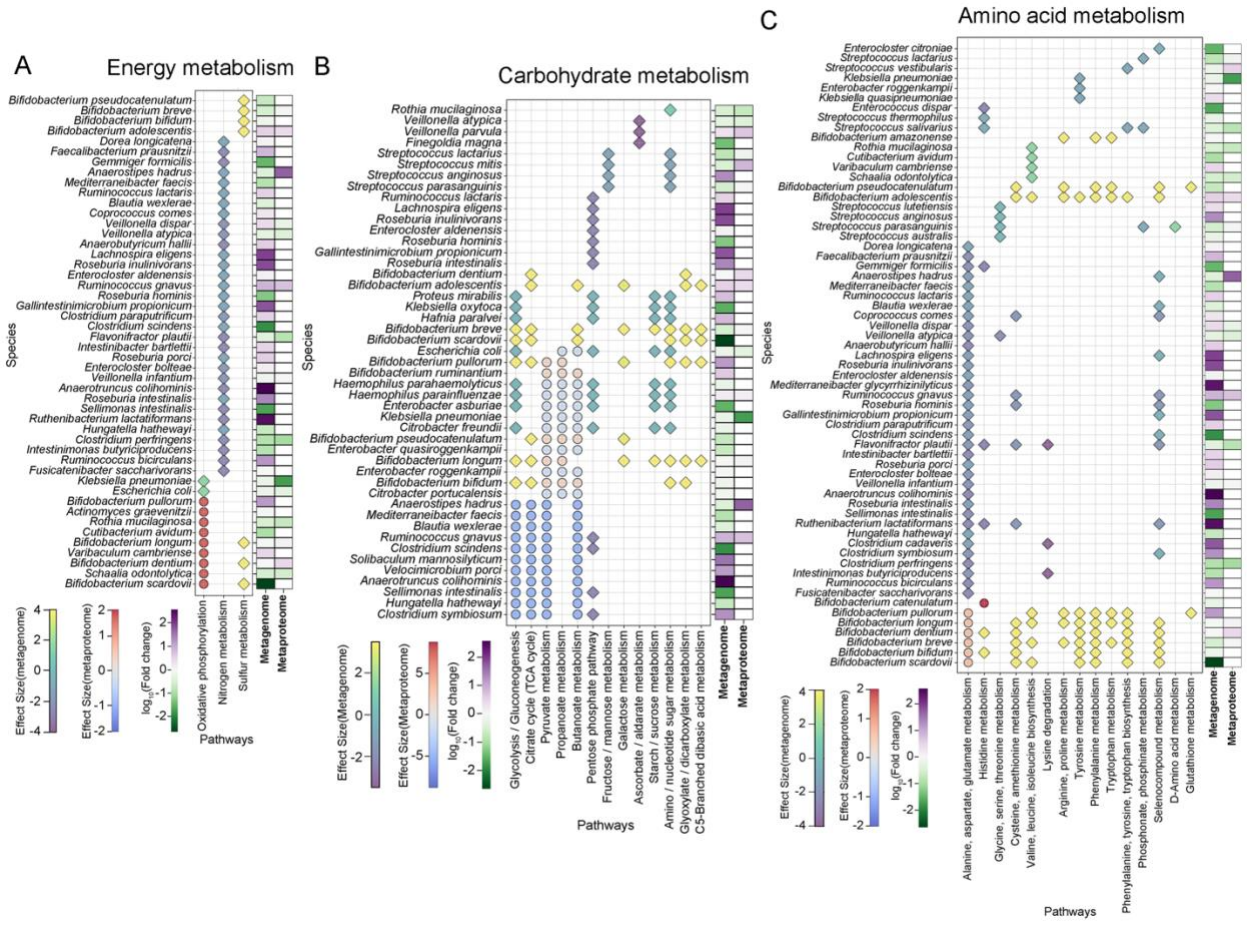

Figure 5.5 Species-specific changes in metabolic pathways in the infant's microbiome. (A) Energy Metabolism. (B) Carbohydrate Metabolism. (C) Amino Acid Metabolism. Circle size represents the fold change, and color indicates the effect size for each species across the different metabolic pathways. Positive effect sizes reflect increased species contributions to specific metabolic functions, while negative values indicate decreased contributions.

5.5 Discussion

This study provides critical insights into how dietary interventions during pregnancy can modulate the gut microbiome in women with gestational diabetes mellitus (GDM) and their infants, with implications for both microbial composition and functional capacity. The findings highlight the importance of dietary composition, particularly the balance of complex carbohydrates versus fat, in shaping the microbial ecosystem and its metabolic outputs. These insights may contribute to developing precision nutrition strategies aimed at improving maternal and infant health outcomes.

The data indicate that dietary intervention through the CHOICE diet—rich in complex carbohydrates—significantly increased microbial alpha diversity in the maternal gut microbiome. Specifically, alpha diversity increased by 9.6% in the CHOICE group compared to the conventional high-fat (CONV) diet group, a finding consistent with previous studies that link high-carbohydrate, fiber-rich diets to enhanced microbial diversity. Increased diversity is widely regarded as a marker of a resilient and healthy microbiome, which may help mitigate some of the adverse metabolic effects associated with GDM, such as inflammation and insulin resistance [263, 264].

However, while metagenomic analyses did not reveal significant taxonomic differences between the two diet groups, metaproteomic data showed clear functional differentiation. Notably, the CHOICE diet led to enhanced expression of proteins involved in short-chain fatty acid (SCFA) production, a key microbial function associated with anti-inflammatory properties and improved metabolic health. This finding underscores the importance of moving beyond taxonomic profiling to explore microbial

function, particularly in understanding how dietary interventions may affect metabolic health [265, 266].

The influence of maternal diet extended to the infant microbiome, particularly in terms of species composition and functional potential. Metagenomic analysis revealed significant species-specific enrichment in the infant microbiome, with key taxa such as *Bifidobacterium catenulatum* dominating. This species is known for its role in carbohydrate metabolism and early colonization of the infant gut, indicating potential benefits for infant gut health [267, 268]. However, the functional capacity of these species, as measured by metaproteomic analysis, remained largely undeveloped at this early stage of life, suggesting a lag in the activation of metabolic pathways.

This developmental lag in microbial function has important implications for early-life metabolic programming. While species colonization begins early, the full functional maturation of the microbiome—especially in terms of SCFA production and other metabolic processes—may take longer to establish [269, 270]. This observation is consistent with previous studies showing that microbial species are often acquired early in infancy but may require several months to reach functional maturity. The maternal CHOICE diet appeared to influence the transmission and early establishment of beneficial microbial species, which may have long-term implications for the infant's metabolic health, particularly in preventing conditions such as obesity and type 2 diabetes [271].

The integration of metagenomic and metaproteomic data revealed clear differences in the functional metabolic profiles of both the maternal and infant microbiomes. In the maternal microbiome, both genomic potential and protein

expression data pointed to significant enrichment in pathways related to energy metabolism, carbohydrate metabolism, and amino acid metabolism. This functional diversity reflects a metabolically active microbial community capable of supporting maternal energy balance and metabolic homeostasis, particularly through enhanced SCFA production in the CHOICE diet group [272].

In contrast, the infant microbiome, while exhibiting significant enrichment in similar metabolic pathways at the genomic level, demonstrated limited functional activity at the protein level. This finding highlights a critical period of microbiome development during which the genetic potential for metabolic function is present but has not yet translated into active protein expression. The delay in the functional activation of metabolic pathways, particularly those involved in SCFA production and lipid metabolism, may have important implications for the infant's immune and metabolic development. The maternal diet's influence on microbial species establishment, even without immediate functional activity, suggests potential long-term benefits as these pathways become fully activated.

The results of this study suggest that targeted dietary interventions, such as the CHOICE diet, may offer a promising approach to improving metabolic outcomes in both mothers and infants affected by GDM. By promoting a more diverse and functionally active microbial community, particularly one capable of producing SCFAs, the CHOICE diet could help reduce inflammation, support metabolic regulation, and mitigate the long-term health risks associated with GDM, such as type 2 diabetes [242, 273].

Moreover, the functional capacity of the microbiome, rather than taxonomic composition alone, appears to be a critical determinant of metabolic health. The

metaproteomic data reveal that while microbial diversity and taxonomic composition are important, the functional activities of microbial communities—specifically their ability to produce key metabolites such as SCFAs—may play an even more significant role in shaping health outcomes. This suggests that dietary interventions should not only aim to increase microbial diversity but also focus on enhancing the metabolic functions of the gut microbiome.

While the findings of this study provide valuable insights into the relationship between maternal diet, microbial composition, and metabolic function, several limitations must be acknowledged. First, the study's sample size was relatively small, limiting the generalizability of the results. Larger studies are needed to confirm these findings and further explore the long-term health implications of dietary interventions in GDM. Second, the follow-up period for infants was limited to a few months, leaving unanswered questions about the lasting effects of early microbiome changes on childhood and adult health outcomes. Longitudinal studies are essential to determine how early-life microbiome modulation affects long-term metabolic health and disease risk.

Future research should also investigate the specific dietary components responsible for driving the observed microbial and functional changes. For example, fiber types and complex carbohydrates likely play distinct roles in modulating microbial activity, but the exact mechanisms remain unclear. Additionally, more work is needed to explore the interactions between maternal diet, the microbiome, and other factors such as breastfeeding, which may also influence the infant microbiome's development and functional maturation.

Overall, this study demonstrates that maternal dietary interventions can significantly alter the taxonomic and functional landscape of the gut microbiome in women with GDM and their infants. The CHOICE diet, rich in complex carbohydrates, was particularly effective in promoting microbial diversity and enhancing the metabolic function of the microbiome, particularly SCFA production. These findings underscore the potential of precision nutrition strategies to optimize maternal and infant health by targeting both the composition and functionality of the gut microbiome. Further research is warranted to explore the long-term effects of these dietary interventions on metabolic health and disease prevention in both mothers and their children.

Chapter 6 Summary and Outlook

6.1 Summary of Findings

The microbial communities govern numerous processes that are essential for the stability of ecosystems and the functioning of biological systems, including nutrient cycling, energy flow, and interactions within and across species [44, 274]. The studies discussed in these chapters provide critical insights into microbial interactions, ranging from biogeochemical cycles to human health contexts. These findings underscore the complexity and importance of understanding microbial dynamics and open the door to potential applications in biotechnology, ecology, agriculture, and medicine.

6.1.1 Ecological and Biotechnological Implications of Microbial Metabolic Dependencies

Microbial communities operate through a web of metabolic dependencies that are crucial for their survival and functionality in different environments [275, 276]. These dependencies—whether through cross-feeding (where one microorganism produces a metabolite used by another), syntrophy (mutualistic metabolic cooperation), or resource partitioning—enable microbial communities to maintain stability, resist environmental stresses, and efficiently cycle nutrients.

In recent years, multi-omics technologies such as metagenomics, metaproteomics, and metabolomics, coupled with computational modeling, have provided a more nuanced understanding of how these metabolic dependencies shape community structure and function [275]. This chapter highlights how these advancements have revealed the critical roles microbial interactions play not only in natural ecosystems but also in engineered environments, such as wastewater treatment systems and bioreactors.

The ecological implications are vast, with these interactions driving nutrient cycling and organic matter decomposition, processes that are essential for sustaining life on Earth. From a biotechnological standpoint, manipulating these interactions offers the potential for optimizing microbial consortia in industrial processes, such as biofuel production, bioremediation, and the sustainable management of agricultural systems [277-279]. Future research should focus on the application of these insights to develop more robust microbial consortia capable of performing complex tasks in diverse and dynamic environments.

6.1.2 Emergent Properties of Quad-Culture Microbial Communities

This study of synthetic microbial consortia, composed of four species performing distinct but interconnected metabolic roles, demonstrates the potential of engineered microbial systems to perform complex tasks. The quad-culture system, which included a cellulolytic bacterium (*R. cellulolyticum*), a hydrogenotrophic methanogen (*M. hungatei*), an acetoclastic methanogen (*M. concilii*), and a sulfate-reducing bacterium (*D. vulgaris*), highlighted the emergent properties of microbial interactions. These interactions are greater than the sum of their parts, as shown by the increased methane production and decreased cellulose degradation compared to simpler configurations (e.g., bi- and tri-cultures).

The discovery of both positive and negative synergies in microbial cooperation offers new insights into how higher-order interactions (i.e., interactions among three or more species) influence community metabolism [4, 171]. These findings are important for the design of synthetic microbial consortia for industrial processes such as bioenergy production and waste management. Understanding the conditions under which positive

synergies occur can lead to the development of more efficient and sustainable bioprocesses.

Future work should explore the role of environmental factors in influencing these emergent properties and investigate how changes in nutrient availability, pH, or temperature might enhance or hinder these interactions. By doing so, researchers can fine-tune microbial consortia for specific industrial applications, potentially unlocking new avenues for bioengineering.

6.1.3 Higher-Order Interactions in Anaerobic Microbial Communities

Microbial communities in anaerobic environments are involved in key processes such as methanogenesis, a critical component of the global carbon cycle. In this study, bi-, tri-, and quad-cultures were analyzed to understand how higher-order interactions influence community structure and functionality. One notable finding was that the inclusion of *D. vulgaris* in the quad-culture reduced metabolic redundancy and facilitated balanced interactions, resulting in a substantial increase in methane production.

Higher-order interactions often give rise to emergent properties—traits or behaviors that are not present in simpler systems. In this case, the presence of multiple interacting species led to enhanced methanogenic efficiency and reduced competition for resources. These findings suggest that understanding microbial interactions in complex systems can inform the design of microbial consortia that are more efficient and resilient.

In future research, the focus should be on exploring the dynamic reorganization of metabolic pathways in response to environmental changes, such as the introduction of new substrates or perturbations in environmental conditions. This will help in

predicting microbial community behavior and designing consortia that can adapt to different industrial or environmental challenges.

6.1.4 Effects of Climate Change on Wetland Microbial Communities

Wetlands are vital ecosystems that play a significant role in the global carbon cycle. However, climate change, through processes such as sea-level rise and droughts, is altering the microbial communities that govern carbon cycling in these environments. This study investigates how two key stressors—elevated oxygen and sulfate levels—impact microbial interactions and, consequently, greenhouse gas emissions.

The results indicate that sulfate and oxygen exposure lead to a significant reduction in methane (CH_4) emissions, with hydrogenotrophic methanogenesis being more suppressed than acetoclastic methanogenesis. The shift from methane to carbon dioxide (CO_2) emissions under elevated oxygen conditions suggests that climate change could alter the balance of greenhouse gases emitted from wetlands, potentially reducing the overall warming effect of these emissions.

The findings from this study provide critical insights into how microbial communities might respond to future climate scenarios. However, predicting the exact outcomes of these changes will require further research that integrates both field data and laboratory-based studies. By understanding how microbial interactions are reshaped under climate stress, we can better model future emissions and develop strategies to mitigate the impact of climate change on wetland ecosystems.

6.1.5 Gut Microbiome and Gestational Diabetes Mellitus (GDM)

The human gut microbiome is an increasingly important area of research, particularly in understanding how it influences health outcomes in both mothers and infants. This study of women with gestational diabetes mellitus (GDM) investigates how dietary interventions can modulate the gut microbiome and improve health outcomes. The results indicate that maternal diet significantly alters microbial diversity in both mothers and infants, with higher alpha diversity observed in those following a complex carbohydrate-rich diet (CHOICE diet).

The ability of dietary interventions to shift the composition and function of the gut microbiome highlights the potential for precision medicine approaches that target specific microbiome profiles to prevent or manage disease. In this case, the study offers promising evidence that dietary manipulation can positively affect the gut microbiome in the context of GDM, a pregnancy complication that can have long-term effects on both maternal and infant health.

Future research should explore the mechanistic links between dietary interventions, microbiome composition, and health outcomes. In addition, personalized nutrition approaches could be developed that consider individual microbiome profiles to optimize dietary recommendations for managing GDM and other metabolic disorders.

6.2 Outlook and Future Directions

The collective insights from these chapters highlight the pivotal role of microbial interactions across diverse ecosystems and health contexts. While significant progress has been made, there are still many avenues for future research and applications.

6.2.1 Advances in Multi-Omics and Computational Modeling

The rapid advancements in multi-omics technologies, combined with increasingly sophisticated computational models, are transforming our understanding of microbial ecosystems [79, 280]. These tools allow for the comprehensive analysis of microbial communities, revealing previously hidden interactions and dependencies. Moving forward, researchers should focus on integrating multi-omics data from diverse ecosystems to build predictive models of microbial behavior.

As computational models become more advanced, they can be used to simulate how microbial communities respond to environmental changes, nutrient inputs, or perturbations. This will have significant implications for managing ecosystems under stress, as well as for designing synthetic microbial consortia with desired properties for industrial applications.

6.2.2 Synthetic Microbial Communities for Biotechnological Innovation

Synthetic biology offers exciting opportunities for engineering microbial consortia that perform specific tasks, such as waste degradation, biofuel production, or bioremediation. The findings from the quad-culture study highlight the potential for designing microbial systems that capitalize on emergent properties, such as increased metabolic efficiency or synergistic cooperation.

Future work should aim to create modular and adaptive microbial consortia that can be fine-tuned for different environments or industrial processes. Additionally, exploring how environmental factors influence these interactions will be critical for scaling up these systems for real-world applications.

6.2.3 Microbial Responses to Climate Change

As climate change intensifies, understanding how microbial communities respond to environmental stressors will be crucial for predicting changes in ecosystem function and greenhouse gas emissions [281]. Wetlands are sensitive to shifts in oxygen and sulfate levels, and microbial communities in these ecosystems are key drivers of carbon cycling.

Future research should focus on integrating microbial dynamics into global climate models, helping to predict how climate change will impact microbial-driven processes such as methanogenesis and carbon sequestration. These insights will inform conservation strategies and guide efforts to mitigate the effects of climate change on critical ecosystems.

6.2.4 Precision Medicine and the Human Microbiome

The growing understanding of the human microbiome opens new possibilities for precision medicine, where treatments are tailored to an individual's microbiome profile. The GDM study demonstrates the potential for dietary interventions to modulate the microbiome and improve health outcomes.

In the future, personalized nutrition and microbiome-based therapies could be developed to target specific health conditions, such as metabolic disorders, autoimmune diseases, and pregnancy complications. By continuing to explore the complex interactions between diet, microbiome, and health, researchers can develop more effective, individualized treatment plans.

6.3 Conclusion

Microbial interactions play a foundational role in shaping ecosystems and human health. The studies presented in these chapters provide valuable insights into how microbial communities function, how they respond to environmental changes, and how they can be harnessed for biotechnological and medical applications. As our understanding of microbial interactions deepens, we are poised to unlock new strategies for managing ecosystems, improving human health, and mitigating the impacts of climate change. The future of microbiome research lies in the integration of multi-omics data, advanced modeling, and innovative applications that capitalize on the power of microbial ecosystems.

Appendix A: Supplementary Figures

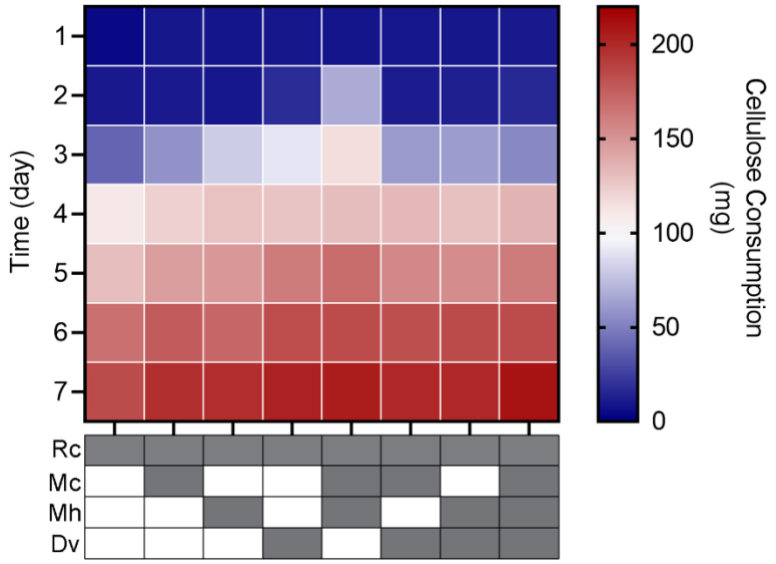

Figure S2.1 Cellulose consumption by the synthetic communities in the control condition. *Ruminiclostridium cellulolyticum* (Rc) *Methanosaeta concilii* (Mc) *Methanospirillum hungatei* (Mh) and *Desulfovibrio vulgaris* (Dv). Grey filling indicates the microorganisms contained in the corresponding cultures.

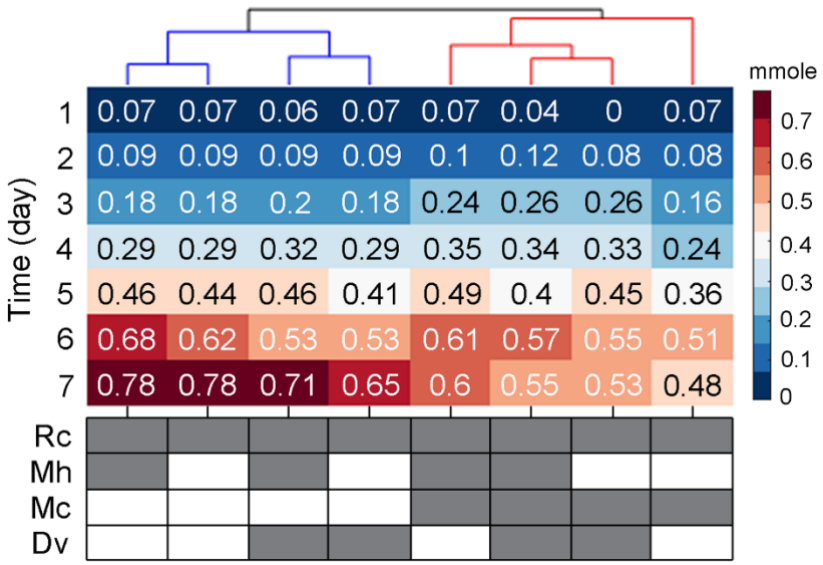

Figure S2.2 Acetate accumulation over 7 days of cultivation in the control condition. *Ruminiclostridium cellulolyticum* (Rc) *Methanosaeta concilii* (Mc) *Methanospirillum hungatei* (Mh) and *Desulfovibrio vulgaris* (Dv). Grey filling indicates the microorganisms contained in the corresponding cultures.

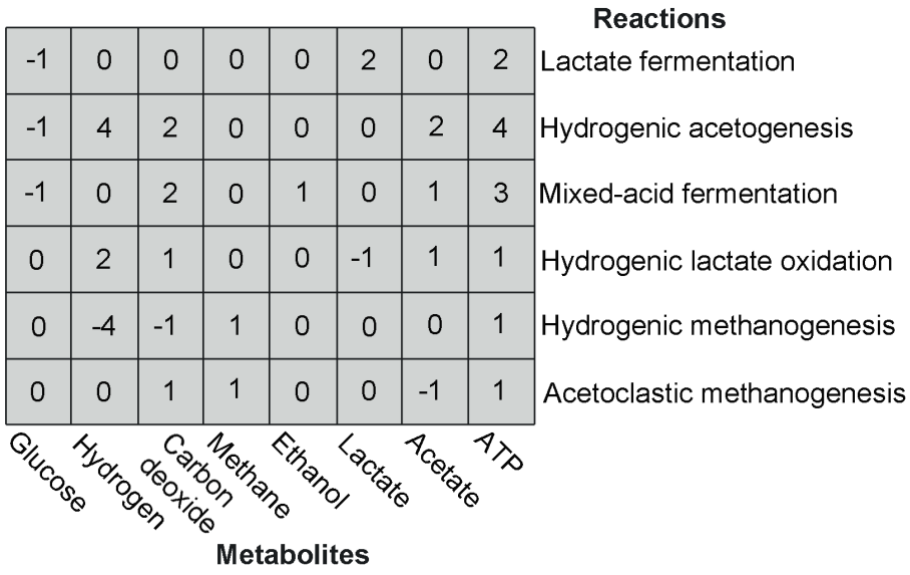

Figure S3.1 The stoichiometric matrix in modeling analysis. Each matrix element is the stoichiometric coefficient of a metabolite in a reaction. Positive values correspond to the amounts of metabolites produced by the reaction. Negative values denote consumption. A value of zero indicates no involvement of metabolites in the reaction.

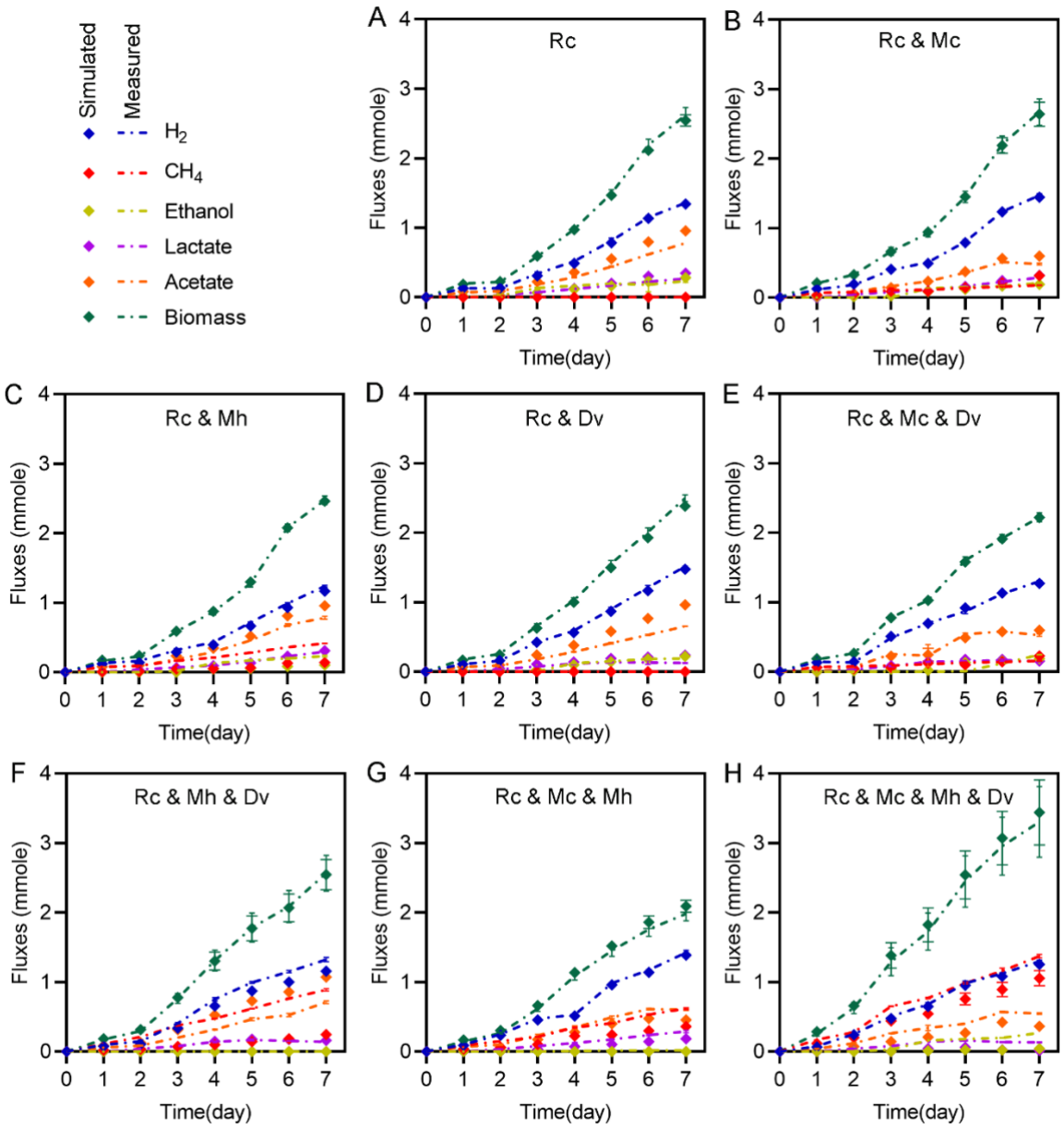

Figure S3.2 Model fitting and average fluxes across all the cultures. The resulting fits indicate the relative contribution of each reaction to the overall observed transformations. Deviations between the inferred metabolic transformations and the measured transformations indicate uncertainty in the understanding of metabolic transformations or limitations in analytical capacity.

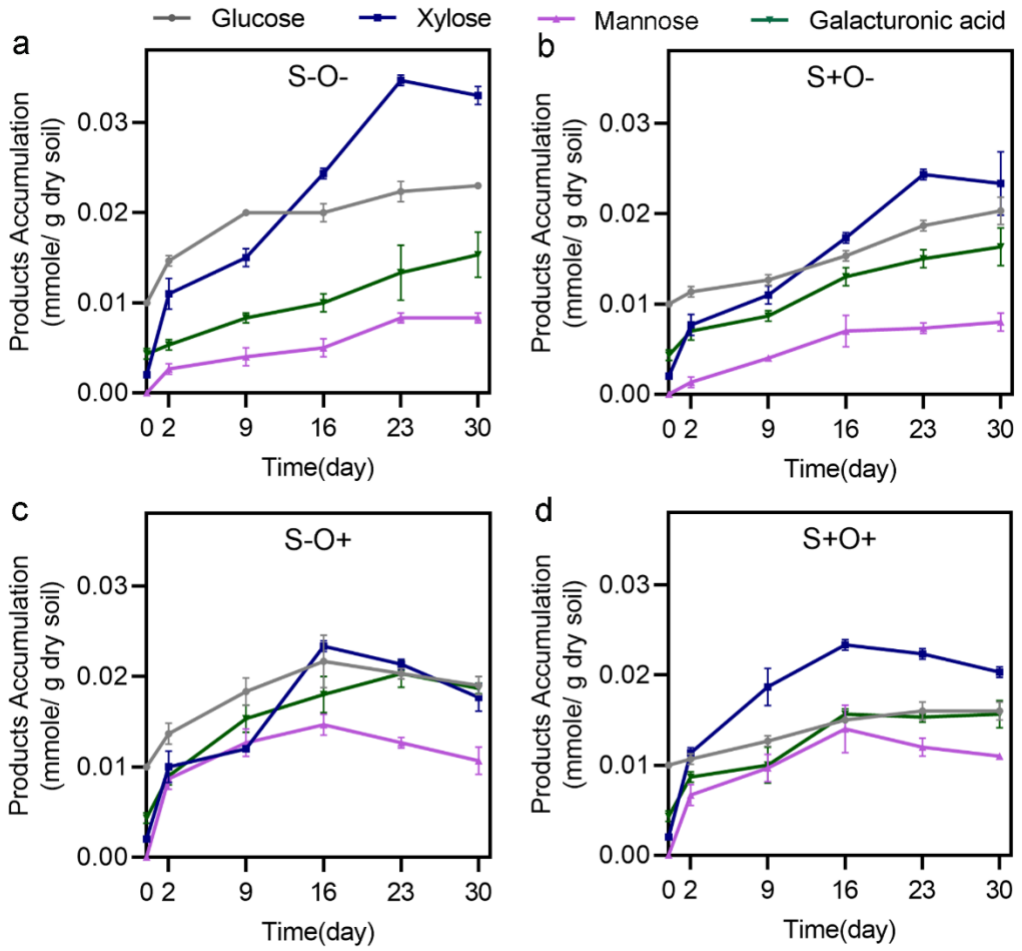

Figure S4.1 Accumulation of monosaccharides over a 30-day incubation under the four conditions. The error bars are defined as standard deviation.

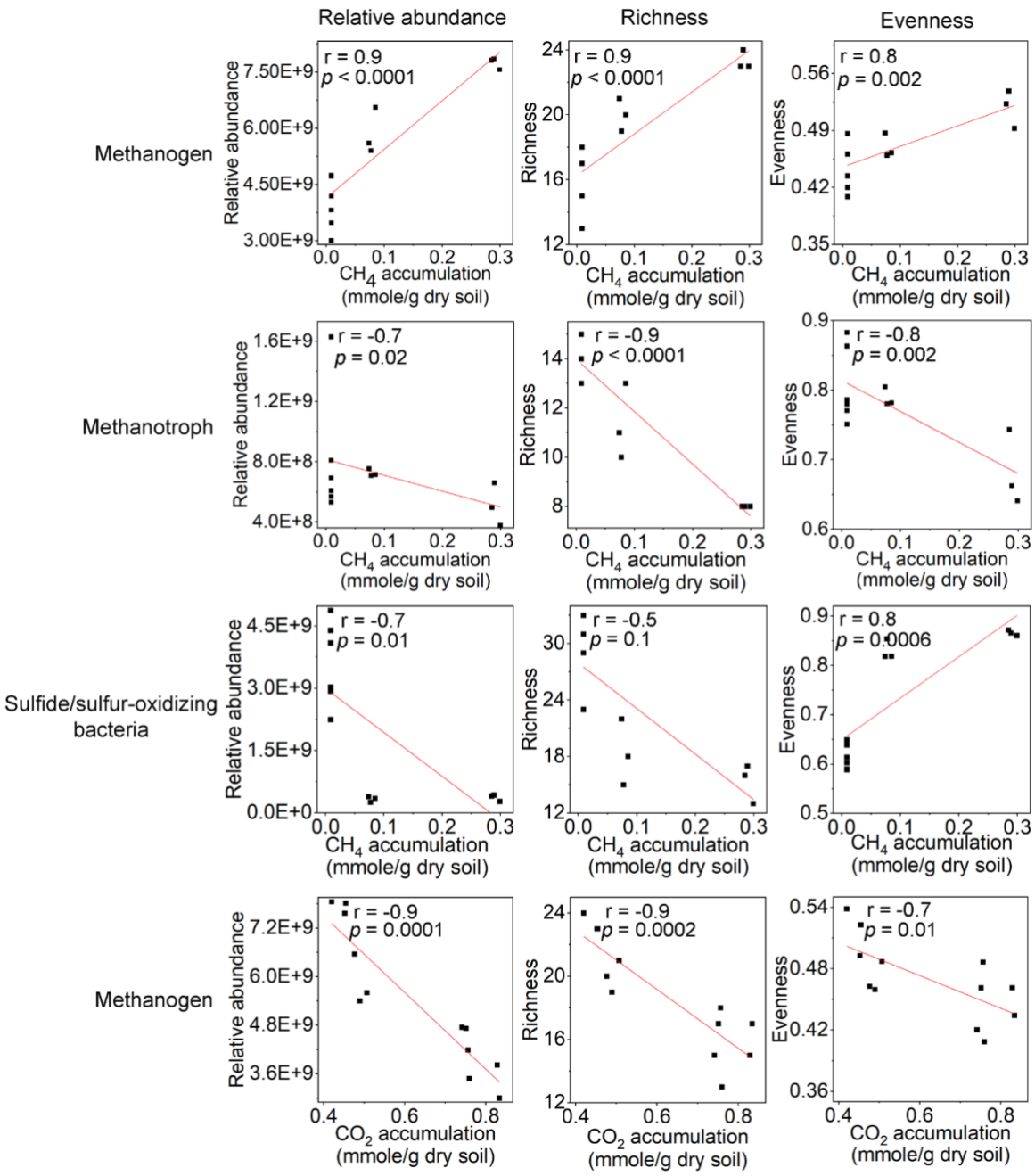

Figure 4.2 Correlation between the accumulations of CH_4 and CO_2 , and the proteome abundance, richness, and evenness of methanogen, methanotroph, and sulfide/sulfur-oxidizing bacterial communities. Each dot represents an experimental measurement (X-axis for geochemical measurements, Y-axis for metaproteomic measurements) from the four conditions with three replicates, and the red line displays best linear fit. r is the Pearson correlation coefficient, and *p* values were determined by t-test.

Glucose	Hydrogen	Carbon deoxide	Methane	Sulfide	Lactate	Acetate	Butyrate	Reactions
-1	0	6	0	0	0	0	0	Aerobic heterotroph
-1	0	0	0	0	2	0	0	Lactate fermentation
-1	4	2	0	0	0	2	0	Hydrogenic acetogenesis
0	0	1	0	0.5	-1	1	0	Sulfidogenic lactate oxidation
0	-2	0	0	0.5	0	0	0	Sulfidogenic hydrogen oxidation
0	-4	-1	1	0	0	0	0	Hydrogenic methanogenesis
0	0	1	1	0	0	-1	0	Acetoclastic methanogenesis
0	0	1	-1	0	0	0	0	Methane oxidation
-1	2	2	0	0	0	0	1	Butyrate production

Metabolites

Figure S4.3 The stoichiometric matrix in modeling analysis. Each matrix element is the stoichiometric coefficient of a metabolite in a reaction. Positive values correspond to the amounts of metabolites produced by the reaction. Negative values denote consumption. A value of zero indicates no involvement of metabolites in the reaction.

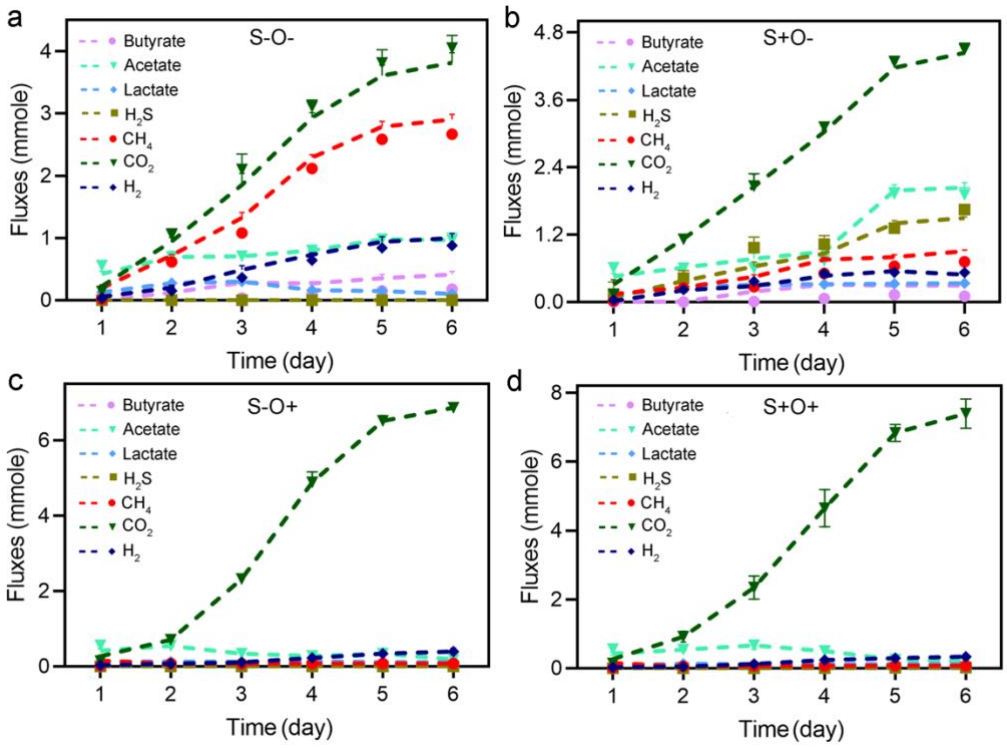

Figure S4.4 Model fitting and average fluxes under four conditions. (a-d) Modeling fitting in the S-O- (A), S+O- (B), S-O+ (C) and S+O+ (D) conditions. The resulting fits indicate the relative contribution of each reaction to the overall observed transformations. Deviations between the inferred metabolic transformations and the measured transformations indicate uncertainty in the understanding of metabolic transformations or limitations in analytical capacity.

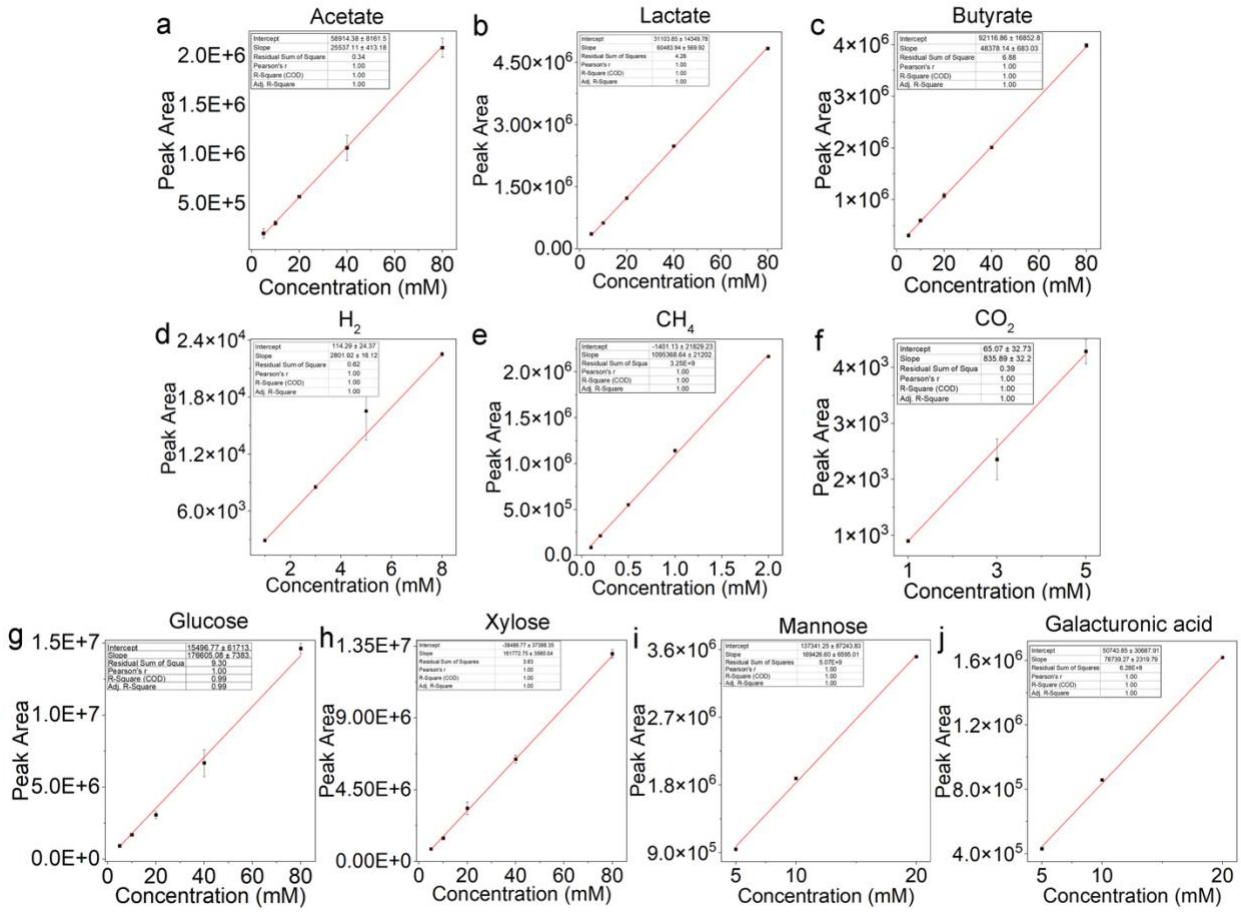

Figure S4.5 Calibration curves of known standards.

Table S2.1 General concept of the stoichiometric model under control condition.

Measured data		Overall catabolic reaction stoichiometries							Fit of measurements	
		R. cellulolyticum		*D. vulgaris*			*M. hungatei*	*M. concilii*	Sum of contributions	
Metabolites	mmoles accumulated	Lactate fermentation	Hydrogenic acetogenesis	Hydogenic lactate oxidation	Sulfidogenic lactate oxidation	Sulfidogenic hydrogen oxidation	Excluding Hydrogenic acetogenesis	Excluding Hydogenic lactate oxidation		
Glucose	-1.17	-1	-1	0	0	0	0	0	-0.90	-0.90
Lactate	0.13	2	0	-1	-1	0	0	0	0.22	0.22
Acetate	0.55	0	2	1	1	0	0	-1	0.62	0.62
Hydrogen	1.30	0	4	2	0	-2	-4	0	1.31	1.31
Carbon Dioxide	1.28	0	2	1	1	0	-1	1	2.07	2.07
Methane	1.37	0	0	0	0	0	1	1	1.42	1.42
Sulfide	0.00	0	0	0	0.5	0.5	0	0	0.00	0.00
									$\sum(x_{measured} - x_{fit})^2$	
Flux through each reaction	Scenario 1	0.90	0.00	1.57	0.00	0.00	0.46	0.96	0.71	
	Scenario 2	0.11	0.79	0.00	0.00	0.00	0.46	0.96		0.71

Table S2.2 General concept of the stochiometric model under sulfate addition condition.

Measured data		Overall catabolic reaction stoichiometries							Fit of measurements		
		R. cellulolyticum		*D. vulgaris*			*M. hungatei*	*M. concilii*	Sum of contributions		
Metabolites	mmoles accumulated	Lactate fermentation	Hydrogenic acetogenesis	Hydogenic lactate oxidation	Sulfidogenic lactate oxidation	Sulfidogenic hydrogen oxidation	Hydrogenotrophic methanogenesis	Acetotrophic methanogenesis	Excluding lactate fermentation	Excluding sulfidogenic lactate oxidation	Excluding hydrogenic acetogenesis
Glucose	-1.14	-1	-1	0	0	0	0	0	-1.11	-0.87	-0.098
Lactate	0.23	2	0	-1	-1	0	0	0	2.03	0.00	0
Acetate	0.49	0	2	1	1	0	0	-1	0.00	0.24	1.02
Hydrogen	1.07	0	4	2	0	-2	-4	0	0.00	1.55	0
Carbon Dioxide	1.00	0	2	1	1	0	-1	1	1.55	0.00	1.55
Methane	1.21	0	0	0	0	0	1	1	0.00	0.00	0
Sulfide	1.17	0	0	0	0.5	0.5	0	0	1.38	1.38	1.38
									$\sum(x_{measured} - x_{fit})^2$		
Flux through each reaction	Scenario 1	1.12	0.00	2.03	0.00	1.55	0.00	1.38	6.44		
	Scenario 2	0.87	0.24	0.00	1.55	0.00	0.00	1.38		2.93	
	Scenario 3	0.09	1.02	0	0	1.55	0	1.38			4.38

Table S2.3 Comparison of stoichiometric fluxes and marker protein abundances.

Species		Modeling					Proteomics			
		Control Condition		Sulfate addition condition			Protein Name	Change	Fold Change	*q*-value
	Reaction \ Scenario	Scenario 1	Scenario 2	Scenario 1	Scenario 2	Scenario 3				
R. cellulolyticum	Lactate fermentation	0.90 ± 0.011	0.11 ± 0.002	1.12 ± 0.008	0.87 ± 0.009	0.099 ± 0.001	L-lactate dehydrogenase (Ldh)	Up	3.7	0.04
	Hydrogenic acetogenesis	0 ± 0	0.79 ± 0.009	0 ± 0	0.24 ± 0.001	1.02 ± 0.008	Acetate kinase (Ack)	Null	1.2	0.9
D. vulgaris	Hydrogenic lactate oxidation	1.58 ± 0.018	0 ± 0	2.03 ± 0.016	0 ± 0	0 ± 0	L-lactate dehydrogenase (Ldh)	Null	1.3	NA
	Sulfidogenic lactate oxidation	0 ± 0	0 ± 0	0 ± 0	1.55 ± 0.02	0 ± 0	Sulfide reductase (Srd)	Up	2.0	0.009
	Sulfidogenic hydrogen oxidation	0 ± 0	0 ± 0	1.55 ± 0.02	0 ± 0	1.55 ± 0.02	FeS cluster assembly ATPase	Up	1.8	0.001
M. hungatei	Hydrogenotrophic methanogenesis	0.46 ± 0.005	0.46 ± 0.005	0 ± 0	0 ± 0	0 ± 0	Formate dehydrogenase (Fdh)	Down	27.8	<0.0001
M. concilii	Acetoclastic methanogenesis	0.97 ± 0.02	0.97 ± 0.02	1.38 ± 0.02	1.38 ± 0.02	1.38 ± 0.02	Methyl-coenzyme M reductase (Mcr)	Down	2.2	0.001

Table S5.1 Comparison of stoichiometric fluxes and marker protein abundances.

Modeling				Proteomics			
Reactions	Treatments			Maker proteins	Treatments		
	F (1,8) (*p*-value)				F (1,8) (*p*-value)		
	SO_4^{2-}	O_2	Interaction		SO_4^{2-}	O_2	Interaction
Aerobic Heterotroph	5.1	3633 (***)	5.1	Cytochrome c oxidase (ccoN)	72.8 (***)	141.9 (***)	72.8 (***)
Lactate Fermentation	113.7 (***)	34.8 (***)	44.1 (***)	L-lactate dehydrogenase (Ldh)	1.7	0.02	0.1
Hydrogenic acetogenesis	16.2 (**)	4545 (***)	24.5 (**)	Acetate kinase (Ack)	0.6	0.6	1.4
Sulfidogenic lactate oxidation	50.4 (***)	50.4 (***)	50.4 (***)	Sulfide reductase (Srd)	0.7	0.2	0.08
Sulfidogenic hydrogen oxidation	14784 (***)	14784 (***)	14784 (***)	Dissimilatory sulfite reductase (Dsr)	10.6 (**)	0.03	0
Hydrogenic Methanogenesis	1147 (***)	1064 (***)	1141 (***)	Ferredoxin oxidoreductase (Frt)	0.8	0.6	4.9
Acetoclastic Methanogenesis	1728 (***)	19020 (***)	1744 (***)	Phosphate acetyltransferase (Pta)	9.1 (*)	0.01	0.7
Methane oxidation	2.1	145.8 (***)	2.1	Methane/ammonia monooxygenase (Pmo)	5.2	17.9 (**)	1.7
Butyrate production	6.2	217.2 (***)	6.2	3-hydroxyisobutyrate dehydrogenase (HIBADH)	2	0	0

Reference

1. Reineke, W. and M. Schlömann, *Microorganisms at different sites: Living conditions and adaptation strategies*, in *Environmental Microbiology*. 2023, Springer. p. 349-396.
2. Mustafa, G., et al., *Microbiology of wetlands and the carbon cycle in coastal wetland mediated by microorganisms.* Science of The Total Environment, 2024: p. 175734.
3. Banerjee, S. and M.G. van der Heijden, *Soil microbiomes and one health.* Nature Reviews Microbiology, 2023. **21**(1): p. 6-20.
4. Peng, X., et al., *Metabolic interdependencies in thermophilic communities are revealed using co-occurrence and complementarity networks.* Nature Communications, 2024. **15**(1): p. 8166.
5. Kost, C., et al., *Metabolic exchanges are ubiquitous in natural microbial communities.* Nature Microbiology, 2023. **8**(12): p. 2244-2252.
6. Custer, G.F., L. Bresciani, and F. Dini-Andreote, *Toward an integrative framework for microbial community coalescence.* Trends in Microbiology, 2024. **32**(3): p. 241-251.
7. Abreu, N.A. and M.E. Taga, *Decoding molecular interactions in microbial communities.* FEMS Microbiology Reviews, 2016. **40**(5): p. 648-663.
8. Freilich, S., et al., *Competitive and cooperative metabolic interactions in bacterial communities.* Nature communications, 2011. **2**(1): p. 589.
9. Konopka, A., S. Lindemann, and J. Fredrickson, *Dynamics in microbial communities: unraveling mechanisms to identify principles.* The ISME journal, 2015. **9**(7): p. 1488-1495.
10. Madsen, E.L., *Microorganisms and their roles in fundamental biogeochemical cycles.* Current opinion in biotechnology, 2011. **22**(3): p. 456-464.
11. Hemkemeyer, M., et al., *Functions of elements in soil microorganisms.* Microbiological Research, 2021. **252**: p. 126832.
12. Trudinger, P., D. Swaine, and G. Skyring, *Biogeochemical cycling of elements–general considerations*, in *Studies in Environmental Science*. 1979, Elsevier. p. 1-27.
13. Sanyal, S.K., J. Shuster, and F. Reith, *Cycling of biogenic elements drives biogeochemical gold cycling.* Earth-Science Reviews, 2019. **190**: p. 131-147.
14. Moran, M.A., et al., *Microbial metabolites in the marine carbon cycle.* Nature microbiology, 2022. **7**(4): p. 508-523.
15. Prasad, S., et al., *Soil microbiomes for healthy nutrient recycling.* Current trends in microbial biotechnology for sustainable agriculture, 2021: p. 1-21.
16. Richter, D.d., et al., *Long-term soil experiments: Keys to managing Earth's rapidly changing ecosystems.* Soil Science Society of America Journal, 2007. **71**(2): p. 266-279.
17. Powers, J.S. and E. Marín-Spiotta, *Ecosystem processes and biogeochemical cycles in secondary tropical forest succession.* Annual Review of Ecology, Evolution, and Systematics, 2017. **48**(1): p. 497-519.

18. Round, J.L. and S.K. Mazmanian, *The gut microbiota shapes intestinal immune responses during health and disease.* Nature reviews immunology, 2009. **9**(5): p. 313-323.
19. Fan, Y. and O. Pedersen, *Gut microbiota in human metabolic health and disease.* Nature Reviews Microbiology, 2021. **19**(1): p. 55-71.
20. Aziz, Q., et al., *Gut microbiota and gastrointestinal health: current concepts and future directions.* Neurogastroenterology & Motility, 2013. **25**(1): p. 4-15.
21. Flint, H.J., et al., *The role of the gut microbiota in nutrition and health.* Nature reviews Gastroenterology & hepatology, 2012. **9**(10): p. 577-589.
22. Blaak, E., et al., *Short chain fatty acids in human gut and metabolic health.* Beneficial microbes, 2020. **11**(5): p. 411-455.
23. Fusco, W., et al., *Short-chain fatty-acid-producing bacteria: key components of the human gut microbiota.* Nutrients, 2023. **15**(9): p. 2211.
24. Juarez, V.M., A.N. Montalbine, and A. Singh, *Microbiome as an immune regulator in health, disease, and therapeutics.* Advanced drug delivery reviews, 2022. **188**: p. 114400.
25. Schnupf, P., V. Gaboriau-Routhiau, and N. Cerf-Bensussan, *Modulation of the gut microbiota to improve innate resistance.* Current Opinion in Immunology, 2018. **54**: p. 137-144.
26. Boulangé, C.L., et al., *Impact of the gut microbiota on inflammation, obesity, and metabolic disease.* Genome medicine, 2016. **8**: p. 1-12.
27. Sultan, S., et al., *Metabolic influences of gut microbiota dysbiosis on inflammatory bowel disease.* Frontiers in physiology, 2021. **12**: p. 715506.
28. Tilg, H., et al., *The intestinal microbiota fuelling metabolic inflammation.* Nature Reviews Immunology, 2020. **20**(1): p. 40-54.
29. Vethathirri, R.S., E. Santillan, and S. Wuertz, *Microbial community-based protein production from wastewater for animal feed applications.* Bioresource Technology, 2021. **341**: p. 125723.
30. Angenent, L.T., et al., *Production of bioenergy and biochemicals from industrial and agricultural wastewater.* TRENDS in Biotechnology, 2004. **22**(9): p. 477-485.
31. Gilmore, S.P. and M.A. O'Malley, *Microbial communities for bioprocessing: lessons learned from nature.* Current Opinion in Chemical Engineering, 2016. **14**: p. 103-109.
32. El-Metwally, M.M., et al., *Symbiotic relationships with fungi: From Mutualism to parasitism*, in *Plant mycobiome: diversity, interactions and uses*. 2023, Springer. p. 375-413.
33. Hagen, M., et al., *Biodiversity, species interactions and ecological networks in a fragmented world*, in *Advances in ecological research*. 2012, Elsevier. p. 89-210.
34. Woodward, G., et al., *Ecological networks in a changing climate*, in *Advances in ecological research*. 2010, Elsevier. p. 71-138.
35. Strogatz, S.H., *Exploring complex networks.* nature, 2001. **410**(6825): p. 268-276.
36. Wootton, J.T., *The nature and consequences of indirect effects in ecological communities.* Annual review of ecology and systematics, 1994: p. 443-466.
37. Mus, F., et al., *Symbiotic nitrogen fixation and the challenges to its extension to nonlegumes.* Applied and environmental microbiology, 2016. **82**(13): p. 3698-3710.

38. Costa, S.R., J.L.P. Ng, and U. Mathesius, *Interaction of symbiotic rhizobia and parasitic root-knot nematodes in legume roots: from molecular regulation to field application*. Molecular Plant-Microbe Interactions, 2021. **34**(5): p. 470-490.
39. Stevens, E.J., K.A. Bates, and K.C. King, *Host microbiota can facilitate pathogen infection*. PLoS pathogens, 2021. **17**(5): p. e1009514.
40. Sarsan, S., et al., *Synergistic interactions among microbial communities*. Microbes in microbial communities: ecological and applied perspectives, 2021: p. 1-37.
41. Wang, C. and Y. Kuzyakov, *Mechanisms and implications of bacterial–fungal competition for soil resources*. The ISME Journal, 2024. **18**(1): p. wrae073.
42. Mataigne, V., et al., *Microbial systems ecology to understand cross-feeding in microbiomes*. Frontiers in Microbiology, 2021. **12**: p. 780469.
43. Pontrelli, S., et al., *Metabolic cross-feeding structures the assembly of polysaccharide degrading communities*. Science advances, 2022. **8**(8): p. eabk3076.
44. Gralka, M., et al., *Trophic interactions and the drivers of microbial community assembly*. Current Biology, 2020. **30**(19): p. R1176-R1188.
45. van den Berg, N.I., et al., *Ecological modelling approaches for predicting emergent properties in microbial communities*. Nature ecology & evolution, 2022. **6**(7): p. 855-865.
46. Lopatkin, A.J. and J.J. Collins, *Predictive biology: modelling, understanding and harnessing microbial complexity*. Nature Reviews Microbiology, 2020. **18**(9): p. 507-520.
47. Gowda, K., et al., *Genomic structure predicts metabolite dynamics in microbial communities*. Cell, 2022. **185**(3): p. 530-546. e25.
48. Matchado, M.S., et al., *Network analysis methods for studying microbial communities: A mini review*. Computational and structural biotechnology journal, 2021. **19**: p. 2687-2698.
49. Joseph, T.A., et al., *Compositional Lotka-Volterra describes microbial dynamics in the simplex*. PLoS computational biology, 2020. **16**(5): p. e1007917.
50. Aguadé-Gorgorió, G., A.R. Anderson, and R. Solé, *Modeling tumors as complex ecosystems*. Iscience, 2024. **27**(9).
51. Picot, A., et al., *Microbial interactions in theory and practice: when are measurements compatible with models?* Current Opinion in Microbiology, 2023. **75**: p. 102354.
52. Mao, S., et al., *Coopetition analysis in industry upgrade and urban expansion based on fractional derivative gray Lotka–Volterra model*. Soft Computing, 2021. **25**: p. 11485-11507.
53. Muscarella, M.E. and J.P. O'Dwyer, *Species dynamics and interactions via metabolically informed consumer-resource models*. Theoretical Ecology, 2020. **13**(4): p. 503-518.
54. Lobanov, V., A. Gobet, and A. Joyce, *Ecosystem-specific microbiota and microbiome databases in the era of big data*. Environmental Microbiome, 2022. **17**(1): p. 37.

55. Zhong, C., et al., *Integrating pan-genome with metagenome for microbial community profiling*. Computational and Structural Biotechnology Journal, 2021. **19**: p. 1458-1466.
56. Van Santen, J.A., et al., *Microbial natural product databases: moving forward in the multi-omics era*. Natural Product Reports, 2021. **38**(1): p. 264-278.
57. Ma, B., et al., *A comprehensive non-redundant gene catalog reveals extensive within-community intraspecies diversity in the human vagina*. Nature communications, 2020. **11**(1): p. 940.
58. Garner, R.E., et al., *A genome catalogue of lake bacterial diversity and its drivers at continental scale*. Nature Microbiology, 2023. **8**(10): p. 1920-1934.
59. Ishizawa, H., et al., *Learning beyond-pairwise interactions enables the bottom–up prediction of microbial community structure*. Proceedings of the National Academy of Sciences, 2024. **121**(7): p. e2312396121.
60. Jones, E.W., et al., *Stochastic microbiome assembly depends on context*. Proceedings of the National Academy of Sciences, 2022. **119**(7): p. e2115877119.
61. Gibbs, T., S.A. Levin, and J.M. Levine, *Coexistence in diverse communities with higher-order interactions*. Proceedings of the National Academy of Sciences, 2022. **119**(43): p. e2205063119.
62. Paquette, A. and A.L. Hargreaves, *Biotic interactions are more often important at species' warm versus cool range edges*. Ecology Letters, 2021. **24**(11): p. 2427-2438.
63. Kern, L., et al., *Commensal inter-bacterial interactions shaping the microbiota*. Current opinion in microbiology, 2021. **63**: p. 158-171.
64. Ganesan, R., et al., *How it all begins: bacterial factors mediating the colonization of invertebrate hosts by beneficial symbionts*. Microbiology and Molecular Biology Reviews, 2022. **86**(4): p. e00126-21.
65. Kleinhesselink, A.R., et al., *Detecting and interpreting higher-order interactions in ecological communities*. Ecology letters, 2022. **25**(7): p. 1604-1617.
66. Arellano-García, M.E., J.A. Camacho-Gutiérrez, and S. Solorza-Calderon, *Machine learning approach for higher-order interactions detection to ecological communities management*. Applied Mathematics and Computation, 2021. **411**: p. 126499.
67. Korkmazhan, E. and A.R. Dunn, *High-order correlations in species interactions lead to complex diversity-stability relationships for ecosystems*. Physical Review E, 2022. **105**(1): p. 014406.
68. Barrows, C.W., et al., *A framework for monitoring multiple-species conservation plans*. The Journal of wildlife management, 2005. **69**(4): p. 1333-1345.
69. Delmas, E., et al., *Analysing ecological networks of species interactions*. Biological Reviews, 2019. **94**(1): p. 16-36.
70. Diener, C. and S.M. Gibbons, *More is different: metabolic modeling of diverse microbial communities*. Msystems, 2023. **8**(2): p. e01270-22.
71. Cardona, C., et al., *Network-based metabolic analysis and microbial community modeling*. Current Opinion in Microbiology, 2016. **31**: p. 124-131.

72. Meroz, N., et al., *Community composition of microbial microcosms follows simple assembly rules at evolutionary timescales.* Nature communications, 2021. **12**(1): p. 2891.
73. Muller, E.E., et al., *Using metabolic networks to resolve ecological properties of microbiomes.* Current Opinion in Systems Biology, 2018. **8**: p. 73-80.
74. Haruta, S. and K. Yamamoto, *Model microbial consortia as tools for understanding complex microbial communities.* Current Genomics, 2018. **19**(8): p. 723-733.
75. Pinto, S., et al., *Species abundance correlations carry limited information about microbial network interactions.* PLoS computational biology, 2022. **18**(9): p. e1010491.
76. Gupta, G., A. Ndiaye, and M. Filteau, *Leveraging experimental strategies to capture different dimensions of microbial interactions.* Frontiers in Microbiology, 2021. **12**: p. 700752.
77. O'Donnell, S.T., R.P. Ross, and C. Stanton, *The progress of multi-omics technologies: determining function in lactic acid bacteria using a systems level approach.* Frontiers in microbiology, 2020. **10**: p. 3084.
78. Franzosa, E.A., et al., *Sequencing and beyond: integrating molecular'omics' for microbial community profiling.* Nature Reviews Microbiology, 2015. **13**(6): p. 360-372.
79. Liu, Z., et al., *Network analyses in microbiome based on high-throughput multi-omics data.* Briefings in bioinformatics, 2021. **22**(2): p. 1639-1655.
80. Hassa, J., et al., *Metagenome, metatranscriptome, and metaproteome approaches unraveled compositions and functional relationships of microbial communities residing in biogas plants.* Applied microbiology and biotechnology, 2018. **102**: p. 5045-5063.
81. García-Jiménez, B., J. Torres-Bacete, and J. Nogales, *Metabolic modelling approaches for describing and engineering microbial communities.* Computational and Structural Biotechnology Journal, 2021. **19**: p. 226-246.
82. Du, H., M. Li, and Y. Liu, *Towards applications of genome-scale metabolic model-based approaches in designing synthetic microbial communities.* Quantitative Biology, 2023. **11**(1): p. 15-30.
83. Sampara, P., et al., *Advancing environmental biotechnology with microbial community modeling rooted in functional 'omics.* Current Opinion in Biotechnology, 2024. **88**: p. 103165.
84. Giordano, N., et al., *Genome-scale community modelling reveals conserved metabolic cross-feedings in epipelagic bacterioplankton communities.* Nature Communications, 2024. **15**(1): p. 2721.
85. Hoagland, B., et al., *Metal-oxide precipitation influences microbiome structure in hyporheic zones receiving acid rock drainage.* Applied and Environmental Microbiology, 2024. **90**(3): p. e01987-23.
86. Milani, C., et al., *Multi-omics approaches to decipher the impact of diet and host physiology on the mammalian gut microbiome.* Applied and Environmental Microbiology, 2020. **86**(23): p. e01864-20.

87. Herold, M., et al., *Integration of time-series meta-omics data reveals how microbial ecosystems respond to disturbance.* Nature communications, 2020. **11**(1): p. 5281.
88. Pierce, E.C. and R.J. Dutton, *Putting microbial interactions back into community contexts.* Current Opinion in Microbiology, 2022. **65**: p. 56-63.
89. McDaniel, E.A., et al., *Prospects for multi-omics in the microbial ecology of water engineering.* Water Research, 2021. **205**: p. 117608.
90. Shahrajabian, M.H. and W. Sun, *Survey on multi-omics, and multi-omics data analysis, integration and application.* Current Pharmaceutical Analysis, 2023. **19**(4): p. 267-281.
91. Arikan, M. and T. Muth, *Integrated multi-omics analyses of microbial communities: A review of the current state and future directions.* Molecular Omics, 2023: p. 1-17.
92. Tolani, P., et al., *Big data, integrative omics and network biology.* Advances in protein chemistry and structural biology, 2021. **127**: p. 127-160.
93. Shi, L.-D., et al., *Coupled anaerobic methane oxidation and reductive arsenic mobilization in wetland soils.* Nature Geoscience, 2020. **13**(12): p. 799-805.
94. Broucek, J., *Options to methane production abatement in ruminants: A review.* J. Anim. Plant Sci, 2018. **28**(2): p. 348-364.
95. Yang, S. and L. Song, *Succession of bacterial community structure and metabolic function during solid waste decomposition.* Bioresource technology, 2019. **291**: p. 121865.
96. Amin, F.R., et al., *Functions of bacteria and archaea participating in the bioconversion of organic waste for methane production.* Science of The Total Environment, 2021. **763**: p. 143007.
97. Santos, A.M.d., et al., *Lactate as an effective electron donor in the sulfate reduction: impacts on the microbial diversity.* Environmental Technology, 2021: p. 1-12.
98. Zhang, G., et al., *Salinity controls soil microbial community structure and function in coastal estuarine wetlands.* Environmental Microbiology, 2021. **23**(2): p. 1020-1037.
99. Gómez-Gener, L., et al., *Drought alters the biogeochemistry of boreal stream networks.* Nature communications, 2020. **11**(1): p. 1-11.
100. Walker, C.B., et al., *Functional responses of methanogenic archaea to syntrophic growth.* The ISME journal, 2012. **6**(11): p. 2045-2055.
101. Zan, F., et al., *Diversion of food waste into the sulfate-laden sewer: Interaction and electron flow of sulfidogenesis and methanogenesis.* Water Research, 2021. **202**: p. 117437.
102. Tsola, S.L., et al., *Diversity of dimethylsulfide -degrading methanogens and sulfate -reducing bacteria in anoxic sediments along the Medway Estuary, UK.* Environmental Microbiology, 2021.
103. Großkopf, T. and O.S. Soyer, *Synthetic microbial communities.* Current opinion in microbiology, 2014. **18**: p. 72-77.
104. Kong, W., et al., *Designing microbial consortia with defined social interactions.* Nature Chemical Biology, 2018. **14**(8): p. 821-829.
105. Summers, Z.M., et al., *Direct exchange of electrons within aggregates of an evolved syntrophic coculture of anaerobic bacteria.* Science, 2010. **330**(6009): p. 1413-1415.

106. LaSarre, B., et al., *Covert cross-feeding revealed by genome-wide analysis of fitness determinants in a synthetic bacterial mutualism.* Applied and environmental microbiology, 2020. **86**(13): p. e00543-20.
107. An, D., et al., *Quorum sensing and motility mediate interactions between Pseudomonas aeruginosa and Agrobacterium tumefaciens in biofilm cocultures.* Proceedings of the National Academy of Sciences, 2006. **103**(10): p. 3828-3833.
108. Doloman, A., et al., *Stimulating Effect of Trichococcus flocculiformis on a Coculture of Syntrophomonas wolfei and Methanospirillum hungatei.* Applied and Environmental Microbiology, 2022: p. e00391-22.
109. Zhou, A., et al., *Rapid selective sweep of pre-existing polymorphisms and slow fixation of new mutations in experimental evolution of Desulfovibrio vulgaris.* The ISME journal, 2015. **9**(11): p. 2360-2372.
110. Tao, X., et al., *Precise promoter integration improves cellulose bioconversion and thermotolerance in clostridium cellulolyticum.* Metabolic engineering, 2020. **60**: p. 110-118.
111. Ferry, J.G., P.H. Smith, and R. Wolfe, *Methanospirillum, a new genus of methanogenic bacteria, and characterization of Methanospirillum hungatii sp. nov.* International Journal of Systematic and Evolutionary Microbiology, 1974. **24**(4): p. 465-469.
112. Hemme, C.L., et al., *Correlation of genomic and physiological traits of Thermoanaerobacter species with biofuel yields.* Applied and environmental microbiology, 2011. **77**(22): p. 7998-8008.
113. Li, Y., et al., *Combined inactivation of the Clostridium cellulolyticum lactate and malate dehydrogenase genes substantially increases ethanol yield from cellulose and switchgrass fermentations.* Biotechnology for biofuels, 2012. **5**(1): p. 1-13.
114. Li, Z., et al., *Genome-resolved proteomic stable isotope probing of soil microbial communities using 13CO2 and 13C-methanol.* Frontiers in microbiology, 2019. **10**: p. 2706.
115. Yao, Q., et al., *Community proteogenomics reveals the systemic impact of phosphorus availability on microbial functions in tropical soil.* Nature ecology & evolution, 2018. **2**(3): p. 499-509.
116. Walker, J.M., *The bicinchoninic acid (BCA) assay for protein quantitation.* The protein protocols handbook, 2009: p. 11-15.
117. Guo, X., et al., *Sipros Ensemble improves database searching and filtering for complex metaproteomics.* Bioinformatics, 2018. **34**(5): p. 795-802.
118. Wang, Y., et al., *Sipros/ProRata: a versatile informatics system for quantitative community proteomics.* Bioinformatics, 2013. **29**(16): p. 2064-2065.
119. Pan, C., et al., *ProRata: a quantitative proteomics program for accurate protein abundance ratio estimation with confidence interval evaluation.* Analytical chemistry, 2006. **78**(20): p. 7121-7131.
120. Li, Z., et al., *Diverse and divergent protein post-translational modifications in two growth stages of a natural microbial community.* Nature communications, 2014. **5**(1): p. 1-11.

121. Li, Z., et al., *Integrated proteomics and metabolomics suggests symbiotic metabolism and multimodal regulation in a fungal-endobacterial system*. Environmental microbiology, 2017. **19**(3): p. 1041-1053.
122. Love, M., S. Anders, and W. Huber, *Differential analysis of count data–the DESeq2 package*. Genome Biol, 2014. **15**(550): p. 10.1186.
123. Love, M., S. Anders, and W. Huber, *Differential analysis of count data–the DESeq2 package*. Genome Biol, 2014. **15**(550): p. 10-1186.
124. Pan, C. and J.F. Banfield, *Quantitative Metaproteomics: Functional Insights into Microbial Communities*, in *Environmental Microbiology: Methods and Protocols*, I.T. Paulsen and A.J. Holmes, Editors. 2014, Humana Press: Totowa, NJ. p. 231-240.
125. Flowers, J.J., et al., *Constraint-based modelling captures the metabolic versatility of Desulfovibrio vulgaris*. Environmental microbiology reports, 2018. **10**(2): p. 190-201.
126. Stolyar, S., et al., *Metabolic modeling of a mutualistic microbial community*. Molecular systems biology, 2007. **3**(1): p. 92.
127. Lu, H., et al., *Physiological and molecular characterizations of the interactions in two cellulose-to-methane cocultures*. Biotechnology for biofuels, 2017. **10**(1): p. 1-14.
128. Liu, W., *Biofuels (hydrogen and ethanol) production of clostridium by cellulose bioconversion*. 2018.
129. Liang, C., J.P. Schimel, and J.D. Jastrow, *The importance of anabolism in microbial control over soil carbon storage*. Nature microbiology, 2017. **2**(8): p. 1-6.
130. Mayumi, D., et al., *Carbon dioxide concentration dictates alternative methanogenic pathways in oil reservoirs*. Nature communications, 2013. **4**(1): p. 1-6.
131. Pacheco, A.R., M. Moel, and D. Segrè, *Costless metabolic secretions as drivers of interspecies interactions in microbial ecosystems*. Nature communications, 2019. **10**(1): p. 1-12.
132. Senne de Oliveira Lino, F., et al., *Complex yeast–bacteria interactions affect the yield of industrial ethanol fermentation*. Nature communications, 2021. **12**(1): p. 1-12.
133. Canto-Encalada, G., et al., *Flux balance analysis of the ammonia-oxidizing bacterium Nitrosomonas europaea ATCC19718 unravels specific metabolic activities while degrading toxic compounds*. PLOS Computational Biology, 2022. **18**(2): p. e1009828.
134. Bordbar, A., et al., *Constraint-based models predict metabolic and associated cellular functions*. Nature Reviews Genetics, 2014. **15**(2): p. 107-120.
135. Li, X. and M.A. Henson, *Metabolic modeling of bacterial co-culture systems predicts enhanced carbon monoxide-to-butyrate conversion compared to monoculture systems*. Biochemical engineering journal, 2019. **151**: p. 107338.
136. Montecchio, D., et al., *Anaerobic co-digestion of food waste and waste activated sludge: ADM1 modelling and microbial analysis to gain insights into the two substrates' synergistic effects*. Waste Management, 2019. **97**: p. 27-37.
137. Martins Conde, P.d.R., T. Sauter, and T. Pfau, *Constraint based modeling going multicellular*. Frontiers in molecular biosciences, 2016. **3**: p. 3.

138. Hunt, K.A., et al., *Stoichiometric modelling of assimilatory and dissimilatory biomass utilisation in a microbial community.* Environmental microbiology, 2016. **18**(12): p. 4946-4960.
139. Doroski, A.A., A.M. Helton, and T.M. Vadas, *Greenhouse gas fluxes from coastal wetlands at the intersection of urban pollution and saltwater intrusion: A soil core experiment.* Soil Biology and Biochemistry, 2019. **131**: p. 44-53.
140. Yang, J., et al., *Effect of salinity on soil respiration in relation to dissolved organic carbon and microbial characteristics of a wetland in the Liaohe River estuary, Northeast China.* Science of the total environment, 2018. **642**: p. 946-953.
141. Dang, C., et al., *Novel microbial community composition and carbon biogeochemistry emerge over time following saltwater intrusion in wetlands.* Global change biology, 2019. **25**(2): p. 549-561.
142. Dar, S.A., et al., *Competition and coexistence of sulfate-reducing bacteria, acetogens and methanogens in a lab-scale anaerobic bioreactor as affected by changing substrate to sulfate ratio.* Applied microbiology and biotechnology, 2008. **78**(6): p. 1045-1055.
143. Ozuolmez, D., et al., *Methanogenic archaea and sulfate reducing bacteria co-cultured on acetate: teamwork or coexistence?* Frontiers in microbiology, 2015. **6**: p. 492.
144. Sela-Adler, M., et al., *Co-existence of methanogenesis and sulfate reduction with common substrates in sulfate-rich estuarine sediments.* Frontiers in microbiology, 2017. **8**: p. 766.
145. Gieg, L.M., S.J. Fowler, and C. Berdugo-Clavijo, *Syntrophic biodegradation of hydrocarbon contaminants.* Current opinion in biotechnology, 2014. **27**: p. 21-29.
146. Walker, D.J., et al., *The archaellum of Methanospirillum hungatei is electrically conductive.* MBio, 2019. **10**(2): p. e00579-19.
147. Watanabe, T., et al., *Three-megadalton complex of methanogenic electron-bifurcating and CO2-fixing enzymes.* Science, 2021. **373**(6559): p. 1151-1156.
148. Coyte, K.Z., J. Schluter, and K.R. Foster, *The ecology of the microbiome: Networks, competition, and stability.* Science, 2015. **350**(6261): p. 663-666.
149. Lin, Q., et al., *Functional conservation of microbial communities determines composition predictability in anaerobic digestion.* The ISME Journal, 2023. **17**(11): p. 1920-1930.
150. Coban, O., G.B. De Deyn, and M. van der Ploeg, *Soil microbiota as game-changers in restoration of degraded lands.* Science, 2022. **375**(6584): p. abe0725.
151. Sobral, M., et al., *Mammal diversity influences the carbon cycle through trophic interactions in the Amazon.* Nature Ecology & Evolution, 2017. **1**(11): p. 1670-1676.
152. Lee, H., B. Bloxham, and J. Gore, *Resource competition can explain simplicity in microbial community assembly.* Proceedings of the National Academy of Sciences, 2023. **120**(35): p. e2212113120.
153. Weber, K.A., L.A. Achenbach, and J.D. Coates, *Microorganisms pumping iron: anaerobic microbial iron oxidation and reduction.* Nature Reviews Microbiology, 2006. **4**(10): p. 752-764.

154. Candry, P., et al., *Microbially mediated climate feedbacks from wetland ecosystems.* Global Change Biology, 2023. **29**(18): p. 5169-5183.
155. Gralka, M., S. Pollak, and O.X. Cordero, *Genome content predicts the carbon catabolic preferences of heterotrophic bacteria.* Nature Microbiology, 2023. **8**(10): p. 1799-1808.
156. Dal Bello, M., et al., *Resource–diversity relationships in bacterial communities reflect the network structure of microbial metabolism.* Nature Ecology & Evolution, 2021. **5**(10): p. 1424-1434.
157. Friedman, J., L.M. Higgins, and J. Gore, *Community structure follows simple assembly rules in microbial microcosms.* Nature ecology & evolution, 2017. **1**(5): p. 0109.
158. Hu, J., et al., *Emergent phases of ecological diversity and dynamics mapped in microcosms.* Science, 2022. **378**(6615): p. 85-89.
159. Culp, E.J. and A.L. Goodman, *Cross-feeding in the gut microbiome: Ecology and mechanisms.* Cell Host & Microbe, 2023. **31**(4): p. 485-499.
160. Holbrook-Smith, D., J. Trouillon, and U. Sauer, *Metabolomics and Microbial Metabolism: Toward a Systematic Understanding.* Annual Review of Biophysics, 2023. **53**.
161. Blair, E.M., K.L. Dickson, and M.A. O'Malley, *Microbial communities and their enzymes facilitate degradation of recalcitrant polymers in anaerobic digestion.* Current Opinion in Microbiology, 2021. **64**: p. 100-108.
162. Bharti, R. and D.G. Grimm, *Current challenges and best-practice protocols for microbiome analysis.* Briefings in bioinformatics, 2021. **22**(1): p. 178-193.
163. Jansson, J.K. and K.S. Hofmockel, *The soil microbiome—from metagenomics to metaphenomics.* Current opinion in microbiology, 2018. **43**: p. 162-168.
164. Moreira, Z.P.M., et al., *Engineering plant microbiomes by integrating eco-evolutionary principles into current strategies.* Current Opinion in Plant Biology, 2023. **71**: p. 102316.
165. Dhanda, A., et al., *Anodic inoculum pre-treatment with green strategies for enhanced electron shuttling and suppressing methanogens in microbial fuel cell: A review.* Bioresource Technology Reports, 2023: p. 101593.
166. Wang, D., et al., *Cross-Feedings, Competition, and Positive and Negative Synergies in a Four-Species Synthetic Community for Anaerobic Degradation of Cellulose to Methane.* Mbio, 2023. **14**(2): p. e03189-22.
167. Yang, Y., *Emerging patterns of microbial functional traits.* Trends in Microbiology, 2021. **29**(10): p. 874-882.
168. Goldschmidt, F., L. Caduff, and D.R. Johnson, *Causes and consequences of pattern diversification in a spatially self-organizing microbial community.* The ISME Journal, 2021. **15**(8): p. 2415-2426.
169. Wang, D., et al., *Metaproteomics-informed stoichiometric modeling reveals the responses of wetland microbial communities to oxygen and sulfate exposure.* npj Biofilms and Microbiomes, 2024. **10**(1): p. 55.

170. Machado, D., et al., *Fast automated reconstruction of genome-scale metabolic models for microbial species and communities.* Nucleic acids research, 2018. **46**(15): p. 7542-7553.
171. Zelezniak, A., et al., *Metabolic dependencies drive species co-occurrence in diverse microbial communities.* Proceedings of the National Academy of Sciences, 2015. **112**(20): p. 6449-6454.
172. Griffin, N.M., et al., *Label-free, normalized quantification of complex mass spectrometry data for proteomic analysis.* Nature biotechnology, 2010. **28**(1): p. 83-89.
173. Vogel, C. and E.M. Marcotte, *Calculating absolute and relative protein abundance from mass spectrometry-based protein expression data.* Nature protocols, 2008. **3**(9): p. 1444-1451.
174. Matzke, M.M., et al., *A comparative analysis of computational approaches to relative protein quantification using peptide peak intensities in label-free LC-MS proteomics experiments.* Proteomics, 2013. **13**(3-4): p. 493-503.
175. Sahraeian, S.M.E. and B.-J. Yoon, *SMETANA: accurate and scalable algorithm for probabilistic alignment of large-scale biological networks.* PloS one, 2013. **8**(7): p. e67995.
176. He, X., et al., *Controls on interspecies electron transport and size limitation of anaerobically methane-oxidizing microbial consortia.* MBio, 2021. **12**(3): p. 10.1128/mbio. 03620-20.
177. Yu, R.-Q., et al., *Syntrophic pathways for microbial mercury methylation.* The ISME Journal, 2018. **12**(7): p. 1826-1835.
178. Basile, A., et al., *Revealing metabolic mechanisms of interaction in the anaerobic digestion microbiome by flux balance analysis.* Metabolic Engineering, 2020. **62**: p. 138-149.
179. Rafieenia, R., E. Atkinson, and R. Ledesma-Amaro, *Division of labor for substrate utilization in natural and synthetic microbial communities.* Current Opinion in Biotechnology, 2022. **75**: p. 102706.
180. Wang, B., et al., *Microbial fingerprints of methanation in a hybrid electric-biological anaerobic digestion.* Water Research, 2022. **226**: p. 119270.
181. Stams, A.J. and C.M. Plugge, *Electron transfer in syntrophic communities of anaerobic bacteria and archaea.* Nature Reviews Microbiology, 2009. **7**(8): p. 568-577.
182. Treitli, S.C., et al., *Hydrogenotrophic methanogenesis is the key process in the obligately syntrophic consortium of the anaerobic ameba Pelomyxa schiedti.* The ISME Journal, 2023. **17**(11): p. 1884-1894.
183. Sasaki, D., et al., *Acceleration of cellulose degradation and shift of product via methanogenic co-culture of a cellulolytic bacterium with a hydrogenotrophic methanogen.* Journal of bioscience and bioengineering, 2012. **114**(4): p. 435-439.
184. Jansson, J.K. and K.S. Hofmockel, *Soil microbiomes and climate change.* Nature Reviews Microbiology, 2020. **18**(1): p. 35-46.
185. Kirwan, M.L., et al., *Geomorphic and ecological constraints on the coastal carbon sink.* Nature Reviews Earth & Environment, 2023: p. 1-14.

186. Candry, P., et al., *Microbially mediated climate feedbacks from wetland ecosystems*. Global Change Biology, 2023.
187. Bao, T., G. Jia, and X. Xu, *Weakening greenhouse gas sink of pristine wetlands under warming*. Nature Climate Change, 2023. **13**(5): p. 462-469.
188. Chen, H., et al., *Differences in the temperature dependence of wetland CO2 and CH4 emissions vary with water table depth*. Nature Climate Change, 2021. **11**(9): p. 766-771.
189. Rillig, M.C., et al., *Increasing the number of stressors reduces soil ecosystem services worldwide*. Nature Climate Change, 2023: p. 1-6.
190. Xu, X., et al., *Wetland ecosystem services research: A critical review*. Global Ecology and Conservation, 2020. **22**: p. e01027.
191. Mobilian, C., et al., *Differential effects of press vs. pulse seawater intrusion on microbial communities of a tidal freshwater marsh*. Limnology and Oceanography Letters, 2023. **8**(1): p. 154-161.
192. Solohin, E., S.E. Widney, and C.B. Craft, *Declines in plant productivity drive loss of soil elevation in a tidal freshwater marsh exposed to saltwater intrusion*. Ecology, 2020. **101**(12): p. e03148.
193. Cavicchioli, R., et al., *Scientists' warning to humanity: microorganisms and climate change*. Nature Reviews Microbiology, 2019. **17**(9): p. 569-586.
194. Hartmann, M. and J. Six, *Soil structure and microbiome functions in agroecosystems*. Nature Reviews Earth & Environment, 2023. **4**(1): p. 4-18.
195. Van Rossum, T., et al., *Diversity within species: interpreting strains in microbiomes*. Nature Reviews Microbiology, 2020. **18**(9): p. 491-506.
196. Lu, Z. and J.A. Imlay, *When anaerobes encounter oxygen: mechanisms of oxygen toxicity, tolerance and defence*. Nature reviews microbiology, 2021. **19**(12): p. 774-785.
197. Berrier, D.J., S.C. Neubauer, and R.B. Franklin, *Cooperative microbial interactions mediate community biogeochemical responses to saltwater intrusion in wetland soils*. FEMS Microbiology Ecology, 2022. **98**(3): p. fiac019.
198. Conrad, R., *Soil microorganisms as controllers of atmospheric trace gases (H2, CO, CH4, OCS, N2O, and NO)*. Microbiological reviews, 1996. **60**(4): p. 609-640.
199. Lee, J.-Y., R.M. Tsolis, and A.J. Bäumler, *The microbiome and gut homeostasis*. Science, 2022. **377**(6601): p. eabp9960.
200. Hakemian, A.S. and A.C. Rosenzweig, *The biochemistry of methane oxidation*. Annu. Rev. Biochem., 2007. **76**: p. 223-241.
201. He, S., et al., *Patterns in Wetland Microbial Community Composition and Functional Gene Repertoire Associated with Methane Emissions*. mBio, 2015. **6**(3): p. 10.1128/mbio.00066-15.
202. Martins, P.D., et al., *Wetland Sediments Host Diverse Microbial Taxa Capable of Cycling Alcohols*. Applied and Environmental Microbiology, 2019. **85**(12): p. e00189-19.
203. Noyce, G.L., et al., *Oxygen priming induced by elevated CO2 reduces carbon accumulation and methane emissions in coastal wetlands*. Nature Geoscience, 2023. **16**(1): p. 63-68.

204. Chen, X., et al., *Priming effects of root exudates on the source-sink stability of benzo [a] pyrene in wetlands: A microcosm experiment.* Journal of Hazardous Materials, 2022. **429**: p. 128364.
205. Wilmoth, J.L., et al., *The role of oxygen in stimulating methane production in wetlands.* Global Change Biology, 2021. **27**(22): p. 5831-5847.
206. Bittleston, L.S., et al., *Context-dependent dynamics lead to the assembly of functionally distinct microbial communities.* Nature communications, 2020. **11**(1): p. 1440.
207. Diamond, S., et al., *Mediterranean grassland soil C–N compound turnover is dependent on rainfall and depth, and is mediated by genomically divergent microorganisms.* Nature Microbiology, 2019. **4**(8): p. 1356-1367.
208. Bushnell, B., *BBTools software packag.* e, 2014.
209. Nurk, S., et al., *metaSPAdes: a new versatile metagenomic assembler.* Genome research, 2017. **27**(5): p. 824-834.
210. Hyatt, D., et al., *Prodigal: prokaryotic gene recognition and translation initiation site identification.* BMC bioinformatics, 2010. **11**: p. 1-11.
211. Aramaki, T., et al., *KofamKOALA: KEGG Ortholog assignment based on profile HMM and adaptive score threshold.* Bioinformatics, 2020. **36**(7): p. 2251-2252.
212. Menzel, P., K.L. Ng, and A. Krogh, *Fast and sensitive taxonomic classification for metagenomics with Kaiju.* Nature communications, 2016. **7**(1): p. 11257.
213. Kang, D.D., et al., *MetaBAT 2: an adaptive binning algorithm for robust and efficient genome reconstruction from metagenome assemblies.* PeerJ, 2019. **7**: p. e7359.
214. Chaumeil, P.-A., et al., *GTDB-Tk: a toolkit to classify genomes with the Genome Taxonomy Database*. 2020, Oxford University Press.
215. Wang, D., et al., *Cross-Feedings, Competition, and Positive and Negative Synergies in a Four-Species Synthetic Community for Anaerobic Degradation of Cellulose to Methane.* Mbio, 2023: p. e03189-22.
216. Cheng, K., et al., *MetaLab: an automated pipeline for metaproteomic data analysis.* Microbiome, 2017. **5**: p. 1-10.
217. Xiao, J., et al., *Metagenomic taxonomy-guided database-searching strategy for improving metaproteomic analysis.* Journal of proteome research, 2018. **17**(4): p. 1596-1605.
218. Easterly, C.W., et al., *metaQuantome: an integrated, quantitative metaproteomics approach reveals connections between taxonomy and protein function in complex microbiomes.* Molecular & Cellular Proteomics, 2019. **18**(8): p. S82-S91.
219. Dixon, P., *VEGAN, a package of R functions for community ecology.* Journal of vegetation science, 2003. **14**(6): p. 927-930.
220. Fremin, B.J., H. Sberro, and A.S. Bhatt, *MetaRibo-Seq measures translation in microbiomes.* Nature communications, 2020. **11**(1): p. 3268.
221. Lin, Y., et al., *Revealing taxon-specific heavy metal-resistance mechanisms in denitrifying phosphorus removal sludge using genome-centric metaproteomics.* Microbiome, 2021. **9**: p. 1-17.
222. Debeljak, P., et al., *Seasonal patterns in microbial carbon and iron transporter expression in the Southern Ocean.* Microbiome, 2023. **11**(1): p. 187.

223. Canfield, D.E. and J. Farquhar, *Animal evolution, bioturbation, and the sulfate concentration of the oceans*. Proceedings of the National Academy of Sciences, 2009. **106**(20): p. 8123-8127.
224. Santos, A.M.d., et al., *Lactate as an effective electron donor in the sulfate reduction: impacts on the microbial diversity*. Environmental Technology, 2022. **43**(20): p. 3149-3160.
225. Ward, N.D., et al., *Representing the function and sensitivity of coastal interfaces in Earth system models*. Nature Communications, 2020. **11**(1): p. 2458.
226. Segarra, K., et al., *High rates of anaerobic methane oxidation in freshwater wetlands reduce potential atmospheric methane emissions*. Nature Communications, 2015. **6**(1): p. 7477.
227. Timmers, P.H., et al., *Anaerobic oxidation of methane associated with sulfate reduction in a natural freshwater gas source*. The ISME journal, 2016. **10**(6): p. 1400-1412.
228. Lawson, C.E., et al., *Common principles and best practices for engineering microbiomes*. Nature Reviews Microbiology, 2019. **17**(12): p. 725-741.
229. Des Marais, D.L., K.M. Hernandez, and T.E. Juenger, *Genotype-by-environment interaction and plasticity: exploring genomic responses of plants to the abiotic environment*. Annual Review of Ecology, Evolution, and Systematics, 2013. **44**: p. 5-29.
230. Chebbi, A., et al., *Photocatalytic conversion of carbon dioxide, methane, and air for green fuels synthesis*. Catalysis Science & Technology, 2023.
231. Lovley, D.R., D.F. Dwyer, and M.J. Klug, *Kinetic analysis of competition between sulfate reducers and methanogens for hydrogen in sediments*. Applied and Environmental Microbiology, 1982. **43**(6): p. 1373-1379.
232. Dar, S.A., et al., *Competition and coexistence of sulfate-reducing bacteria, acetogens and methanogens in a lab-scale anaerobic bioreactor as affected by changing substrate to sulfate ratio*. Applied microbiology and biotechnology, 2008. **78**: p. 1045-1055.
233. Ye, R., et al., *pH controls over anaerobic carbon mineralization, the efficiency of methane production, and methanogenic pathways in peatlands across an ombrotrophic–minerotrophic gradient*. Soil Biology and Biochemistry, 2012. **54**: p. 36-47.
234. Nguyen, D. and S.K. Khanal, *A little breath of fresh air into an anaerobic system: How microaeration facilitates anaerobic digestion process*. Biotechnology advances, 2018. **36**(7): p. 1971-1983.
235. Lim, J.W. and J.-Y. Wang, *Enhanced hydrolysis and methane yield by applying microaeration pretreatment to the anaerobic co-digestion of brown water and food waste*. Waste Management, 2013. **33**(4): p. 813-819.
236. Rillig, M.C., et al., *The role of multiple global change factors in driving soil functions and microbial biodiversity*. Science, 2019. **366**(6467): p. 886-890.
237. Yang, G., et al., *Multiple anthropogenic pressures eliminate the effects of soil microbial diversity on ecosystem functions in experimental microcosms*. Nature Communications, 2022. **13**(1): p. 4260.

238. Loreau, M., et al., *Biodiversity and ecosystem functioning: current knowledge and future challenges*. science, 2001. **294**(5543): p. 804-808.
239. McIntyre, H.D., et al., *Gestational diabetes mellitus*. Nature reviews Disease primers, 2019. **5**(1): p. 47.
240. Choudhury, A.A. and V.D. Rajeswari, *Gestational diabetes mellitus-A metabolic and reproductive disorder*. Biomedicine & Pharmacotherapy, 2021. **143**: p. 112183.
241. Egan, A.M., M.L. Dow, and A. Vella. *A review of the pathophysiology and management of diabetes in pregnancy*. in *Mayo Clinic Proceedings*. 2020. Elsevier.
242. Saravanan, P., et al., *Gestational diabetes: opportunities for improving maternal and child health*. The Lancet Diabetes & Endocrinology, 2020. **8**(9): p. 793-800.
243. Ringholm, L., P. Damm, and E.R. Mathiesen, *Improving pregnancy outcomes in women with diabetes mellitus: modern management*. Nature Reviews Endocrinology, 2019. **15**(7): p. 406-416.
244. Aloke, C., et al., *Current advances in the management of diabetes mellitus*. Biomedicines, 2022. **10**(10): p. 2436.
245. Zheng, Z.-X., X. Feng, and L. Zhuang, *The effect of oxidative stress and antioxidants treatment on gestational diabetes mellitus outcome: A scoping review*. Cell Biochemistry and Biophysics, 2024: p. 1-11.
246. Martín, M.Á. and S. Ramos, *Impact of dietary flavanols on microbiota, immunity and inflammation in metabolic diseases*. Nutrients, 2021. **13**(3): p. 850.
247. Shao, T., et al., *The gut ecosystem and immune tolerance*. Journal of Autoimmunity, 2023: p. 103114.
248. Zakaria, Z.Z., et al., *Physiological changes and interactions between microbiome and the host during pregnancy*. Frontiers in Cellular and Infection Microbiology, 2022. **12**: p. 824925.
249. Mesa, M.D., et al., *The evolving microbiome from pregnancy to early infancy: a comprehensive review*. Nutrients, 2020. **12**(1): p. 133.
250. Mao, L., et al., *Interaction and Metabolic Pathways: Elucidating the Role of Gut Microbiota in Gestational Diabetes Mellitus Pathogenesis*. Metabolites, 2024. **14**(1): p. 43.
251. Sindi, A.S., et al., *Can we modulate the breastfed infant gut microbiota through maternal diet?* FEMS microbiology reviews, 2021. **45**(5): p. fuab011.
252. Sassin, A.M., et al., *Crucial nuances in understanding (mis) associations between the neonatal microbiome and cesarean delivery*. Trends in molecular medicine, 2022. **28**(10): p. 806-822.
253. Bolte, E.E., D. Moorshead, and K.M. Aagaard, *Maternal and early life exposures and their potential to influence development of the microbiome*. Genome Medicine, 2022. **14**(1): p. 4.
254. Forgie, A.J., et al., *The impact of maternal and early life malnutrition on health: a diet-microbe perspective*. BMC medicine, 2020. **18**: p. 1-15.
255. O'Neill, I.J., et al., *Maternal and infant factors that shape neonatal gut colonization by bacteria*. Expert Review of Gastroenterology & Hepatology, 2020. **14**(8): p. 651-664.

256. Singh, P., et al., *Maternal microbiota and gestational diabetes: impact on infant health*. Journal of Translational Medicine, 2023. **21**(1): p. 364.
257. Mirpuri, J., *Evidence for maternal diet-mediated effects on the offspring microbiome and immunity: implications for public health initiatives*. Pediatric research, 2021. **89**(2): p. 301-306.
258. Selma-Royo, M., et al., *Maternal diet during pregnancy and intestinal markers are associated with early gut microbiota*. European journal of nutrition, 2021. **60**: p. 1429-1442.
259. Parks, D.H., et al., *CheckM: assessing the quality of microbial genomes recovered from isolates, single cells, and metagenomes*. Genome research, 2015. **25**(7): p. 1043-1055.
260. Pérez-Rodríguez, I., et al., *Detection and phylogenetic analysis of the membrane-bound nitrate reductase (Nar) in pure cultures and microbial communities from deep-sea hydrothermal vents*. FEMS microbiology ecology, 2013. **86**(2): p. 256-267.
261. Letunic, I. and P. Bork, *Interactive Tree of Life (iTOL) v6: recent updates to the phylogenetic tree display and annotation tool*. Nucleic Acids Research, 2024: p. gkae268.
262. Fu, L., et al., *CD-HIT: accelerated for clustering the next-generation sequencing data*. Bioinformatics, 2012. **28**(23): p. 3150-3152.
263. Wu, N., et al., *The gut microbial signature of gestational diabetes mellitus and the association with diet intervention*. Frontiers in Cellular and Infection Microbiology, 2022. **11**: p. 800865.
264. Bokoliya, S., et al., *Exploring the influence of microbiota on gestational diabetes and its potential as a biomarker*. Frontiers in Bacteriology, 2024. **3**: p. 1352227.
265. Valles-Colomer, M., et al., *Cardiometabolic health, diet and the gut microbiome: a meta-omics perspective*. Nature Medicine, 2023. **29**(3): p. 551-561.
266. Metwaly, A., S. Reitmeier, and D. Haller, *Microbiome risk profiles as biomarkers for inflammatory and metabolic disorders*. Nature reviews Gastroenterology & hepatology, 2022. **19**(6): p. 383-397.
267. Liu, J., et al., *Comparative genomic analysis revealed genetic divergence between Bifidobacterium catenulatum subspecies present in infant versus adult guts*. BMC microbiology, 2022. **22**(1): p. 158.
268. Zhu, L., et al., *Captive common marmosets (Callithrix jacchus) are colonized throughout their lives by a community of Bifidobacterium species with species-specific genomic content that can support adaptation to distinct metabolic niches*. MBio, 2021. **12**(4): p. 10.1128/mbio. 01153-21.
269. Wang, S., et al., *A good start in life is important—perinatal factors dictate early microbiota development and longer term maturation*. FEMS microbiology reviews, 2020. **44**(6): p. 763-781.
270. Tsukuda, N., et al., *Key bacterial taxa and metabolic pathways affecting gut short-chain fatty acid profiles in early life*. The ISME journal, 2021. **15**(9): p. 2574-2590.
271. Lubin, J.-B., et al., *Arresting microbiome development limits immune system maturation and resistance to infection in mice*. Cell host & microbe, 2023. **31**(4): p. 554-570. e7.

272. Carmody, R.N. and J.E. Bisanz, *Roles of the gut microbiome in weight management*. Nature Reviews Microbiology, 2023. **21**(8): p. 535-550.
273. Wan, J. and J. Ma, *Efficacy of dietary supplements targeting gut microbiota in the prevention and treatment of gestational diabetes mellitus*. Frontiers in Microbiology, 2022. **13**: p. 927883.
274. Philippot, L., B.S. Griffiths, and S. Langenheder, *Microbial community resilience across ecosystems and multiple disturbances*. Microbiology and Molecular Biology Reviews, 2021. **85**(2): p. 10.1128/mmbr. 00026-20.
275. Machado, D., et al., *Polarization of microbial communities between competitive and cooperative metabolism*. Nature Ecology & Evolution, 2021. **5**(2): p. 195-203.
276. Hernandez, D.J., et al., *Environmental stress destabilizes microbial networks*. The ISME Journal, 2021. **15**(6): p. 1722-1734.
277. Saleem, M. and L.A. Moe, *Multitrophic microbial interactions for eco-and agro-biotechnological processes: theory and practice*. Trends in Biotechnology, 2014. **32**(10): p. 529-537.
278. Cao, Z., et al., *Construction of microbial consortia for microbial degradation of complex compounds*. Frontiers in Bioengineering and Biotechnology, 2022. **10**: p. 1051233.
279. Islam, M.A., et al., *Interspecies microbial interactions in bioelectrochemical system and biodegradation: A state of the art review*. Science of The Total Environment, 2023. **891**: p. 164623.
280. Jiang, D., et al., *Microbiome multi-omics network analysis: statistical considerations, limitations, and opportunities*. Frontiers in genetics, 2019. **10**: p. 995.
281. Stein, L.Y., *The long-term relationship between microbial metabolism and greenhouse gases*. Trends in microbiology, 2020. **28**(6): p. 500-511.